# FUNCTIONS OF THE VIRAL ATTACHMENT PROTEIN IN REOVIRUS NEUROVIRULENCE

By

Danica Marie Sutherland

Dissertation

Submitted to the Faculty of the

Graduate School of Vanderbilt University

in partial fulfillment of the requirements

for the degree of

DOCTOR OF PHILOSOPHY

in

Microbiology and Immunology

August 31, 2018

Nashville, Tennessee

Approved:

Terence Dermody, M.D.

Bruce Carter, Ph.D.

Jim Chappell, M.D., Ph.D.

Dana Borden Lacy, Ph.D.

Earl Ruley, Ph.D.

## DEDICATION

To world-class mentors and friends.

## ACKNOWLEDGMENTS

I am grateful for the financial support that made this research possible, including the public health service awards Reovirus Attachment Mechanisms (R01 AI118887), Molecular Basis of Reovirus Pathogenesis (R01 AI038296), and the Molecular Microbial Pathogenesis Training Program (T32 AI007281). Additionally, I am thankful for funding provided by the Elizabeth B. Lamb Center for Pediatric Research at Vanderbilt University.

Words cannot express the overwhelming thanks that I wish to share with Terence Dermody, my Ph.D. mentor. Terry is an active and exceptional mentor, and I doubt I will ever meet anyone as selfless or hard working as this man. I thank him for welcoming me into the lab and working tirelessly to provide an environment tailored to trainees. The teachings I have received under Terry's thoughtful leadership have shaped the individual I am today in innumerable and immeasurable ways. I am a better scientist, a better leader, and a better person for the time that I have spent in his company. I especially want to thank Terry for his dedication over the years, patiently coaching me to write, think, and speak like a scientist.

I want to thank Borden Lacy, Bruce Carter, Jim Chappell, Earl Ruley, and John Williams for support provided as my thesis committee. The helpful discussions and advice they have shared over the years has enhanced my training, each member providing a unique and important perspective. I appreciate that they made me feel like a colleague, and their kindness and suggestions over the years have meant so much to me. I will miss conversations with this group.

I am so very grateful for members of the Dermody lab, both past and present. You have all been my scientific cheerleaders, my teachers, my best friends, and my family during the best days, and importantly, during the toughest days. Being a part of this team has been the greatest joy of my training. I want to thank my first labmates, Bernardo Mainou and Jennifer Konopka-Anstadt, for letting me join their island of talent and leading by example in all ways. In particular, I want to thank Jennifer Konopka-Anstadt for being a patient and supportive mentor during my rotation in the lab and encouraging me to join the lab. Thanks to Laurie Silva, Anthony Lentscher and Nicole McAllister for sharing countless meals, game nights, and laughs. Thanks to Kristen

Ogden and Pavithra Aravamudhan for never shying away from asking the tough, but important, questions. I thank Jonathan Knowlton for his infectious curiosity and assistance in helping to identify a viral ligand for NgR1. I would like to thank Mine Ikizler for opening her home and heart to me and for generating plasmid reagents used in these studies. I want to thank two terrific lab managers and friends, Andrea Pruijssers and Gwen Taylor, for providing expert lab infrastructure and selflessly advancing the work of those around them.

I thank Thilo Stehle, Melanie Dietrich, and Kerstin Reiss for enumerable helpful discussions regarding protein expression, purification, and folding and σ1 chimera sequences. I especially want to thank Thilo Stehle for allowing me to train in his laboratory in Tubingen, Germany with members of his lab to learn crystallography techniques. Both Thilo Stehle and Melanie Dietrich were instrumental in designing and developing σ1-chimeric reoviruses and demonstrated steadfast patience, kindness, and support in helping me solve difficult problems over the last six years. I am grateful to BVV Prasad, Rodolfo Moreno, and Liya Hu for helpful collaborations and discussions. I thank Steve Harrison and Tobias Herrmann for purified protein.

I am forever grateful to the staff of the Interdepartmental Graduate Program at Vanderbilt University, for inviting me to train at Vanderbilt University and supporting my first year as a graduate student, both financially and practically. I want to thank Michelle Grundy, Jim Patton, and Erika Thompson for their support. I thank my FOCUS leaders Mark deCaestecker, Remy Betous, and Stephanie Fretham for encouraging me to ask questions and providing a welcoming environment to learn how to discuss scientific research in my early training. I also want to thank Chris Aiken and Lorie Franklin for support in the Department of Microbiology and Immunology at Vanderbilt University.

I want to thank all of my friends, both old and new, for providing healthy and happy breaks between science. To my Circle of Brunch friends, Cody Wenthur, Brielle Wenthur, Tim Shaver and Cassie Retzlaff – your friendship has meant the world to me and I hope we're still finding a way to share a meal together fifty years from now. I thank Daniel LePage for many supportive conversations and care packages that helped in tough times. I am so grateful to my german twin, Emily Hay, for showing me how a fulfilled life should be led. I want to thank Natalie O'Neal for always finding a way to get

my shy self on the phone. A life without friends is no life at all, and you guys make every day a better day.

And finally, I want to thank the individuals who took on the challenge of raising a human life and still made the time to encourage my curiosity and passion to explore the unknown. To my stepfather, Steve Webb, for countless hours teaching me how to use every tool from a paintbrush to a table saw. I am forever grateful to Amanda Dunn, who took me in as one of her own and inspired me to learn more about more. And to my mother - my first, and most important teacher. You are the strongest woman I have ever met and a dear friend. I grow to be more like you each day, and for that, I am exceptionally grateful. You always joke, with a smile not far behind, that you brought me into this world and you can take me back out. Well, thank you for keeping me around. It has been an honor to be your daughter and to learn from you.

## TABLE OF CONTENTS

**Page**

## LIST OF FIGURES

**Figure** **Page**

## LIST OF TABLES

**Table** **Page**

## LIST OF ABBREVIATIONS

| | |
|---|---|
| 3D | Three dimension(al) |
| $^{35}S$ | Radioactive isotope of sulfur with 35 nucleons |
| Å | Angstrom(s) |
| a.a. | Amino acids |
| ANOVA | One-way analysis of variance |
| AUG | Adenine – uracil – guanine; translation initiation codon |
| APC | Antigen presenting cell |
| BHK(-T7) | Baby hamster kidney cells (expressing the T7 phage RNA polymerase) |
| BRV | Baboon orthoreovirus |
| CAR | Coxsackievirus and adenovirus receptor |
| CHO | Chinese hamster ovary cells |
| cryo-EM | Cryo-electron-microscopy |
| CNS | Central nervous system |
| DAPI | 4’,6-diamidino-2-phenylindole |
| DC | Dendritic cell(s) |
| DNA | Deoxyribonucleic acid |
| dsRNA | Double-stranded RNA |
| EM | Electron microscopy |
| FDA | United States Food and Drug Administration |
| h | Hour(s) |
| HSV-1 | Herpes simplex virus 1 |
| hpi | Hours post-infection |
| IgG | Immunoglobulin G |
| ISVP | Infectious subvirion particle |
| JAM-A | Junctional adhesion molecule-A |
| kDa | Kilodalton |
| M | Molar |
| MEF | Murine embryonic fibroblast cells |
| MEL | Murine erythroleukemia T3cl.2 cells |

| | |
|---|---|
| min | Minute(s) |
| mRNA | messenger RNA |
| NgR1 | Nogo receptor 1 (Reticulon 4 receptor) |
| PAGE | Polyacrylamide gel electrophoresis |
| PBS | Phosphate-buffered saline |
| PFU | Plaque forming unit |
| ORF(s) | Open reading frame(s) |
| RRL(s) | Rabbit reticulocyte lysates |
| Reovirus | Mammalian orthoreovirus |
| RNA | Ribonucleic acid |
| rpm | Revolutions per minute |
| RT | Room temperature |
| SDS | Sodium dodecyl sulfate |
| siRNA | Short-interfering RNA |
| ssRNA | Single-stranded RNA |
| T1 | Serotype 1 reovirus |
| T1+/- | Type 1 Lang (+, WT; -, S370P/Q271E) |
| T1- | Type 1 Lang with S370P and Q371E mutations |
| T1L | Type 1 Lang |
| T2 | Serotype 2 reovirus |
| T2J | Serotype 2 Jones |
| T3 | Serotype 3 reovirus |
| T3D | Type 3 Dearing |
| T3+/- | T3SA+ or T3SA- reovirus |
| $TCID_{50}$ | 50% Tissue-culture infectious dose |
| UTR(s) | Untranslated region(s) |

# CHAPTER I

# INTRODUCTION

## Thesis Overview

Viral invasion of the central nervous system (CNS) is a significant cause of morbidity and mortlity worldwide, particularly in young children (1). The nervous system presents a challenging site for viruses to access, with multiple physical and immunological barriers that limit pathogen invasion. To invade the CNS, viruses must access cell-surface receptors for binding and entry events. Virus-receptor interactions also govern tropism and often control disease type and severity. For many viruses, the identities of receptors and other cellular determinants of viral tropism remain elusive. Understanding where and how viral capsid components engage neural receptors and the effect of these interactions on tropism and disease may illuminate targets to prevent viral neuroinvasion.

Mammalian orthoreoviruses (reoviruses) provide a highly tractable and well-established system to identify mechanisms of viral entry into the CNS. Reoviruses are nonenveloped particles containing a 10-segmented, double-stranded (ds) RNA genome that replicate well in culture and can be altered via a robust reverse-genetics system (2, 3). While reovirus causes similar age-restricted disease in many young mammals (4-6), most studies employ newborn mice. Following peroral or intracranial inoculation of newborn mice, reovirus displays serotype-specific patterns of tropism in the brain and concomitant disease (**Fig. I-1**). Serotype 1 (T1) strains infect ependymal cells lining the ventricles of the brain and cause a non-lethal hydrocephalus (7). In contrast, serotype 3 (T3) strains infect specific neuron populations in the CNS and produce a fulminant, and often lethal, encephalitis (8). These differences in tropism and disease have been genetically mapped to the reovirus S1 gene using single-gene reassortant viruses (9). However, viral and host gene sequences that mediate either T1 or T3 tropism have not been defined.

In Chapter I of my dissertation, I introduce key themes about mechanisms of neuroinvasion and the disease consequences of CNS infection. I describe fundamental knowledge and open areas of research pertaining to reovirus infection in the CNS and

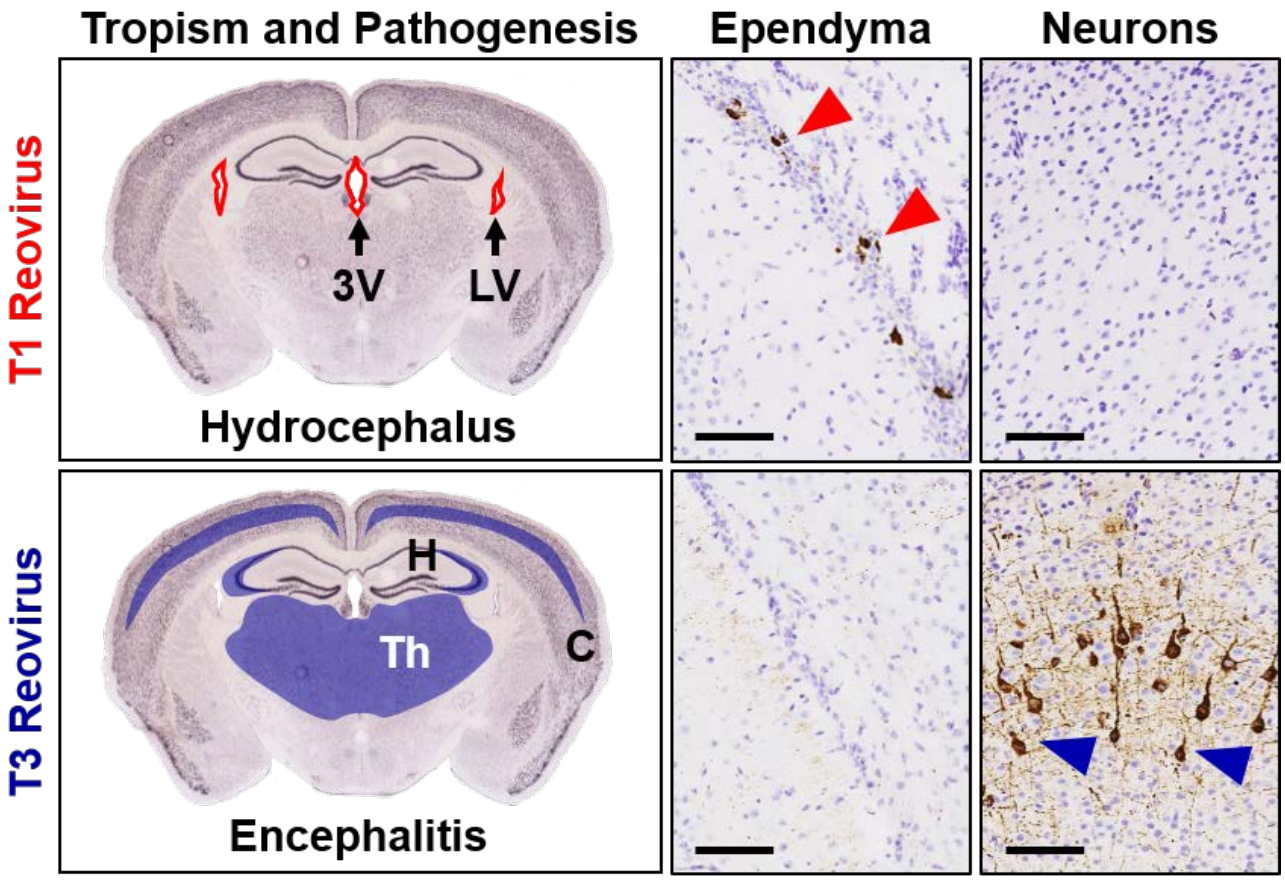


**Figure I-1: Reovirus exhibits serotype-dependent tropism and pathogenesis in the CNS.** Serotype 1 (T1) and serotype (T3) reoviruses target different cell types in the CNS. Commonly infected regions in the mouse brain are depicted by colored overlay on a coronal brain section of a mouse (left panels) (Allen Brain Atlas). Representative micrographs of the lateral ventricle (middle panels) or cortex (right panels), with immunohistochemical detection of reovirus antigen (brown) and nuclei (blue). T1 reovirus strains (red, top panels) infect ependymal cells (red arrowheads) and cause non-lethal hydrocephalus, whereas T3 reovirus strains (blue) infect neurons (blue arrowheads) and cause lethal encephalitis. 3V, Third ventricle; LV, Lateral ventricle; C, Cortex; H, Hippocampus; Th, Thalamus.

expand on reovirus-receptor interactions. I conclude Chapter I with a summary of viral oncolytic therapies and highlight strengths and opportunities for improvement of reovirus oncolytics. In Chapter II, I describe the design and implementation of σ1-chimeric reoviruses to identify sequences in the S1 gene that dictate neurotropism and virulence in the CNS. In these studies, I found that homologous sequences at the virion-distal end of the viral attachment protein are responsible for neuron and ependymal cell targeting. In Chapter III, I identify sequences of the NgR1 reovirus receptor that are required for binding and post-binding functions and elucidate the viral ligand for NgR1, which is the σ3 outer-capsid protein, using a combination of genetic, biochemical, and structural approaches. Finally, in Chapter IV, I review conclusions from results presented in Chapters II and III, examine new questions raised by these studies, and discuss future directions of this work. Collectively, my dissertation research has unveiled viral and host sequences that contribute to neural cell targeting and will improve strategies and knowledge to design targeted oncolytic therapies.

## Multifunctional Virus Proteins

Viruses rely on host cells for every step in the replication cycle. This dependency, combined with their small size and evolutionary pressure to replicate efficiently, promotes a requirement for multifunctional virus proteins. Multifunctional virus proteins are described as virus-encoded proteins that have several roles in the viral life cycle and may segregate these different functions to distinct viral domains or oligomerization states (10). In particular, viral capsid components are often multifunctional (10, 11). Capsid proteins have several essential functions, including self-assembly, genome encapsidation, and interaction with host receptors. They mediate diverse steps throughout the viral replication cycle, including cell adhesion, entry, replication, particle egress, and immune evasion. Capsid proteins must be sufficiently stable to withstand the environment but also susceptible to cell-cued conformational changes to permit entry. Moreover, specific capsid components, called viral attachment proteins, engage cellular receptors and dictate important functions in tropism and pathogenesis. Understanding how multiple functions are mediated by a single protein is the subject of

ongoing research and requires a coordinated and multidisciplinary approach combining structural, biochemical, and animal model systems.

## Viral Infections of the Central Nervous System

Neuroinvasion by any pathogen in the central nervous system is a dangerous and often life-threatening condition. Children are significantly more at risk for CNS infections (1), and even short, self-limited infections can cause lasting neurological impairment. In the United States, viruses account for more infections of the CNS than do bacteria, protozoa, and fungi combined (12, 13). Despite these facts, mechanisms of viral neuroinvasion and pathogenesis are not well understood. Furthermore, viral infections of the CNS are underreported and treatment is often limited to supportive care. Not only are better prophylactics, diagnostic tests, and therapies needed to improve outcomes of viral CNS infections, but it is necessary to develop a mechanistic understanding of how viruses first invade the CNS and then produce disease at these specialized sites.

### Viral routes into the central nervous system

To enter the CNS, viruses must bypass several complex mechanical and immunological barriers and use specific host factors, such as cell receptors, to establish and propagate infection. In general, viruses enter the CNS by one of two routes – hematogenously (via the blood) or neurally (via infection of peripheral or olfactory nerves). Some viruses demonstrate a preference, while others are capable of using both routes. Once in the blood, viruses must cross one of two additional barriers to access the brain parenchyma (**Fig. I-2**). The blood-brain barrier (BBB) and the blood-cerebrospinal fluid (CSF) barrier (BCSFB) serve to regulate molecular exchange between the brain and the outside environment and contribute to the immune specialization of the brain.

The BBB is formed at the interface of brain microvascular endothelial cells with specialized tight junctions and basement membranes and is supported by critical contacts with glial pericytes and astrocytes. For perspective, the microvasculature accounts for only 3% of the brain's volume, but it occupies a massive 15-25 $m^2$ of

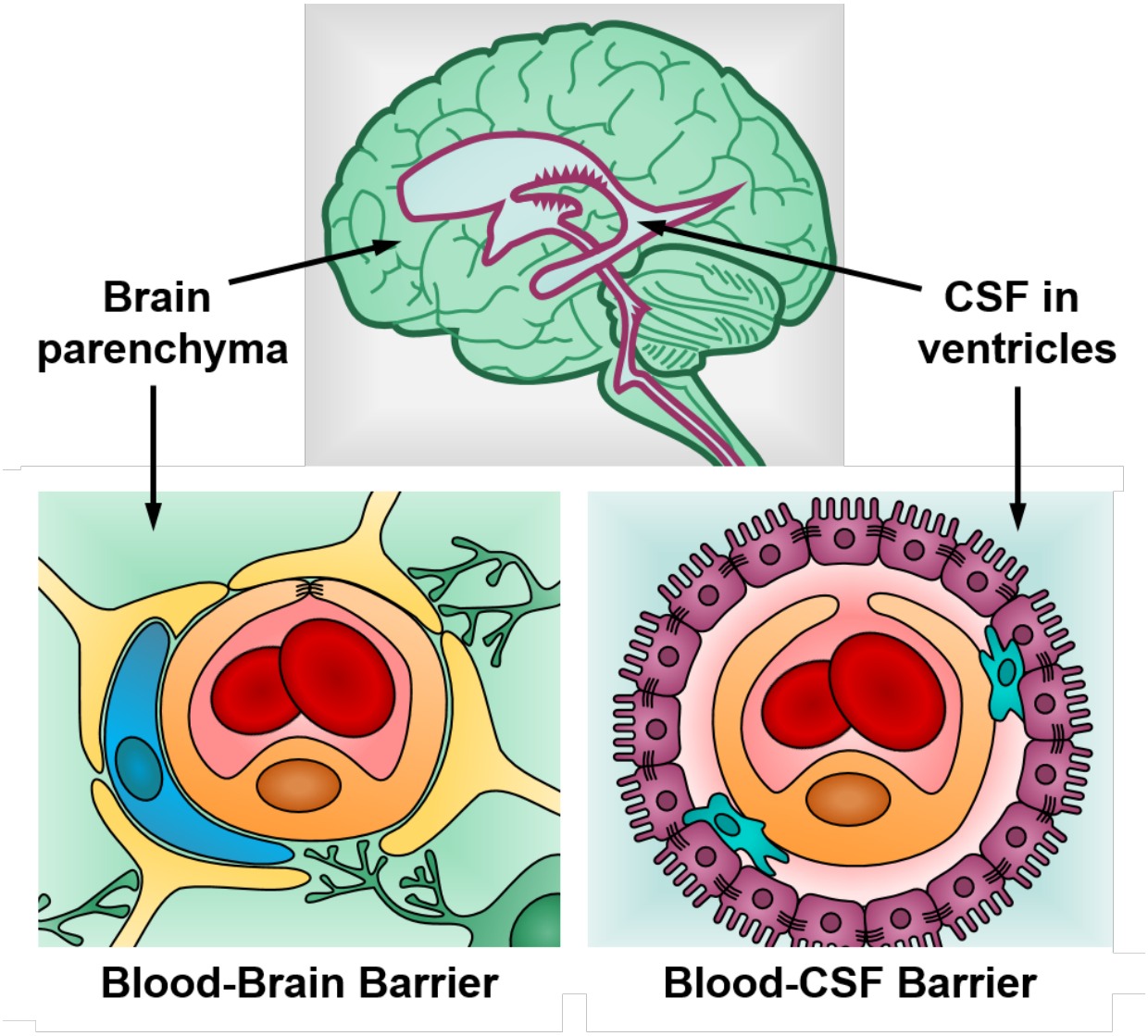


**Figure I-2: Initial Barriers to Infection in the Brain.** For T1 and T3 reovirus to exit the bloodstream and access ependymal cells and neurons, virus must first bypass several barriers. The blood-CSF barrier is present in specialized structures of the ventricle called the choroid plexus, which are depicted as thickenings of the ependymal cell layer (purple) in the top panel. Green, neurons and brain parenchyma; purple, ependymal cell; orange, brain microvascular endothelial cell; yellow, astrocyte foot; red, erythrocyte; blue, pericyte; teal, leukocyte; hatched black lines, tight junctions.

surface area in the average adult brain (14). This surface area is required for expedient glucose and oxygen exchange to energy-demanding neurons, but also serves as an entry point for viruses. The BCSFB is located in the choroid plexus adjacent to specialized ependymal cells that secrete CSF into the ventricles (**Fig. I-2**). The BCSFB displays significantly different barrier function, when compared to the BBB. At the BCSFB, fenestrations replace tight junctions between microvascular endothelial cells and blood bathes the stroma underlying ependymal cells (15). The BCSFB is thought to be a primary site of immune surveillance by patrolling leukocytes (16) and is hypothesized to be an entry point into the brain for many neurotropic viruses (17).

To overcome these mechanical and immunological barriers, viruses can use transcellular, paracellular, or “Trojan horse” mechanisms. A transcellular mechanism involves bypass of tight junctions by directly infecting brain microvascular endothelial cells and release to the basolateral surface. Some viruses, such as HIV-1 (18), are thought to migrate directly between tight junctions in a paracellular transport mechanism. HIV-1 (19) and other viruses can use a “Trojan horse” mechanism to enter the CNS by transiting barriers within extravasating phagocytic cells. Bloodborne cytokines, free radicals, and matrix metalloproteinases can mediate an indirect barrier disruption and enhance virus entry into otherwise immune-protected CNS sites (20, 21). Collectively, viruses are not limited to one route or mechanism of entry into the CNS and often use several entry points.

<u>Inflammation and damage in the CNS</u>

Inflammation caused by infections in the CNS can affect the meninges (meningitis), brain parenchyma (encephalitis), or both (meningoencephalitis). The most common symptoms of CNS inflammation in patients include fever, headache, irritability, depression, photophobia, and loss of appetite. Meningitis is often suspected when patients feel neck stiffness. Encephalitis is suspected if a patient additionally presents with cognitive impairment, such as confusion, altered mobility, or lethargy. Severe complications of CNS infection can include seizures, paralysis, coma, and death. There are also several neurologic disorders that can occur after a virus has been cleared. For example, acute disseminated encephalomyelitis (ADEM) is an autoimmune disorder

usually initiated by viral infection and marked by rapid-onset inflammation and demyelination of neurons in the brain and spinal cord (22).

Several viruses can cause meningitis and encephalitis. The large majority of viral meningitis cases identified in the USA (~90%) are caused by enteroviruses (12), which also account for 10 to 20 percent of identifiable cases of viral encephalitis (23). Other commonly identified agents include herpes simplex virus 1 (HSV-1), varicella-zoster virus, Epstein-Barr virus, and influenza virus. Several less commonly identified viral agents of meningitis and encephalitis are limited by effective vaccination campaigns (e.g., measles virus, mumps virus, and rubella virus) or geographic distribution of their respective vector. For example, Colorado tick fever virus is transmitted by *Dermacentor andersoni* ticks that reside at 4,000 to 10,000 feet in poorly populated mountainous areas of the USA (24). Similarly, cases of La Crosse fever virus are generally restricted to wooded areas in the Midwest where the principal vector, the *Aedes triseriatus* mosquito, resides (25). It should be noted that the etiologic agents of aseptic meningitis and encephalitis often go unidentified, precluding a comprehensive understanding of pathogen contributions.

A diagnosis of viral encephalitis is based on patient history and physical exam findings, as described above. Additionally, magnetic resonance imaging (MRI), lumbar puncture, and/or electroencephalogram (EEG) can provide additional evidence of CNS involvement. At a macroscopic view, edema and focal lesions in the brain parenchyma are common and can be detected by MRI. The CSF is a relatively acellular, clear, non-viscous liquid in healthy individuals, but inflammation caused by meningitis and encephalitis induces pleocytosis, or recruitment of inflammatory cells. Lumbar punctures are performed both to exclude biotic infections (e.g., bacteria, protozoa, and fungi) and examine the CSF for cellular infiltrates, total protein levels, and metabolite presence. While EEG's are less specific to viral infections, analysis of electrical patterns in the brain can be informative. For example, severe cases of West Nile virus often present with abnormal EEG findings and demonstrate generalized electrical slowing across multiple brain regions (26).

Viral infections of the CNS elicit a variety of inflammatory and cell-death pathways. Post-mortem analyses of lethal cases of viral encephalitis reveal viral antigen

in brain parenchymal cells (e.g., neurons, microglia, astrocytes, etc.) and inflammatory infiltration (e.g., CD4+ and CD8+ leukocytes, CD68+ macrophages/microglia, neutrophils, etc.) of the parenchyma. Inflammatory infiltration can be diffuse or exhibit concentrated foci such as perivascular cuffing and microglial nodules. Cell death is often evident and may be at sites overlapping with viral infection (27) or as an indirect result of inflammatory cytokines or other byproducts (28). Apoptosis, often detected via cleaved caspase-3 expression, is induced by diverse families of viruses, including alphaviruses (29), enteroviruses (30), and flaviviruses (31). Sites of damage, inflammation, and viral replication are often overlapping and dictated by viral tropism. Therefore, it is essential to understand mechanisms of neuroinvasion and tropism to fully appreciate viral pathogenesis.

## Mammalian Orthoreoviruses (Reoviruses)

Reovirus background

Reoviruses belong to the family *Reoviridae*. *Reoviridae* members are nonenveloped and encapsidate 9 to 12 linear dsRNAs within 1 to 3 protein shells with icosahedral symmetry. Many *Reoviridae* members are pathogenic. For example, rotavirus is a leading cause of gastroenteritis worldwide in young children, causing over 215,000 estimated deaths in 2013 (32). Baboon reovirus initiates a fulminant meningoencephalitis in primates (33). Colorado tick fever virus causes neurologic disease in humans, although these infections are rare. Mechanisms of disease induction, particularly for neurotropic reoviruses, have not been fully elucidated.

Reovirus displays a broad species tropism, causing age-restricted disease in many mammalian species, including mice, ferrets, rabbits, and pigs. While reovirus clinical manifestations in humans are only rarely thought to be severe (34-38), strains isolated from human stools during a gastroenteritis outbreak cause lethal disease in several immunocompetent animal model systems (39). Reovirus infection in animal models can initiate biliary inflammation, pneumonia, hydrocephalus, myocarditis, meningitis, and encephalitis (40). Additionally, reovirus induces loss of oral tolerance in mice to food antigens such as gluten, making it a potential trigger for human disorders like celiac disease (41). Finally, reovirus exhibits preferential cytotoxicity in cancer cells

and is being assessed in clinical trials as an oncolytic agent (42). Therefore, understanding mechanisms of reovirus pathogenesis and specific molecular interactions that dictate reovirus tropism could inform a diverse number of fields.

Reovirus gene organization, virion structure, and reverse genetics

Reovirus particles are nonenveloped with two concentric capsid layers, the inner core and the outer capsid, that encase ten segments of dsRNA (**Fig. I-1** and **I-3**). Large (L), medium (M), and small (S) gene segments lack poly-A tails, contain 5' caps, and encode short, conserved untranslated regions (UTRs) at the 5' and 3' termini (**Fig. I-4**) (43, 44). Combined with flanking protein-coding sequences, UTRs are predicted to engage in end-to-end complementary stem-loop RNA interactions that resemble a "panhandle" and likely promote genome replication and packaging (45). With the exception of the S1 gene, which is bicistronic, reovirus genes are monocistronic and encode a single protein product. Eight structural (λ1, λ2, λ3, μ1, μ2, σ1, σ2, and σ3) and three non-structural viral proteins (σ1s, σNS, and μNS) are produced (**Fig. I-4B**). The outer capsid is primarily composed of repeating heterohexamers of σ3 and μ1 (**Fig. I-3B** and **I-3C**). Three monomers of μ1 interweave to form a pedestal on which three σ3 molecules rest. At the 12 icosahedral vertices, $\sigma3_3\mu1_3$ hexamers are interrupted by pentameric arrangements of λ2. It is at these five-fold axes of symmetry that the trimeric viral attachment protein, σ1, embeds into the virion in a small pore formed by abutting λ2 monomers.

A robust reverse genetics platform allows recovery of altered reovirus strains to assess dsRNA and protein function in discreet stages of the viral replication cycle (3, 46, 47). Briefly, 4 to 10 plasmids containing complementary DNA (cDNA) to all 10 reovirus genes are transfected into a baby hamster kidney (BHK) cell line constitutively expressing the T7 RNA polymerase (BHK-T7). The T7 RNA polymerase combined with a 3' appended ribozyme stimulate transcription of reovirus mRNAs with authentic 5' and 3' termini. Current and ongoing studies have pushed the limits of what is possible with reovirus reverse genetics (more detail in Chapter II discussion).

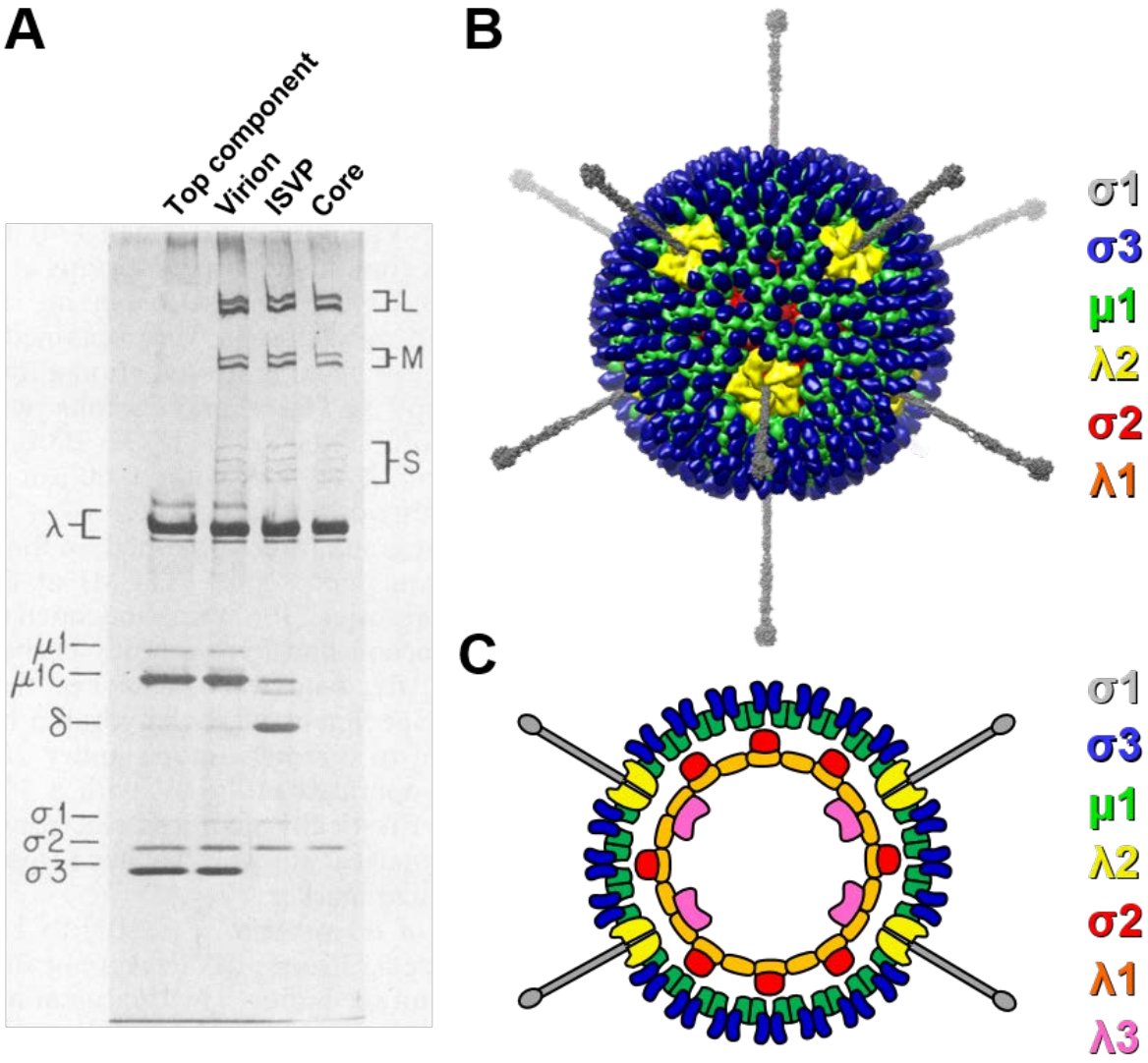


**Figure I-3: Reovirus structure.** (**A**) Resolution of reovirus proteins and dsRNA by SDS-PAGE. Reovirus "top component" consists of virion-like particles that do not encapsidate viral RNA. Virions, ISVPs, and core particles encapsidate 10 segments of dsRNA ($L_{1-3}$, $M_{1-3}$, $S_{1-4}$) but contain different protein compositions. Note the accumulation of the δ-fragment of μ1/μ1C and the loss of σ3 in virion-to-ISVP conversion. Modified from (48). (**B**) The reovirus virion (49) is shown to scale with a model of the extended conformer of σ1 (grey) (50) or shown as a schematic (**C**). Reovirus proteins σ3 (blue), μ1 (green), λ2 (yellow), σ2 (red), λ1 (orange), λ3 (pink) are indicated where appropriate.

**A**

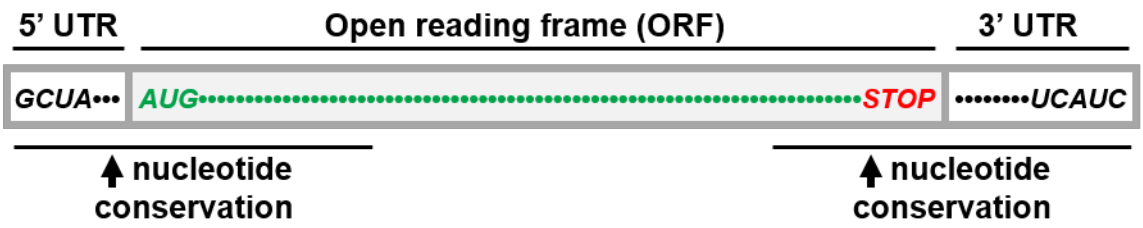


**B**

| | Reovirus gene segment | | | | | | | | | | |
|---|---|---|---|---|---|---|---|---|---|---|---|
| | **S1** | | **S2** | **S3** | **S4** | **M1** | **M2** | **M3** | **L1** | **L2** | **L3** |
| *Protein name* | σ1 | σ1s | σ2 | σNS | σ3 | μ2 | μ1 | μNS | λ3 | λ2 | λ1 |
| *Abundance* | ≥12 | - | 150 | - | 600 | ~24 | 600 | - | 120 | 60 | 12 |
| *Location* | OC | NS | C | NS | OC | C | OC | NS | C | OC/C | C |

**Figure I-4: Reovirus gene structure and organization.** (A) Reovirus genes are dsRNA molecules with short 5' and 3' untranslated regions (UTRs). Shorter 5' UTRs are 12-32 nucleotides and longer 3' UTRs are 35-83 nucleotides in length. The open reading frame for prototype reovirus strains ranges from 1095-3867 nucleotides. Gene termini (< 200 nucleotides), which are predicted to function in packaging or replication signals, are more conserved than internal sequences. Modified from (40). (B) Genes and proteins present in reovirus virions. Nonstructural proteins are not included in virion particles. Modified from (40). OC, outer capsid; NS, nonstructural; C, core.

Reovirus lab strains

Reovirus strains are divided into one of three serotypes based on neutralizing antibody responses and hemagglutination-inhibition activity (51-54). In general, serotype 1 (T1) and serotype 2 (T2) strains are more genetically similar to one another, and serotype 3 (T3) strains are more divergent (55, 56). Most reovirus studies have focused on T1 and T3 prototype strains. Examples of prototype lab strains include T1 Lang (T1L; T1+), T2 Jones (T2J), T3 Dearing (T3D), T3SA+ (T3+), and T3SA- (T3-). The σ1 viral attachment protein is the primary target of the neutralizing antibody response and thus dictates the serotype (54).

Reovirus cell entry and replication

The entry of reovirus into host cells has been elucidated primarily using non-polarized, cultured cells, and little is known about mechanisms used by reovirus to infect polarized ependymal cells and neurons. Following receptor-mediated endocytosis in cultured cells, the majority of virus appears to enter using clathrin-dependent mechanisms (57), but other pathways can be used (58). Following endocytosis of reovirus, outer-capsid proteins σ3 and μ1 undergo acid-dependent proteolytic processing to generate infectious subvirion particles (ISVPs) (59, 60). ISVPs are characterized by loss of major outer-capsid protein σ3, cleavage of μ1 to the δ and φ fragments, and conformational rearrangement of the σ1 protein (**Fig. I-3A**) (59, 61). Further μ1 processing and loss of σ1 enables endosomal membrane penetration and release of the viral core into the cytoplasm (**Fig. I-3A**) (62-64). Fragments of μ1 entering the cytosol trigger apoptotic signaling (65).

Once in the cytosol, transcriptionally active cores synthesize full-length, capped, message-sense RNAs for each gene segment (66, 67). These single-stranded (ss) RNAs are templates for translation and minus-strand synthesis to generate genomic dsRNA (68-70). Newly made proteins and 10 segments of dsRNA coalesce in an enigmatic process to generate progeny particles (71). Following genome replication and new particle assembly, reovirus progeny use both lytic and non-lytic pathways to exit infected cells (72, 73). In the CNS of infected mice, T1 reovirus induces ependymal cell damage and sloughing (4), and T3 reovirus induces apoptosis in neurons (27, 74).

Despite this knowledge, it is not known how reovirus exits cells in the brain and how viral egress contributes to pathogenesis and dissemination within the CNS.

Reovirus S1 gene contributions to CNS tropism and disease

Reovirus transmission occurs primarily through the fecal-oral route. Following oral inoculation of mice, reovirus establishes primary infection in intestinal epithelium and lymphoid tissue (75-77). Reoviruses spread systemically to several sites of secondary replication, including the CNS. Multiple gene products interact with host factors to promote efficient cell entry (78, 79) and neurovirulence (27). However, serotype-dependent differences in CNS spread, tropism, and disease caused by T1 and T3 segregate exclusively with the S1 gene (8, 9, 80), which encodes attachment protein σ1 and non-structural protein σ1s in alternate but overlapping reading frames.

Viruses with a T1 S1 gene spread hematogenously to infect ependymal cells and cause hydrocephalus, whereas viruses with a T3 S1 gene spread by both hematogenous and neural routes to infect neurons, inducing apoptosis and lethal encephalitis (**Fig. I-1**) (27, 74, 80). The nonstructural σ1s protein is dispensable for both T1 (81) and T3 (82) replication in the brain, suggesting that this protein does not mediate serotype-dependent CNS infection. In contrast, the σ1 viral attachment protein is well-suited to mediate tropism differences. Serotype-dependent reovirus binding and infection of multiple non-CNS-derived cultured cells are phenotypes that track with the σ1 protein (83, 84). Moreover, T1 virus preferentially binds ependymal cells (85), and T3 virus preferentially binds neurons (86). Collectively, these data suggest that the σ1 protein mediates these disparate disease manifestations by binding distinct receptors on these cells.

Attachment protein σ1

While T1 and T3 σ1 proteins are structurally similar (87, 88), they share less than 30% amino acid identity (89) and are the most serotype-divergent of reovirus proteins (55). The σ1 protein is a long, filamentous trimer that can extend ~ 40 nm away from the capsid, doubling the virion diameter (**Fig. I-3B** and **I-5A**). Viruses can incorporate between 0 to 12 trimers of σ1, and the number of σ1 trimers incorporated per virion

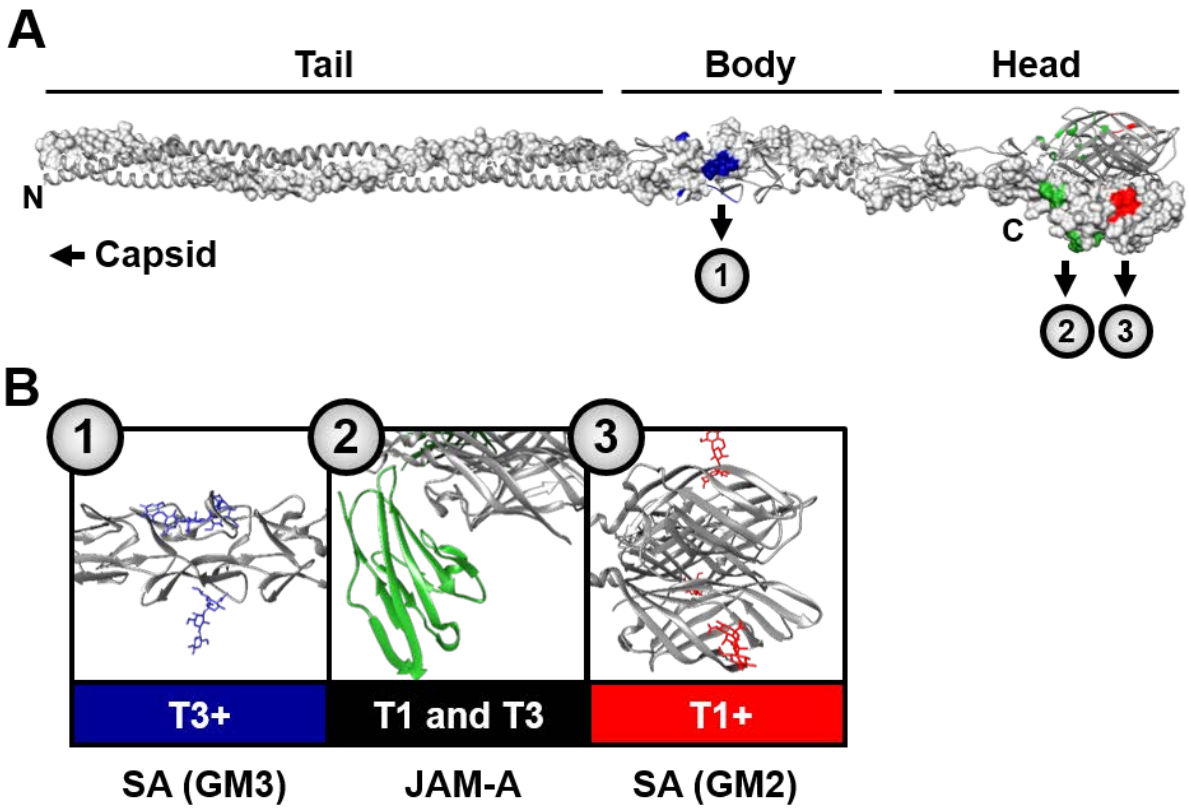


**Figure I-5: Structure of reovirus attachment protein σ1 and its receptors.** (**A**) A model of the reovirus attachment protein, σ1, is shown as a ribbon diagram (grey) with one monomer of the trimer surface-shaded (88). Receptor-binding sites are colored for T1-bound SA (red), T3-bound SA (blue), and JAM-A (green). N and C termini are indicated. The σ1 model was generated by linking two partial, but overlapping structures of σ1 (6GAP and 3S6X) and encompasses residues 27-455 of T3D. The tail domain embeds into the virion capsid. (**B**) Crystal structure insets of σ1 (grey) in complex with receptors. T3D σ1 bound to GM3 glycan (blue) (50) or JAM-A (green) (90); T1L σ1 bound to GM2 glycan (87).

influences infectivity (91). Three σ1 subunits interweave to form multifunctional tail, body, and head domains (**Fig. I-5**). The σ1 trimer structure has an α-helical coiled-coil tail domain that is anchored to the virion (89, 92), followed by a body domain composed of β-spiral repeats interrupted by a short α-helix (50), and terminates in a head domain composed of three β-barrel motifs (50, 87). Despite identification and characterization of three receptors and their cognate receptor-binding domains in reovirus σ1 (**Fig. I-5B**), host determinants of the S1-mediated differences in neurotropism remain elusive.

Similar to fusion proteins of enveloped viruses, the σ1 protein is thought to undergo conformational changes during entry. Virion-associated σ1 is observed extending from the reovirus virion in electron micrographs of negatively stained reovirus particles (48). However, subsequent to particle averaging, only a short λ2-embedded fragment of σ1 is detected. These data support the hypothesis that a flexible conformer of σ1 is displayed on virions. In contrast, EM reconstructions of ISVPs demonstrate additional density at intermediate distances extending from the λ2 vertices, suggesting an altered and perhaps extended conformer of σ1 is present on ISVPs (61). Furthermore, some σ1-specific antibodies differentially recognize virion- and ISVP-associated σ1 (93, 94), indicating structural rearrangement of the epitope. The function of σ1 conformational changes in reovirus infection are not known. However, these changes may modify receptor-binding capacity (95, 96).

Reovirus receptors and their function in viral tropism and pathogenesis

Although multiple receptors have been identified for reovirus, cellular receptors engaged in the CNS by T1 or T3 reovirus have not been defined. Moderately conserved pockets at the base of both the T1 and T3 σ1 head domain engage junctional adhesion molecule A (JAM-A) (90, 97) to mediate hematogenous dissemination in mice (77). JAM-A expression is dispensable for reovirus replication in the brain following intracranial inoculation (77). Another reovirus receptor, Nogo receptor 1 (NgR1), is predominantly expressed in CNS neurons with a distribution that overlaps with sites of T3 neurotropism and, thus, it represents an attractive candidate for a T3-specific receptor (98). However, both T1 and T3 strains can use NgR1 to infect non-neuronal

cell types (98), suggesting it is not the sole cellular determinant of reovirus neuronal tropism.

The only reovirus receptors known to be engaged in a serotype-specific manner are sialylated glycans. Glycans are not thought to directly mediate reovirus entry. Instead, glycans facilitate adhesion strengthening to cells, whereby reovirus transiently binds sialic acid (SA) with low affinity until a higher-affinity receptor like JAM-A is encountered (99). When compared with glycan-binding strains, T1 and T3 reoviruses engineered with mutations that specifically abrogate SA-binding capacity infect similar sites in the brain and produce similar yields (100, 101), leaving the viral and cellular determinants of reovirus neurotropism unclear. In the following section, I expand on reovirus receptor use, discussing structure-function relationships of the virus with known receptors and highlight their respective roles in tropism and pathogenesis.

*Sialylated glycans*

Many viruses use cell-surface carbohydrates as attachment factors to enhance infectivity. While carbohydrates terminating in SA are commonly bound, neutral-charge glycans and glycosaminoglycans promote adhesion strengthening for different viruses (102-104). SAs are a heterogeneous family of more than fifty monosaccharides that share a 9-carbon core (105). The complexity of the SA family stems not just from varied glycosidic linkages and chemical modifications, but also from the glycans and structures to which they are linked. As the most common terminal glycan on oligosaccharides anchored to proteins or lipids, SAs are expressed by all vertebrate cell types and mediate many important physiological processes such as cell-cell adhesion, protein stability, and macromolecular transport (105). The broad distribution and abundance of SA is likely why many different viruses, including reoviruses, have converged to interact with SA as a receptor. Most reovirus field-isolate strains engage SA as an attachment factor at the cell surface to mediate adhesion strengthening. The low-affinity interaction of reovirus with SA allows rapid on/off kinetics (99) and affords an opportunity for reovirus to sample nearby SAs and other cell-surface moieties to eventually engage in higher-affinity contacts with a receptor capable of mediating cell entry. Engagement of SA alone is not thought to yield a productive infection for reovirus. However, virus

binding to SA could fortuitously allow its uptake by an internalization event already underway.

Despite similarities in sequence and structure, T1 and T3 σ1 use different domains to engage distinct sialylated glycans (**Fig. I-5** and **I-6A**). For both serotypes, each σ1 subunit has an independent SA-binding site (50, 87). T1 reoviruses specifically bind the terminal α2,3-linked *N*-acetyl-SA on GM2 glycan (displayed on glycoproteins or GM2 ganglioside) in a shallow groove located on the σ1 head domain (87, 101). In contrast, T3 strains demonstrate more promiscuous glycan engagement and bind terminal α2,3-, α2,6-, or α2,8-linked SA using a deeper, larger groove located on the σ1 body domain (50). Point mutations engineered in these binding grooves specifically abrogate glycan engagement and convert SA-binding strains (denoted by "+") to non-SA-binding strains (denoted by "-"). For example, two point mutations in the SA-binding groove of T1L convert a T1+ virus to a T1- virus (101). Multiple single amino acid polymorphisms in T3 σ1 generate T3- viruses in different genetic backgrounds (9, 50, 106). These non-SA binding strains are colloquially referred to as "glycan-blind" and have been instrumental in defining the contribution of SA engagement to reovirus infection of specific cell types.

SA binding is required for efficient reovirus binding and infection of many cell types *in vitro*. Most commonly, cellular glycan requirements for binding and infection are defined genetically using glycan-blind viruses and cell lines deficient in glycan expression or chemically using neuraminidase to remove terminal SAs and lectins to block virus access to SA. Reovirus demonstrates little to no SA requirement for infection of some cell types, such as L929 fibroblasts. Diminishing reovirus access to SA on these cells using any of these methods has a negligible effect on binding or infectivity, and different serotypes replicate comparably (50, 87, 107). However, infection of other cell types, such as primary murine embryonic fibroblasts (MEFs), is efficient only with T1 or T3 strains that exhibit intact glycan binding capacity (87, 107). SA engagement also can permit reovirus infection in a serotype-specific manner. For example, murine erythroleukemia T3cl.2 (MEL) cells are susceptible only to T3 glycan-binding strains (50). These cell-type specific differences in glycan requirement for infection are likely attributable to the relative abundance of other reovirus receptors present (87).

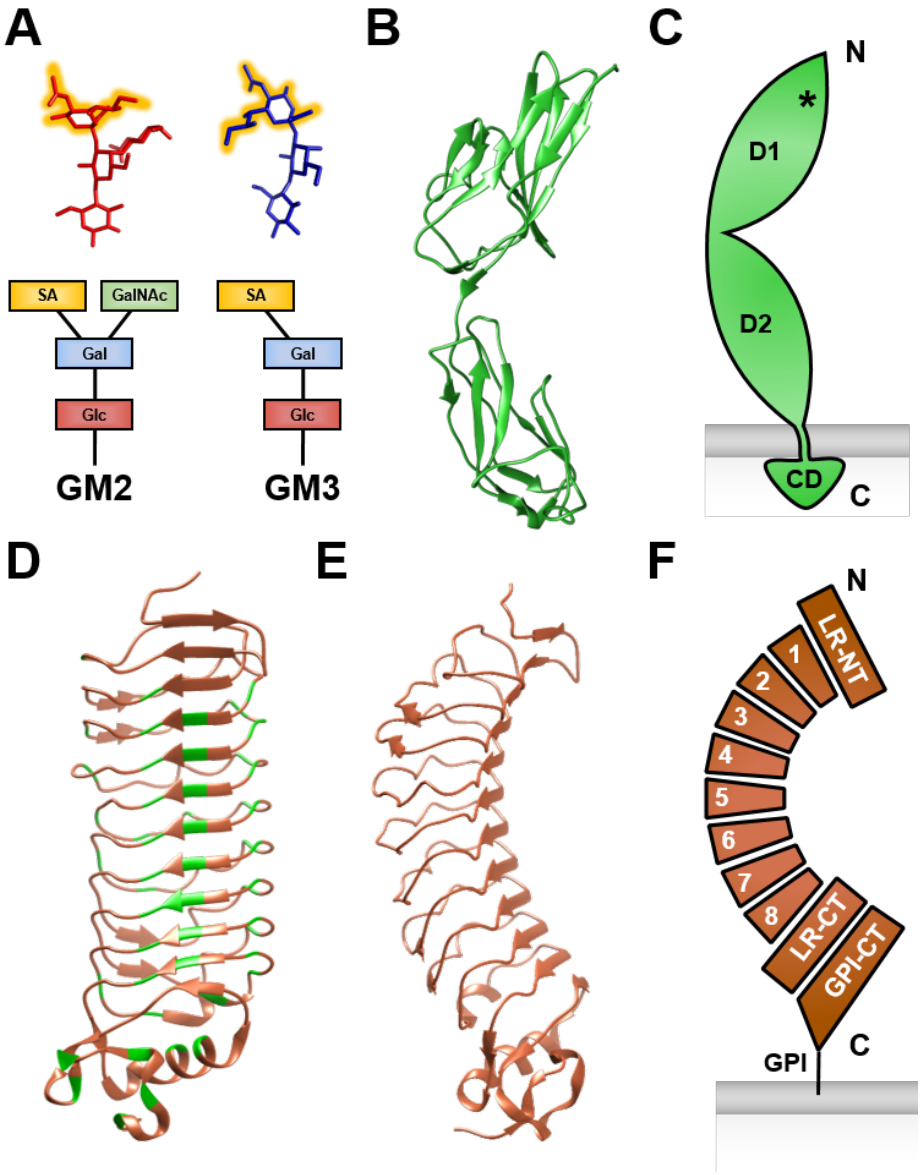


**Figure I-6: Known reovirus receptors.** (**A**) Sialylated glycan portions of GM2 (T1-bound, red) and GM3 (T3-bound, blue) are shown in stick representation with the terminal SA glycan outlined in yellow or as schematics demonstrating glycan composition (SA, *N*-5-acetyl neuraminic acid; GalNAc, *N*-acetylgalactosamine; Gal, galactose; Glc, glucose). These glycan chains can be attached to lipids or proteins. JAM-A is shown as a ribbon tracing (a.a. 27-233) (108) (**B**) or as a schematic with the D1, D2, and cytoplasmic domains (CD) annotated (a.a. 28-299) (**C**). The approximate reovirus binding interface is indicated in (**C**) with an asterisk. NgR1 a.a. 27-311 are shown as a ribbon tracing from a front view with leucine residues highlighted in green (**D**) or a side view (**E**). (**F**) Schematic of NgR1 (a.a. 27-447). NgR1 is formed by eight canonical LRR domains, capped by non-canonical NT and CT domains (LR-NT and LR-CT, respectively). The most C-terminal domain (GPI-CT) is anchored to glycophosphatidylinositol (GPI). N and C termini are indicated. The plasma membrane is depicted as a grey bar.

Interestingly, most cell lines that demonstrate glycan-dependent reovirus infection are more efficiently bound and infected by T3 strains, and, to my knowledge, no cell line has been identified that is exclusively susceptible to infection by T1 strains, likely demonstrating a significant consequence of the more promiscuous SA-binding capacity of T3 reovirus.

The function of SA engagement in reovirus-mediated cell signaling is unclear. Compared to T3-, T3+ virus induces more robust apoptosis in L929 fibroblasts, despite the two strains replicating comparably (107). Pre-incubation of T3+ virus with sialylated glycans or pre-treatment of cells with neuraminidase abrogates apoptosis induction to the level of T3-, under the conditions tested (107). It is not clear whether SA binding activates proapoptotic signaling pathways or alters other steps in viral infection like membrane lipid clustering, internalization, or virus disassembly, as has been observed for other viruses. For example, multivalent engagement of SA by influenza virus leads to clustering of lipid rafts (109). Such ligand-induced clustering activates the epidermal growth factor receptor (EGFR) and leads to influenza virus internalization (109, 110). While σ1 is capable of ligating multiple SA glycans simultaneously (50, 87), it is unclear whether multiple SA moieties are ligated by reovirus on the cell surface or whether SA ligation can mediate signaling processes in the absence of other receptors.

SA engagement contributes to reovirus pathogenesis and disease outcome (106). T1 and T3 glycan-blind viruses induce less severe disease in the CNS, compared with their cognate glycan-binding viruses. Following intracranial inoculation, T1- induces significantly less severe hydrocephalus than T1+, but it reaches similar peak titers in the brain (101). Interestingly, ependymal infection is more localized to the inoculation site for T1-, suggesting that the virus may not efficiently disseminate through the ventricles (101). Reduced infectivity of T1- compared to T1+ also is observed in a human ependymoma cell line (101). A similar trend is true for T3 viruses. Following peroral inoculation, both T3+ and T3- viruses establish efficient replication in the intestine, but T3+ is detected sooner in peripheral sites like the spleen, liver, and brain, suggesting an advantage in dissemination efficiency (106). However, T3- reaches peak titers comparable to those of T3+ at later time points (106). In the CNS, T3+ often replicates to higher titers, induces more apoptosis, and is more neurovirulent than T3- (100, 106).

Cultured primary murine cortical neurons also are more susceptible to T3+ than T3- infection (100). However, while T3+ is more neurovirulent, both T3+ and T3- exhibit comparable CNS tropism. (100). Therefore, although diminished SA-binding capacity alters the virulence of T1 and T3 reovirus, the tropism remains unaltered, supporting a model whereby SA functions as an attachment factor and not as a tropism determinant in reovirus CNS infection.

*Junctional adhesion molecule A (JAM-A)*

In an effort to identify a neural receptor for reovirus, a cDNA library from a neuroblastoma cell line was transfected into non-susceptible COS-7 cells and screened for reovirus binding using T3- as the affinity ligand. Using this strategy, junctional adhesion molecule A (JAM-A) was identified as a receptor for reovirus (111).

JAM-A is an immunoglobulin superfamily protein expressed by hematopoietic, endothelial, and epithelial cells, as well as some types of glial cells (112-115). It serves critical functions in the maintenance of tight junction integrity and immune cell migration across epithelial and endothelial barriers (116, 117). Many tight junction proteins and immunoglobulin superfamily proteins serve as receptors for a variety of viruses (118, 119), suggesting their shared localization provides some type of selective advantage for viruses. As viruses must cross barriers formed by epithelial and endothelial cells to gain access to sites of secondary replication and spread systemically, use of tight junction proteins may be advantageous in establishment of viremia and spread within the host.

JAM-A has two immunoglobulin-like extracellular domains, a single transmembrane domain, and a short cytoplasmic tail that functions in intracellular signaling (**Fig. I-6B** and **C**) (120). The membrane-distal immunoglobulin domain engages in homotypic and heterotypic interactions at the cell surface (120). Reovirus binds to JAM-A at this homodimerization surface via conserved residues within the head domain of σ1 (**Fig. 1-5B**) (90, 97). This interaction is serotype-independent; all prototype and field-isolate strains of the three reovirus serotypes tested to date use JAM-A as a receptor (97, 121). σ1 binds to JAM-A with a thousand-fold higher affinity than JAM-A for itself, which likely disrupts the homodimeric JAM-A interaction (90). Dimer disruption is a common mechanism to trigger cell adhesion molecule

internalization and intracellular signaling (122). Disruption of JAM-A dimers by σ1 could function similarly to induce signaling and recruit additional interaction partners to internalize reovirus.

JAM-A plays an essential role in hematogenous dissemination of both T1 and T3 reovirus from the intestine. Interestingly, primary replication of the virus in intestinal epithelium and other resident intestinal cells does not require JAM-A (77). Studies of reovirus infection using mice with tissue-specific expression of JAM-A revealed that hematopoietic expression of JAM-A is dispensable for the establishment of viremia (123). Additionally, disruption of endothelial cell tight junction integrity *in vitro* (73) or vasculature permeability *in vivo* (123) was not observed following reovirus infection. However, endothelial expression of JAM-A is required for both reovirus entry and egress from the bloodstream, suggesting that JAM-A-dependent uptake, amplification, and apical release of reovirus by polarized endothelial cells promotes viremia and systemic spread of reovirus (73, 123).

Although JAM-A is required for hematogenous spread of reovirus, it is dispensable for neural dissemination. Intracranial or intramuscular inoculation of virus provides direct access to neural routes to study the influence of receptors on neural spread of reovirus. Following intramuscular inoculation of wild-type (WT) mice, T3 reovirus infects sensory and motor neurons to travel the length of the spinal cord and reach the brain (124). Following intramuscular inoculation of mice with genetic ablation of JAM-A (JAM-A$^{-/-}$), T3 virus titers increase in the spinal cord, suggesting that neural pathways of infection are intact (77). Furthermore, following intracranial inoculation, T3 virus tropism, replication, and virulence in the CNS are comparable in WT and JAM-A$^{-/-}$ mice. Infection of cortical neurons cultured from JAM-A$^{-/-}$ mice also demonstrates that JAM-A is dispensable for neuronal infection. Collectively, these data suggest that JAM-A does not mediate serotype-dependent neural spread or infection in the CNS.

*Nogo-66 receptor 1 (NgR1)*

Nogo-66 receptor 1 (NgR1) was first discovered as a mediator of reovirus infectivity in an RNA interference screen to identify host genes required for reovirus-induced cytotoxicity (98). NgR1 is expressed on the cell surface of neurons in a pattern

overlapping with sites of T3 virus tropism in specific neural populations in the cortex, hippocampus, thalamus, and cerebellum (**Fig. 1**) (77, 125). With the postnatal onset of myelination, NgR1 ligands are expressed on myelinating oligodendrocytes that encase neural axons. NgR1 engages these ligands (e.g., nogo-A, myelin-associated glycoprotein (MAG), and oligodendrocyte-myelin glycoprotein(OMgp)), recruits a signaling complex, and suppresses axonal outgrowth in the adult brain (126). The timing of NgR1 occupation by oligodendrocyte ligands coincides with the onset of age restriction for reovirus infection (127, 128). Thus, it is possible that myelination may mechanically block reovirus access to neural receptors.

NgR1 has a curled shape (**Fig. I-6D-F**) (129) characteristic of all leucine-rich repeat (LRR) superfamily proteins, many of which are involved in host detection of pathogens. For example, Toll-like receptors (130), NOD-like receptors (131), and the adaptive immune mediators in jawless vertebrates, variable lymphocyte receptors (132), all have the same LRR solenoid structure. NgR1 is composed of eight canonical LRR motifs capped on either end by non-canonical LRR motifs and a C-terminal domain linked to glycosylphosphatidylinositol (GPI) that anchors the protein to the cell membrane (**Fig. I-6F**). Like many LRR protein-ligand partners (130, 132), ligands in the CNS appear to bind the highly conserved, concave face of NgR1 (133).

Ectopic expression of NgR1 allows infection of normally non-susceptible Chinese hamster ovary (CHO) cells (98). This infection is mediated by direct interaction of reovirus with NgR1, as demonstrated by diminished infectivity following receptor blockade via either pre-incubation of cells with NgR1-specific antibodies or pre-incubation of virus with soluble NgR1 (98). Importantly, these competition assays significantly diminish reovirus infectivity in primary cultures of cortical neurons, suggesting that NgR1 serves as a neural receptor for reovirus. Reovirus virions but not ISVPs directly bind and use NgR1 as a receptor, suggesting that either σ3, which is lost during ISVP formation, or a virion conformer of σ1 interacts with NgR1 (98). Viral and receptor sequences required for binding and infection via NgR1 are not known. Moreover, it is not known whether reovirus competes with NgR1 ligands for binding surfaces.

Mechanisms of internalization, endocytic trafficking, and signaling initiated by reovirus binding to NgR1 also are not known. NgR1 lacks a cytoplasmic domain and likely is incapable of intra-neuronal signaling without cytoplasmic-domain-containing coreceptors. Under physiological conditions, NgR1 binds myelin-associated ligands and recruits two neural coreceptors to form a tri-partite complex that initiates RhoA activation and actin reorganization to prevent axonal outgrowth (134). NgR1 ligands expressed on oligodendrocytes include nogo A, OMgp, and MAG. The tripartite receptor complex on the neural cell surface includes NgR1, p75 neurotrophin receptor (p75 NTR) or TNF receptor superfamily member 19 (TROY), and LRR and immunoglobin-like domain-containing protein 1 (LINGO1) or adhesion molecule with immunoglobulin-like domain 3 (AMIGO3). Many other viruses use the Rho pathway during entry (135), but it is not known whether reovirus binding to NgR1 initiates signaling events or ligation of coreceptors.

The overlapping expression of NgR1 in neural populations targeted by reovirus raises the possibility that NgR1 dictates T3-specific neurotropism (74, 77, 136). However, expression of NgR1 in CHO cells allows infection by both T1 and T3 strains (98). Such promiscuous infection by both serotypes is not observed following inoculation of murine cortical neurons in culture (77). T3 infects these neurons in an NgR1-dependent manner, whereas T1 infects neurons poorly, independent of NgR1 expression (98). The contrasting infectivity profile in different cell types could be due to cell-specific modifications of NgR1. Alternatively, an additional factor that promotes entry by the respective serotypes, possibly glycans or coreceptors, may be differentially expressed in different cell types.

## Viral Oncolytic Therapies

Cancer is the second leading cause of death worldwide, contributing to nearly 1 in every 6 deaths (137). The main challenges to reduce cancer mortality arise from poor access to healthcare and persistence of harmful lifestyle risk factors. The World Health Organization has estimated that between 30% and 50% of current cancer cases could be avoided by lifestyle changes and that many other cases could be ameliorated if detected and treated earlier (137). However, many cancers are detected late and thus

are resistant to traditional treatment options (e.g., surgical removal, radiation therapy, and chemotherapy). Recent advances in understanding the genetic and epigenetic determinants of cancers has led to growing support for precision targeting. Here, therapies are tailored to the specific cancer and address cancer anatomic distribution, biomarker expression, and host immunity.

Oncolytic viruses are a promising addition to the field of precision targeting. While viral infection has been hypothesized to modulate cancer for over 100 years (138), only recently have viruses been produced at clinical-grade quality to treat human cancers. Oncolytic viruses preferentially replicate in and kill cancer cells while sparing normal cells. This localized infection often stimulates a robust antitumor immune response, which can promote enhanced host recognition of malignant cells throughout the body (139). Several viruses are currently being evaluated as oncolytic therapeutics in clinical trials (see **Table I-1** for reference). Only two viruses involved in clinical trials today are unmodified, coxsackievirus and reovirus. Other oncolytic candidates are genetically modified to alter cell-type specificity or immune responses. For example, gene deletions can attenuate viral virulence or replication in normal cells, transgenes can contribute tumor-specific antigens or immune stimulants, and promotor modifications or replacements can drive tumor-specific replication. The ability to improve target specificity, cell killing, and selective immune activation by already-oncolytic viruses makes these biological machines important tools in the fight against cancer.

Only one viral oncolytic, called *talimogene laherparepvec* (Imylgic), is currently approved by the United States Food and Drug Association (FDA). Imlygic is an attenuated HSV-1 strain licensed since 2015 for direct intratumoral inoculation into metastatic melanomas (140, 141). Imlygic lacks two HSV-1 genes and expresses a regulatory cytokine transgene. These genetic manipulations contribute to decreased infection of normal cells, increased recognition of infected cells by the immune system, and enhanced recruitment and activation of antigen-presenting cells (APCs) (142-144). Despite encouraging pre-clinical and clinical results, Imlygic is limited in therapeutic intervention to direct intratumoral inocoulation of visible or palpable tumors, is not suitable for patients with impaired immune function, and has suboptimal killing of tumors

**Table I-1: Summary of recent oncolytic virus clinical trials.**

| Virus backbone | Genetically modified? Yes | Genetically modified? No | Number of clinical trials | Intravenous studies | Combination therapy used |
|---|---|---|---|---|---|
| Reovirus | | X | 3 | 100% | All |
| Adenovirus | X | | 13 | 15% | Some |
| Coxsackie virus | | X | 5 | 60% | All |
| HSV-1 | X | | 8 | 13% | Some |
| Maraba virus | X | | 2 | 100% | All |
| Measles virus | X | | 7 | 29% | Some |
| Poliovirus | X | | 1 | 0% | None |
| Retrovirus | X | | 3 | 33% | All |
| Vaccinia virus | X | | 7 | 43% | Some |
| VSV | X | | 2 | 0% | None |

*Oncolytic virus clinical trials listed on ClinicalTrials.gov as of April 2018 (actively recruiting or ongoing, at that time). Intravenous administration is listed as percent of total trials offering at least an option for intravenous administration. “Combination therapy” indicates viral therapy combined with one or more of the following treatment options: radiotherapy, chemotherapy, antivirals, stem cell therapy, and biologicals. Modified from (Twumasi-Boateng et al., 2018).

at sites distant from inoculation. Clearly, other viral therapeutic interventions are needed.

Reovirus displays a natural predilection to infect transformed cells that was described in 1977 (145). In 1998, reovirus was first assessed in pre-clinical studies as an oncolytic vector (146). Intratumoral inoculation of reovirus efficiently reduced tumor burden in 80% of immunocompromised mice and 65% of immunocompetent mice (146), providing support for the use of reovirus as an oncolytic therapeutic. Since 2000, 26 clinical trials using reovirus to target a variety of cancers in monotherapy or combination therapy have been completed or are ongoing in the U.S. alone (42). A single unmodified strain of reovirus, T3D, has been employed for these studies and is licensed as pelareorep under the trademark REOLYSIN®. Since reovirus rarely causes disease in humans and most patients have pre-existing anti-reovirus antibodies (147-152), reovirus T3D is well-tolerated. High infectious doses ($\geq 1 \times 10^{10}$ PFU/dose) and repeated inoculations have proven safe by intratumoral and intravenous routes (42). When toxicities are observed in clinical trials of reovirus, it is most often limited to acute, low-grade, flu-like symptoms with no lasting toxicities that have been attributed to the virus (42).

Reovirus T3D has been used to treat many cancers, including those of the brain, spine, head and neck, breast, cervix, ovaries, prostate, skin, lung, and pancreas (42). Patient biopsies of tumors inoculated directly (147) or by intravenous routes (148) demonstrate viral replication and cell death in transformed tissues, while neighboring tissues are spared. In addition to direct lysis of infected cells, reovirus infection promotes a robust antitumor immune response. Inoculation stimulates production of cytokines and chemokines that recruit and prime immune cells in the presence of tumor antigens (153-156). Virus-primed, tumor-specific, cytolytic T cells and dendritic cells (DCs) promote antitumor immunity systemically by targeting transformed cells where virus infection is absent, enhancing the efficiency of innate immune cells, and even attacking cancer cells after remission, viral clearance, and tumor recurrence (154, 155, 157). In this way, T3D and other oncolytic viruses can function as anti-cancer vaccines.

Combined with the natural predilection of reovirus to kill cancer cells and stimulate a robust immune response, there are several characteristics of reovirus that

improve its capacity as an oncolytic. For example, cancer progression is often rated by the TNM staging system that characterizes the tumor (T), lymph node (N), and metastatic (M) extent of transformed cells. Most cancers are rated from stage I to stage IV. Stage IV cancer is characterized by metastasis from the original tumor site to other organs within the body and coincides with a substantial decrease in life expectancy. For example, from stage III to stage IV breast cancer, the expected 5-year survival rate drops precipitously from ~ 72% to ~ 22% (158). As cancer spreads, treatment options require harsher, more systemic approaches. Reovirus spreads efficiently by hematogenous routes (159), making it well-suited to target metastatic, or stage IV, cancers. Furthermore, JAM-A expression is a predictive biomarker for tumor proliferation, metastasis, and poor prognosis (160-165). While reovirus cell-killing capacity is not dictated entirely by JAM-A expression (166), the presence of a high-affinity receptor like JAM-A acts as a homing beacon to snare virus for infection.

Reovirus displays a propensity to infect *Ras*-transformed cells (146, 167, 168). Mutations in *Ras* proto-oncogenes are identified in ~ 30% of human cancers and *Ras* mutations are thought to arise early in tumorigenesis. In late stages of tumorigenesis, *Ras* mutations are found in up to 100% of some cancer types, such as pancreatic adenocarcinomas, which are often resistant to traditional therapies and have a 5-year survival rate at diagnosis of ~ 4% (169, 170). Reovirus functions well in combination therapy with established chemotherapies (42). For example, tumor vascularization is an important hallmark of cancer progression. Reovirus infection induces vigorous expression of chemokine interferon-γ-inducible protein 10 (CXCL10), which is synergistically enhanced by multiple chemotherapies (171). CXCL10, in turn, disrupts endothelial branching and angiogenesis (171). Manipulation of reovirus efficiency by targeting cancers with particular biomarkers and using combination therapies will likely improve outcomes and allow use of lower doses of toxic chemotherapies.

While several strains of reovirus have been assessed in pre-clinical studies (172), the only approved therapy in clinical development is T3D REOLYSIN®. Several characteristics of T3D reovirus may be disadvantageous as an oncolytic. Foremost is the efficiency of T3 replication, which is inferior to that of T1 in many cell types (173-175). Reovirus tropism can and should be manipulated by altering the selection of

receptors used. By directing virus to specific, transformed cell populations expressing certain receptors, on-target efficiency of reovirus oncolysis and anticancer immunity can be improved while limiting off-target infection of non-transformed cells. This application brings to light the importance of studying basic virology and mechanisms of receptor-dependent tropism.

## Thesis Goal

Despite identification and characterization of three distinct reovirus receptors (sialylated glycans, JAM-A, and NgR1), mechanisms that mediate serotype-specific tropism in the CNS have not been uncovered. The focus of my thesis is to define viral and receptor sequences required for T1 and T3 neurotropism and virulence. In Chapter II, I elucidate the viral sequences that dictate neurovirulence and neurotropism, and in Chapter III, I define viral and NgR1 sequences required for binding and infection.

## Significance

Infections of the CNS cause life-threatening conditions like hydrocephalus, meningitis, and encephalitis. Even acute infections can dramatically and chronically impair neurologic function. Children are especially vulnerable to the detrimental consequences of viral infections of the CNS. It is imperative to understand the molecular underpinnings of what makes cells susceptible to virus infection. Work presented here seeks to define viral and host determinants of reovirus neural invasion and disease in mice. While reovirus is not a significant pathogen of humans, mounting reports of reovirus infections in humans raise concern that more virulent reovirus strains may emerge. Moreover, reovirus currently is being used in human clinical trials as a last resort to treat refractory cancers. Understanding what receptors are targeted by reovirus and perhaps elucidating the underlying differences between highly susceptible hosts (small, young mammals) and poorly susceptible hosts (adult mammals and humans) will inform diverse fields. These studies could 1) expand a collective understanding of viral pathogenesis in the CNS, 2) identify age- or species-specific interactions dictating susceptibly, 3) help prevent emergence of dangerous reovirus strains by identifying factors that contribute to neuroinvasion, and 4) lead to improved oncolytic strategies.

# CHAPTER II

# THE FUNCTION OF REOVIRUS σ1 PROTEIN DOMAINS IN NEUROTROPISM AND VIRULENCE

## Introduction

The reovirus attachment protein, σ1, is predicted to mediate serotype-specific tropism in the CNS of young mammals. However, reported receptor-binding functions of σ1 (**Fig. I-4**) cannot individually explain serotype-specific patterns of infection and disease in the CNS (**Fig. I-1**). Known proteinaceous receptors of reovirus mediate serotype-independent infection (98, 121). Furthermore, JAM-A expression is dispensable for reovirus replication in the brain (77). Sialylated glycans are engaged in a serotype-specific manner. T1 and T3 viruses with abrogated glycan-binding elicit less disease in the CNS, however, they still infect predicted sites in the CNS (100, 101). Perhaps glycan-blind viruses are not sufficiently "blind" and are still capable of binding sialylated neural and ependymal receptors. Alternatively, unidentified host molecules may mediate infection at sites within the CNS.

In this study, I used reverse genetics to engineer a panel of viruses expressing T1-T3 chimeric σ1 proteins to identify S1 gene sequences and encoded protein domains that dictate reovirus neurotropism and virulence in mice. I validated that chimeric σ1 proteins were expressed, encapsidated, folded, and functional to bind receptors and facilitate efficient viral replication in non-neuronal cells. I found that neurotropism and neurovirulence correlate with sequences in the T3 σ1 head domain. The reciprocal sequences of T1 σ1 track with infection of ependymal cells. Together, these findings indicate that homologous domains of the reovirus viral attachment protein coordinate distinct patterns of tropism in the CNS and suggest that the σ1 head domain engages unknown receptors that target virus to distinct cell populations.

## Results

### Design and recovery of chimeric σ1 viruses

To elucidate determinants of reovirus neurotropism, I designed a panel of viruses that express different S1 genes in an otherwise isogenic T1 background. Four parental,

or control, S1 genes were used to establish well-characterized σ1-specific differences of the two reovirus serotypes and their respective glycan-binding capacities. T1+ and T3+ parental S1 genes (**Fig. II-1B**) encode σ1 proteins (**Fig. II-1A**) that efficiently bind glycan (87, 99) and dictate divergent patterns of tropism in the brain. Viruses with specific mutations introduced into the glycan-binding domains of T1+ (101) and T3+ (99) display diminished glycan-binding capacity and are called T1- and T3-, respectively.

To define domains of T3 σ1 that mediate infection of neurons, I designed gain-of-function constructs in which a T1 σ1 domain was exchanged with homologous T3 sequences and concordantly, loss-of-function constructs in which a T3 σ1 domain was exchanged with homologous T1 sequences. I hypothesized that sequence exchange between serotypes at the two interdomain regions (located at the σ1 tail-body and body-head junctions) would yield replication-competent viruses. Therefore, I used primary sequences and available crystal structures of T1 σ1 and T3 σ1 to identify sequences neighboring the interdomain regions that contain sequence or structural conservation. Using this information, S1 genes were designed to encode the approximate σ1 head, body, or tail domain of one strain exchanged with homologous sequences of the reciprocal strain (**Fig. II-1B**).

Virus and S1 gene nomenclature are interchangeable and reflect the domain that was acquired. For example, T3 Head virus contains sequences of the T3 σ1 head domain appended to sequences of the T1 body and tail domains. The σ1s open reading frame remains intact within the overlapping σ1 tail domain of all S1 genes used in this study. Within a reovirus gene, terminal 5' and 3' sequences are predicted to bind with complementarity and function to promote efficient replication or packaging (44, 45, 176). Chimeric genes containing discordant termini were either modified at the 3' end to include extended 3' untranslated sequences of the parental gene (**Fig. II-1B**) or modified at the 5' end to express the native 5' untranslated region of the parental gene (**Fig. II-1B**). Following design, chimeric S1 genes were engineered using a combination of molecular cloning and *de novo* gene synthesis.

Plasmids encoding parental or chimeric S1 genes were transfected together with the nine remaining T1 genes into BHK-T7 cells to produce recombinant virus strains as

A

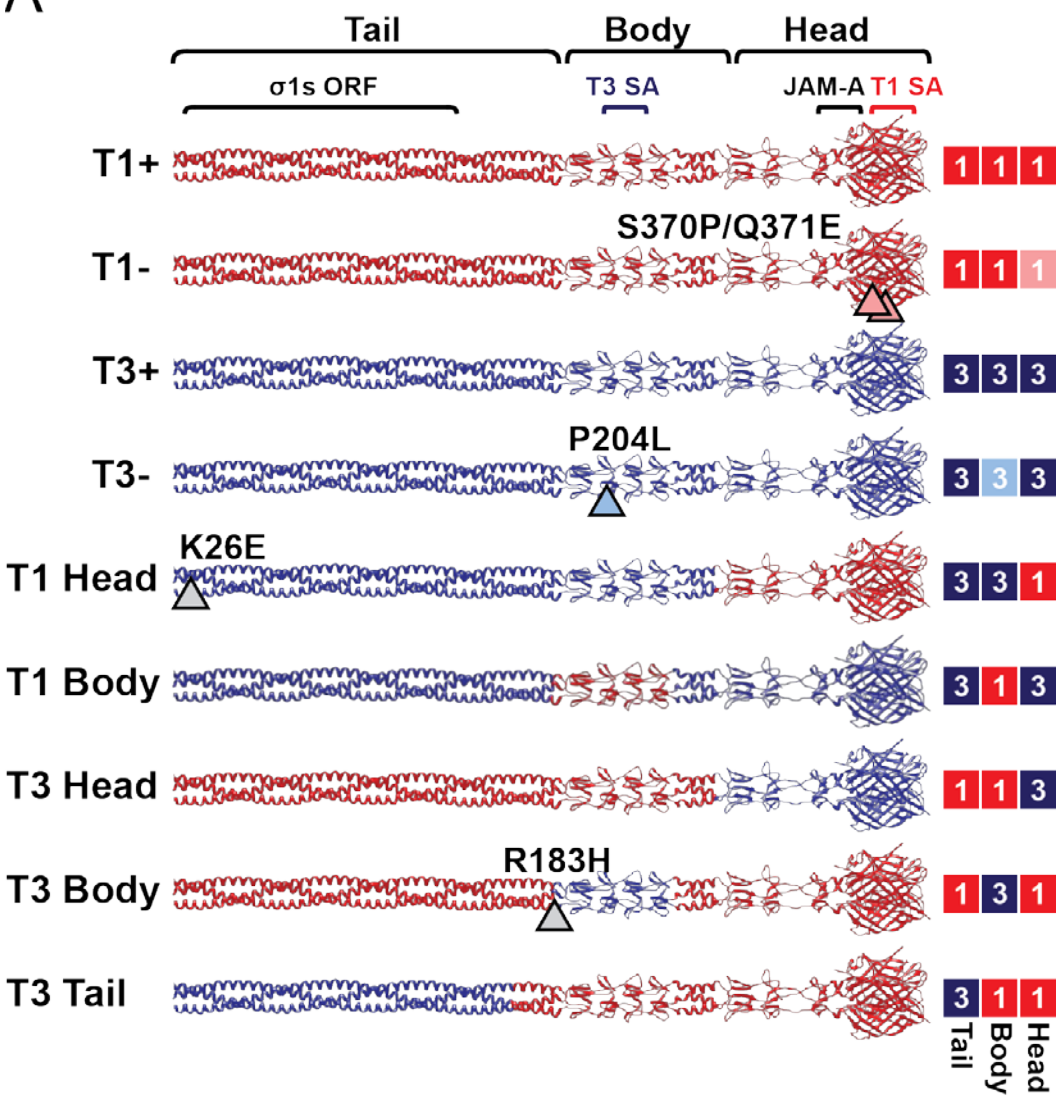


B

| Virus Name | 5' UTR | Tail | Body | Head | UTR | 3' UTR | |
|---|---|---|---|---|---|---|---|
| T1+ | | 1-470 | | | | NA | Parental |
| T1- | | 1-470** | | | | NA | |
| T3+ | | 1-455 | | | | NA | |
| T3- | | 1-455* | | | | NA | |
| T1 Head | | 1-250* | | 263-470 | | | Chimeric |
| T1 Body | | 1-165 | 176-248 | 236-455 | | NA | |
| T3 Head | | 1-262 | | 251-455 | | | |
| T3 Body | | 1-175 | 166-235* | 249-470 | | NA | |
| T3 Tail | | 1-150 | 154-470 | | | NA | |

**Figure II-1: Chimeric σ1-encoding viruses used in this study.** (A) Schematic of engineered σ1 proteins. A model of the σ1 trimer (adapted from Dietrich et al., JVI 2018) is shown as a ribbon diagram (left) or a simplified box schematic (right). T1 sequences (red; 1) and T3 sequences (blue; 3) are indicated for the tail, body, and head domains. T1 and T3 parental strains bind glycans (+) or contain mutations that abrogate glycan-binding (-). Mutations that differ from T1+ and T3+ are indicated by arrowheads and noted. The schematic on the right indicates sequence origin of σ1 domains for each virus (T1-red; T3-blue). (B) T1 (red) or T3 (blue) S1 gene elements are depicted for each virus. The approximate σ1 head, body, and tail domains are noted. Native untranslated regions (UTR) are shown for 5' and 3' gene termini. S1 genes of T1 Head and T3 Head viruses contain additional UTR sequences appended to the 3' termini. Amino acid boundaries are provided for chimeras and numbered by parental strain origin (1-470 of T1 and 1-455 of T3). Asterisks indicate the number of amino acids that differ from either T1+ or T3+ parental strains in the corresponding domain. NA; not applicable.

described (3, 46). BHK-T7 cell lysates yielded plaques on L929 cell monolayers for all viruses shown (**Fig. II-1A** and **II-1B**). However, despite several attempts, T1 Tail virus was not recovered. For other constructs, individual virus plaques were isolated and amplified in L929 cells for two passages before extraction of total RNA and sequence confirmation of the S1 gene.

The S1 genes of most viruses were genetically identical to the input plasmid sequences. However, approximately half of the T3 Body virus clones contained a point mutation (T3 σ1-R183H) near the 5' junction of T1 and T3 sequences (**Fig. II-1A** and **II-1B**). This mutation coincided with higher viral titers, larger plaques, and enhanced replicative capacity (data not shown). Therefore, the S1 gene of T3 Body was modified to encode a histidine at T3-σ1 position 183 and recovered by reverse genetics. A point mutation also was identified in all propagated clones of T1 Head virus (T3 σ1-K26E) in a region of σ1 that is predicted to be embedded into the viral capsid (48, 177). Before introduction into mice, these chimeric strains were evaluated using several *in vitro* correlates of viral fitness.

In vitro validation of chimeric virus function and fitness

To determine whether σ1-chimeric reoviruses faithfully recapitulate properties of parental reoviruses and efficiently encapsidate chimeric σ1 proteins, equivalent particle numbers of each strain were resolved by SDS-PAGE. Proteins were visualized following colloidal blue staining, and the optical densities of bands corresponding to specific viral proteins were quantified. All viruses contain comparable levels of major large (λ), medium (μ), and small (σ) structural proteins (**Fig. II-2A**). Moreover, σ1-chimeric viruses do not demonstrate significant ISVP contamination, a correlate of particle instability that is discerned by the appearance of the δ fragment of μ1 and loss of σ3 (**Fig. II-2A**). However, T1 Head virus incorporates significantly less σ1 protein into virions (**Fig. II-2A** and **II-2B**), perhaps as a consequence of the T3-K26E mutation identified in the σ1 tail domain of this strain. Combined, these data demonstrate that reovirus particles can assemble and encapsidate chimeric σ1 trimers, and most viruses do so with an efficiency comparable to that of the parental strains.

To determine whether chimeric σ1 proteins are correctly folded and displayed on

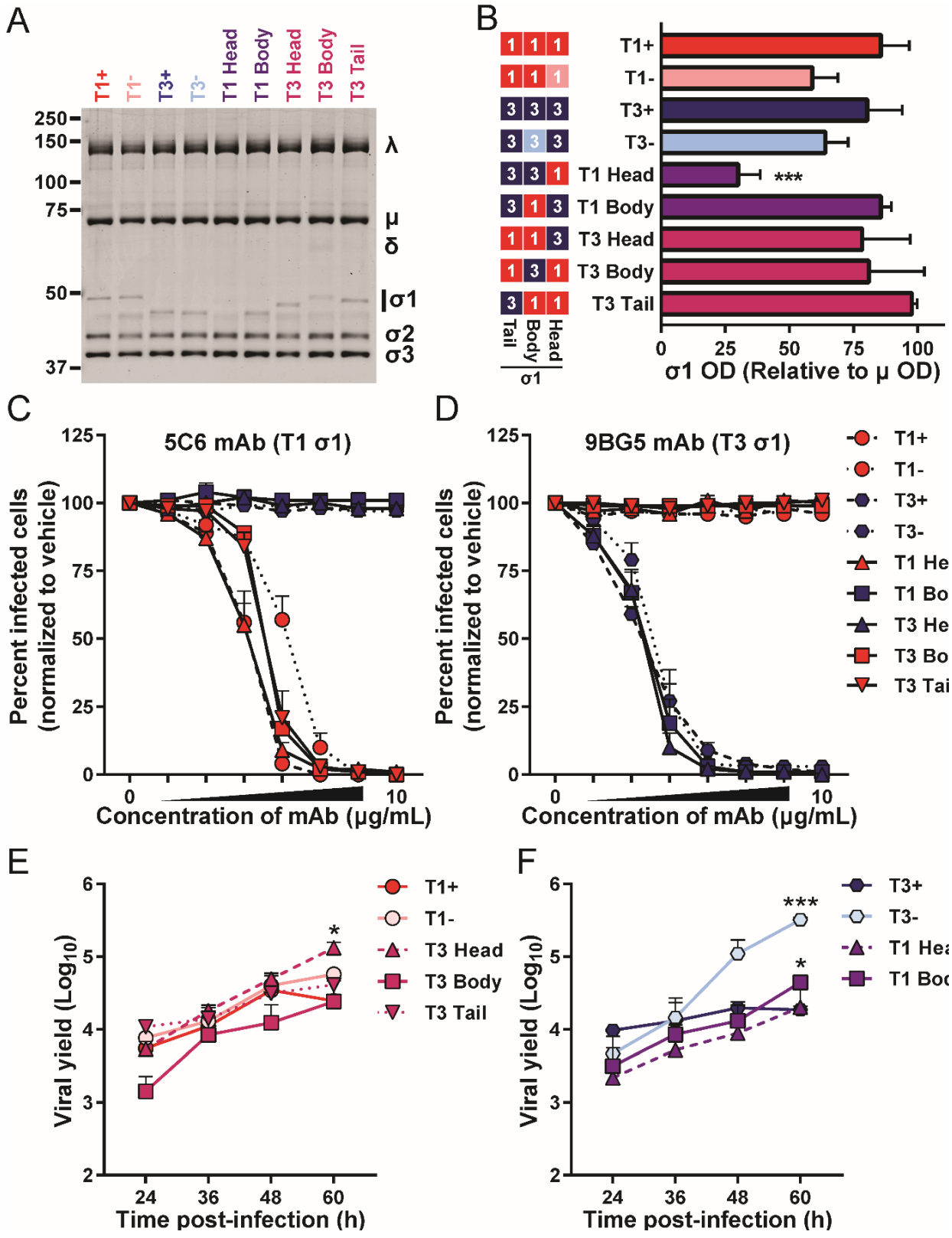
A
T1+
T1-
T3+
T3-
T1 Head
T1 Body
T3 Head
T3 Body
T3 Tail
250
150
100
75
50
37
λ
μ
δ
σ1
σ2
σ3
B
T1+
T1-
T3+
T3-
T1 Head
T1 Body
T3 Head
T3 Body
T3 Tail
***
Tail
Body
Head
σ1
0
25
50
75
100
σ1 OD (Relative to μ OD)
C
5C6 mAb (T1 σ1)
Percent infected cells (normalized to vehicle)
125
100
75
50
25
0
0
10
Concentration of mAb (μg/mL)
D
9BG5 mAb (T3 σ1)
Percent infected cells (normalized to vehicle)
Concentration of mAb (μg/mL)
T1+
T1-
T3+
T3-
T1 He
T1 Bo
T3 He
T3 Bo
T3 Tai
E
Viral yield (Log10)
6
5
4
3
2
*
24
36
48
60
Time post-infection (h)
T1+
T1-
T3 Head
T3 Body
T3 Tail
F
Viral yield (Log10)
***
*
Time post-infection (h)
T3+
T3-
T1 Hea
T1 Boc

**Figure II-2: Fitness correlates of chimeric σ1-containing viruses.** (A,B) Incorporation of σ1 in virions. Purified virus particles ($5 \times 10^{10}$) were resolved by SDS-polyacrylamide gel electrophoresis. Proteins were visualized following colloidal blue staining and imaged using an Odyssey fluorescence scanner. (A) A representative gel is shown. Bands corresponding to viral λ, μ, and σ proteins and molecular weight markers (kD) are indicated. (B) Optical density of bands corresponding to σ1 and μ structural proteins were quantified. Results from three independent experiments are expressed as the mean relative optical density of σ1 bands normalized to μ bands. Error bars indicate SD. The schematic on the left indicates sequence origin of σ1 domains for each virus (T1-red; T3-blue). (C,D) Conformation-specific antibody neutralization of viral infectivity. L929 fibroblasts were inoculated with the virus strains shown pre-incubated with vehicle or four-fold dilutions of monoclonal antibodies 5C6 (C) or 9BG5 (D). Infected cells were enumerated 24 h post-inoculation by indirect immunofluorescence. Antibodies 5C6 and 9BG5 recognize epitopes in the σ1 head domain of T1 or T3, respectively. Symbol color reflects the sequences present in the σ1 head domain (T1-red; T3-blue). Results are expressed as the mean percentage of infected cells relative to vehicle-treated samples for four fields of view per well in duplicate wells for three independent experiments. Error bars indicate SEM. Values that differ significantly from PBS-treated controls by one-way ANOVA and Dunnett's test are indicated (*, $P < 0.05$; **, $P < 0.01$; ***, $P < 0.001$). (E) Viral replication efficiency. L929 fibroblasts were inoculated with the virus strains shown at an MOI of 0.5 PFU/cell. At the times shown post-inoculation, viral titer in cell lysates was determined by plaque assay. Results are expressed as the mean viral yield from duplicate wells for three independent experiments. Error bars indicate SEM. Viral titers that differ significantly from those of T1+ at 60 h post-inoculation by one-way ANOVA and Dunnett's test are indicated (*, $P < 0.05$; **, $P < 0.01$; ***, $P < 0.001$).

the surface of virions, I assessed the capacity of conformationally specific σ1 antibodies to neutralize reovirus infectivity using a fluorescent focus unit (FFU) assay. Monoclonal antibodies 5C6 and 9BG5 recognize distinct epitopes that span subunits in the trimeric σ1 head domain of T1 and T3 reoviruses, respectively (94). Parental and σ1-chimeric reoviruses were pre-incubated with monoclonal antibody or vehicle and adsorbed to L929 cells. Cells were fixed at 24 h post-adsorption, stained with a reovirus-specific antiserum, and imaged to determine the percentage of infected cells. Viruses containing T1 σ1-head sequences (T1+, T1-, T1 Head, T3 Body, and T3 Tail) were efficiently neutralized by T1-specific 5C6 antibody, whereas viruses containing T3 σ1-head sequences (T3+, T3-, T1 Body, and T3 Head) were unaffected by increasing concentrations of 5C6 (**Fig. II-2C**). Similarly, the T3-specific antibody 9BG5 reduced infectivity of viruses containing T3 σ1-head sequences (**Fig. II-2D**), but even at high concentrations, 9BG5 did not diminish infectivity of viruses containing T1 σ1-head sequences. Notably, the efficiencies with which chimeric strains are neutralized by the 5C6 and 9BG5 antibodies are comparable to those of parental strains expressing the same σ1 antibody epitope. Combined, these data suggest that chimeric σ1 trimers are natively folded and displayed on the virion surface.

Reovirus strains are capable of efficiently infecting a broad range of cell types. However, they often do so in a strain-specific manner. In particular, reovirus infectivity of many cultured cell lines is dependent on serotype-specific engagement of sialylated cell-surface glycans (87, 99, 101). Unlike with many other cell lines, reovirus infection of L929 cells is largely glycan- and serotype-independent (99). To determine whether viruses with chimeric σ1 proteins replicate efficiently, L929 cells were adsorbed with equivalent infectious units, and viral titer was determined at multiple intervals post-inoculation by plaque assay. All viruses tested replicated with comparable kinetics and reached similar peak viral titers (**Fig. II-2E** and **II-2F**). T3 Head and T3 Tail display replication kinetics similar to parental strains T1+ and T1-, and T3 Head virus even reached modestly, but significantly, higher titers than did T1+ at 60 h post-adsorption. T3 Body virus produced lower mean yields at early time points than its parental strain, T1+, but reached comparable yields at 60 h post-inoculation (**Fig. II-2E**). Similarly, T1 Head and T1 Body viruses produced slightly lower yields at early time points compared

with their parental strain, T3+, but both chimeric viruses reached yields comparable to T3+ at 60 h post-inoculation (**Fig. II-2F**). Notably, T3- produced significantly higher titers than did T3+ at late time points in this assay, which may be a consequence of diminished cell viability following infection with T3+ (107). Together, these data demonstrate that σ1-chimeric viruses are capable of replicating with similar efficiency and producing equivalent or enhanced peak titers relative to parental strains.

Reovirus strains display serotype-specific patterns of hemagglutination as a consequence of binding to different SA moieties on the surface of erythrocytes (101, 178-181). The T1 glycan-binding site in the σ1 head domain mediates agglutination of human erythrocytes (87), whereas sequences in the T3 σ1 head domain do not contribute to hemagglutination. Instead, the glycan-binding site in the T3 σ1 body domain mediates less efficient agglutination of human erythrocytes and a serotype-specific agglutination of bovine erythrocytes (182).

To evaluate the functionality of SA-binding sequences conferred to chimeric σ1 proteins, I assessed hemagglutination capacity of reovirus particles using human and bovine erythrocytes. T1+ agglutinated human erythrocytes efficiently (mean HA titer = 1024), while disruption of the T1 glycan-binding pocket in the σ1 head domain of T1- virus resulted in a 64-fold reduction in HA titer (**Fig. II-3A**). Residual hemagglutination capacity of T1- is thought to be mediated by σ1 crosslinking non-SA moieties on the cell surface (101). T3+ agglutinated human erythrocytes with a mean HA titer of 32, which is 32-fold less than that of T1+. Disruption of the T3 glycan-binding domain in T3- virus abolished agglutination of these cells. Two σ1-chimeric viruses (T1 Body and T3 Head) do not contain any predicted glycan-binding sequences and, as expected, these strains did not agglutinate human erythrocytes. T3 Tail virus contains a predicted T1 glycan-binding domain and agglutinated human erythrocytes with an HA titer identical to that of T1+, suggesting that the T1 σ1 head domain functions efficiently to engage SA. Two σ1-chimeric viruses (T1 Head and T3 Body) incorporate sequences for both the T1 and T3 glycan-binding domains and were predicted to have identical hemagglutination profiles. However, T1 Head agglutinated human erythrocytes poorly (32-fold less than that of T1+ and 2-fold less than that of T3+), indicating an impairment in binding to human erythrocyte glycans. In contrast, the mean HA titer of T3 Body was 8-fold greater

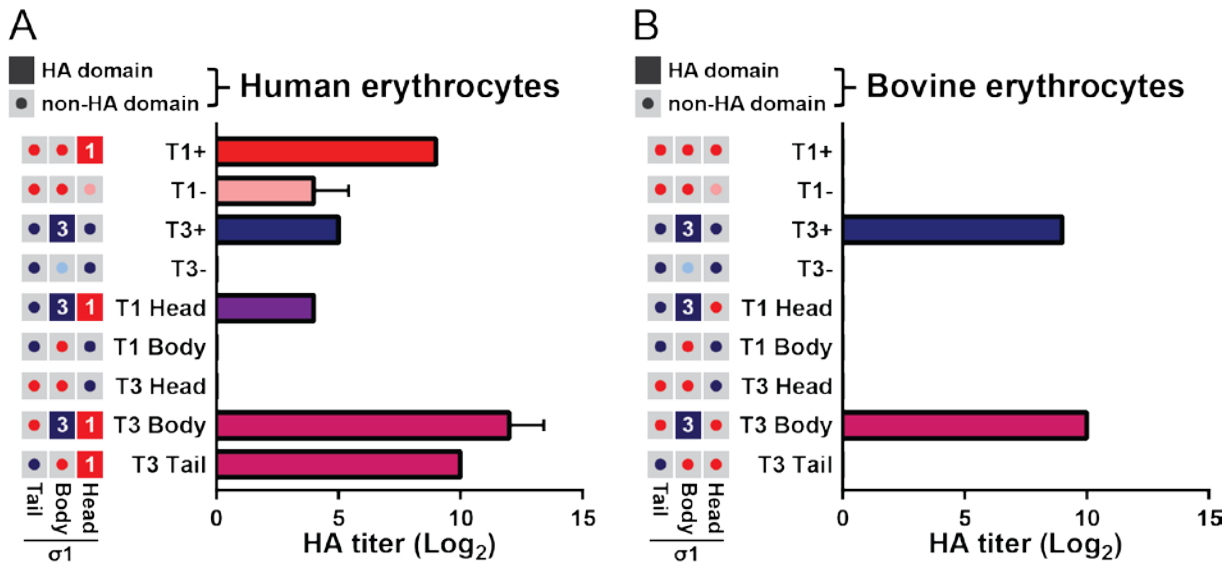


**Figure II-3: Chimeric viruses display distinct sialic-acid binding profiles.** (A,B) Hemagglutination capacity of parental and σ1-chimera viruses. Schematics on left indicate the predicted hemagglutination capacity of σ1 head, body, and tail domains for each virus. Filled boxes (T1+, red; T3+, blue) indicate domains with predicted hemagglutination capacity. Grey boxes with central buttons indicate that the domain is not hypothesized to contribute to hemagglutination (T1+, red; T1-, pink; T3+, dark blue; T3-, light blue). Purified reovirus virions ($10^{11}$) were serially diluted two-fold in PBS. Human (A) or bovine (B) erythrocytes were resuspended in PBS at a concentration of 1% (vol/vol). Equal volumes of virus and erythrocyte mixtures were combined and incubated at 4°C for 4 h, and hemagglutination was assessed. Results are expressed as mean $log_2$-transformed HA titer from three independent experiments. Error bars indicate SD.

than that of T1+ and 128-fold greater than that of T3+, suggesting a synergistic effect of the two glycan-binding domains (**Fig. II-3A**).

Of the viruses tested, only T3+, T1 Head, and T3 Body contain T3 glycan-binding sequences and, therefore, these strains were hypothesized to specifically agglutinate bovine erythrocytes. T3+ and T3 Body viruses agglutinated bovine cells equivalently (**Fig. II-3B**), suggesting that the conferred T3 σ1 body domain is sufficient to mediate SA binding. However, T1 Head virus failed to agglutinate bovine erythrocytes. The combined impairment of T1 Head virus to agglutinate human and bovine erythrocytes is likely attributable to the decreased encapsidation of σ1 onto virions (**Fig. II-2A** and **II-2B**). Together, these data indicate that four of the five chimeric σ1 proteins bind glycan receptors as predicted and provide validated tools to identify σ1 domains required for reovirus neurovirulence.

Analysis of viral loads and disease initiated by chimeric viruses

To define reovirus sequences that govern neurovirulence, I inoculated newborn mice intracranially with ~100 PFU of reovirus and monitored infected animals for symptoms of disease. Moribund animals were euthanized. T1- and T3- viruses were excluded from these studies to reduce the number of mice used, as these viruses display lethality at this dose comparable to their glycan-binding counterparts, T1+ (101) and T3+ (106), respectively. Inoculation with T1+ or T3 Tail virus caused no detectable disease, and all inoculated mice survived infection (**Fig. II-4A**). Following inoculation with T1 Head or T3 Body, one mouse in each cohort was euthanized as a consequence of significantly impaired weight gain over the course of infection. However, lethality following inoculation with these strains did not differ statistically when compared with T1+. In contrast, the majority of mice inoculated with T3+, T1 Body, or T3 Head displayed weight loss, lethargy, and neurological impairment. Neurological signs included agitated behavior, repetitive movements such as scratching or walking in circles, seizures, and ataxia, which are all consistent with reovirus-induced meningoencephalitis (36, 183). Some mice inoculated with T3+, T1 Body, or T3 Head either did not display detectable signs of disease or recovered from illness. Viruses that did not initiate statistically-significant lethal disease in newborn mice all express

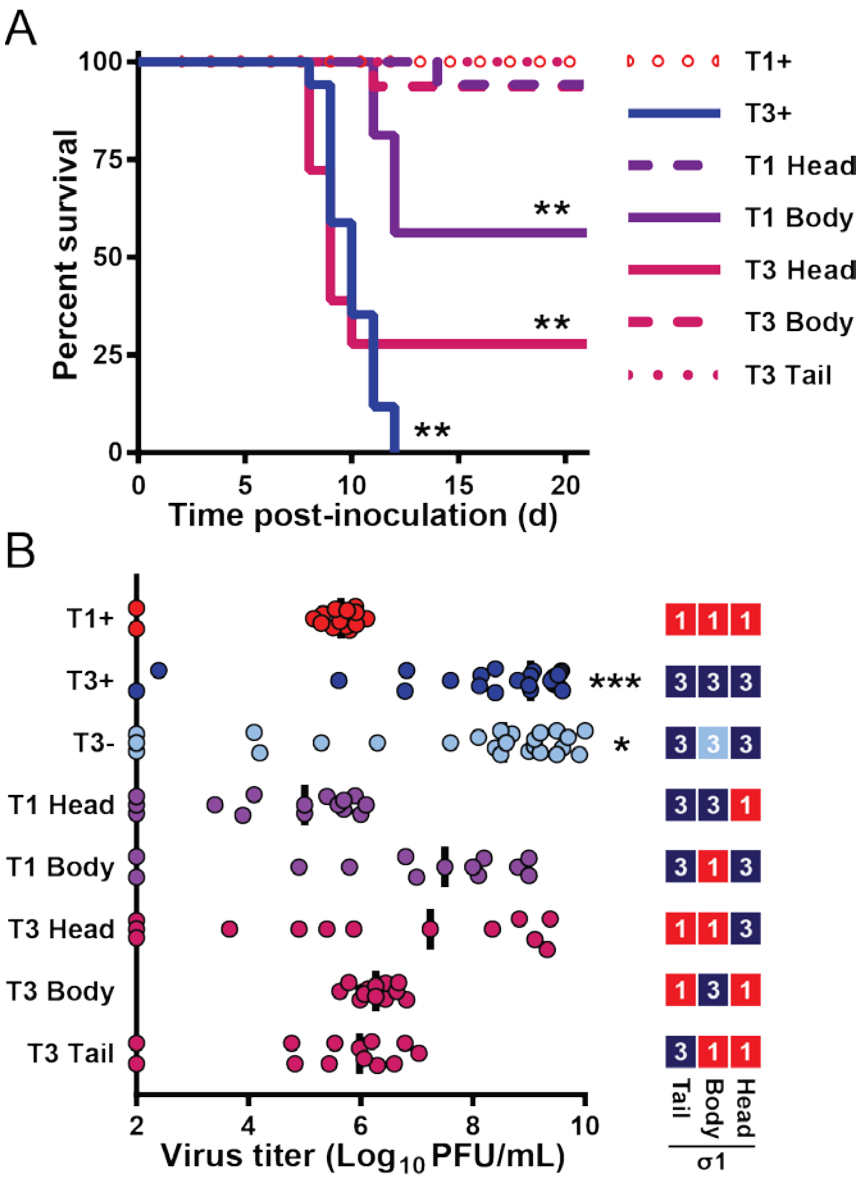


**Figure II-4: The σ1 head domain dictates reovirus neurovirulence and viral replication capacity in the brain.** (A) Survival following intracranial inoculation. Newborn C57BL/6 mice (*n* = 16 to 18 for each virus strain) were inoculated intracranially with 100 PFU of purified virions of the strains shown. Mice were monitored for illness for 21 days and euthanized when moribund. Values that differ significantly from T1+ by log-rank test are indicated (*, $P < 0.05$; **, $P < 0.01$). (B) Viral titers in the brain following intracranial inoculation. Schematic on the left indicates sequence origin of σ1 domains for each virus (T1-red; T3-blue). An independent cohort of identically inoculated mice (*n* = 13 to 26 for each virus strain) were euthanized eight days post-inoculation, and viral titers in the homogenized right brain hemispheres were determined by plaque assay. Each symbol represents the viral titer of a single mouse. Data are log-transformed and displayed with a linear *x*-axis scale. Median viral titer is indicated by a horizontal bar. Values that differ significantly from T1+ by one-way ANOVA and Dunnett's test are indicated (*, $P < 0.05$; ***, $P < 0.001$).

sequences corresponding to the T1 σ1 head domain, whereas viruses causing lethal disease express sequences corresponding to the T3 σ1 head domain.

To determine the replicative capacity of σ1-chimeric viruses in the brain, I inoculated mice intracranially with ~100 PFU of reovirus and euthanized infected animals 8 days post-inoculation to quantify viral titers in the right brain hemisphere by plaque assay. T1- was excluded from these studies to minimize the number of mice used but was previously shown to produce slightly lower titers than T1+ at this dose and time-point (101). Median and peak virus titers in the brain for all other strains were compared to those of T1+ to identify viruses that have enhanced replicative capacity at that site. For viruses expressing T1 σ1 head sequences (T1+, T1 Head, T3 Body, and T3 Tail), maximum titers ranged from 6.1 to 7.0 $\log_{10}$ PFU/brain, and median titers ranged from 5.0 to 6.3 $\log_{10}$ PFU/brain (**Fig. II-4B**). In contrast, viruses expressing T3 σ1 head sequences (T3+, T3-, T1 Body, and T3 Head) displayed maximum titers 770 to 12,000-fold higher than that for T1+ and ranged from 9.0 to 10.2 $\log_{10}$ PFU/brain, while median titers ranged from 7.2 to 9.0 $\log_{10}$ PFU/brain (**Fig. II-4B**). The broader distribution of viral titers in brain tissue observed for higher-replicating viruses may reflect differences in receptor utilization or sites targeted within the brain. Thus, viruses that express T1 σ1 head sequences produce lower viral titers in the brain and do not initiate significant disease, whereas viruses that express T3 σ1 head sequences produce higher viral titers in the brain and induce lethal disease (**Fig. II-4A** and **II-4B**), further implicating the σ1 head domain as the major determinant of reovirus neurovirulence.

Analysis of chimeric virus neurotropism

To test whether the σ1 head domain influences sites of viral replication in the brain, mice were inoculated with ~100 PFU of parental or chimeric reovirus strains and euthanized 8 days post-inoculation. The left-brain hemisphere was sectioned and stained with a reovirus-specific antiserum. With the exception of glial cells (identified by their dendritic morphology), which were sparsely infected by all strains, viral tropism was mutually exclusive to either ependyma or neurons for all tissue sections assessed (**Fig. II-5**).

Following inoculation with T1+, T1 Head, T3 Body, or T3 Tail (all viruses that express T1 σ1 head sequences), reovirus antigen was detected in cells adjacent to the lumen of the lateral ventricle that lack extended processes (**Fig. II-5**). This staining pattern is consistent with both the location and morphology of ependymal cells, as is expected for T1+ tropism (7, 101). Following inoculation with T3+, T3-, T1 Body, or T3 Head (all viruses that express T3 σ1 head sequences), reovirus antigen was detected in specific neuronal subsets throughout the brain (**Fig. II-5**), as described previously for T3+ (100). All neuronal subsets infected by T3+ also were infected by T3-, T1 Body, and T3 Head. In particular, pyramidal neurons of the cortex, neurons of the thalamus and hypothalamus, and Purkinje neurons of the cerebellum were targeted by viruses expressing a T3 σ1 head domain. These findings indicate that the σ1 head domain dictates the tropism of both T1 and T3 reovirus in the brain.

Evaluation of glycan-independent infection of neurons

Results obtained thus far demonstrate that the σ1 head domain of T3 reovirus is required for infection of neurons in the CNS and that glycan engagement by the T3 body domain is dispensable for infection of these cells. To test this hypothesis directly, I quantified reovirus infection of cultured primary neurons with or without neuraminidase pre-treatment to remove cell-surface SA. Vehicle-treated neurons were poorly infected by T1+, T1-, T1 Head, and T3 Tail, moderately infected by T3-, T1 Body, T3 Head, and T3 Body, and most heavily infected by T3+ (**Fig. II-6A** and **II-6B**). These results demonstrate serotype-dependent infection of neurons (when comparing T1+ and T1- with T3+ and T3-) and SA-enhanced infection of neurons (when comparing T3+ with T3-), as shown previously for the parental strains (77). Similar to viral replication efficiency in the brain, T1 Body and T3 Head infected neurons in culture as efficiently as T3-, which also lacks a functional T3 glycan-binding domain. Infectivity of cultured neurons with T1 Head and T3 Tail also mirrored *in vivo* replication capacity, with low-level infectivity similar to T1+ and T1-. Surprisingly, a virus that did not efficiently infect neurons *in vivo*, T3 Body, demonstrated enhanced infectivity in cultured neurons relative to the T1 parental strains. This trend of enhanced infectivity cannot be entirely

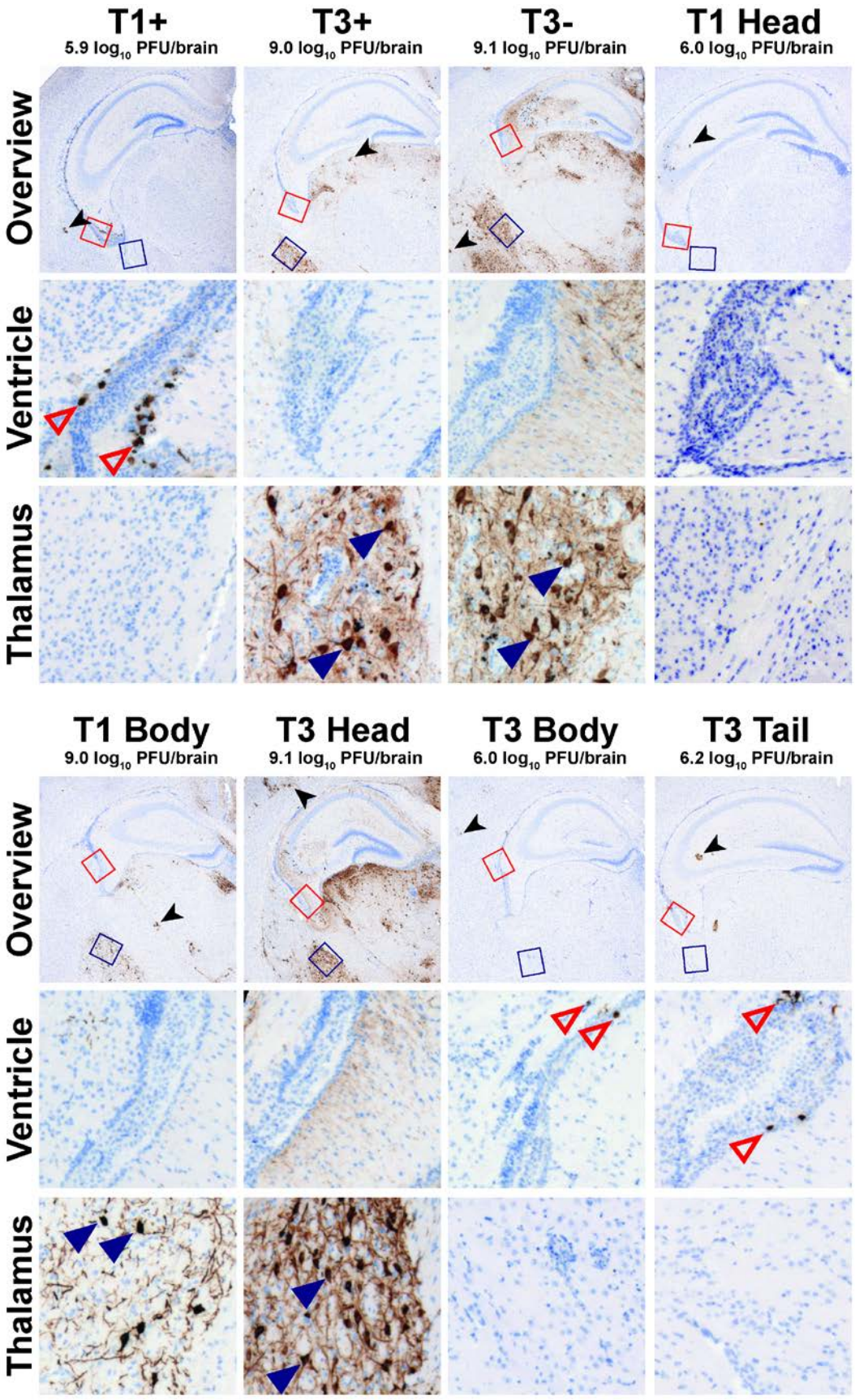
T1+
5.9 log10 PFU/brain
T3+
9.0 log10 PFU/brain
T3-
9.1 log10 PFU/brain
T1 Head
6.0 log10 PFU/brain
Overview
Ventricle
Thalamus
T1 Body
9.0 log10 PFU/brain
T3 Head
9.1 log10 PFU/brain
T3 Body
6.0 log10 PFU/brain
T3 Tail
6.2 log10 PFU/brain
Overview
Ventricle
Thalamus

**Figure II-5: Reovirus neurotropism is dictated by sequences in the σ1 head domain.** Newborn C57BL/6 mice were inoculated intacranially with 100 PFU of purified virions of the strains shown. Mice were euthanized eight days post-inoculation, and brains were resected and hemisected along the longitudinal fissure. Right brain hemispheres were homogenized for determination of viral titer by plaque assay. Left-brain hemispheres were fixed in formalin and embedded in paraffin. Coronal sections of the left-brain hemisphere were stained with reovirus-specific antiserum and hematoxylin. Low-magnification overview images at the depth of the hippocampus are shown. Regions corresponding to high magnification insets of the lateral ventricle and lateral thalamus are indicated in the overview micrographs by red or blue boxes, respectively. Representative sections are shown. Viral titers from the paired right brain hemispheres are displayed above the micrographs. Reovirus-infected ependymal cells (open red triangles), neurons (filled blue triangles), and glia (black arrowhead), all identified using morphological criteria, are indicated.

explained by the presence of T3 body domain sequences, as T1 Head virus does not show this trend.

To determine the influence of SA on infection of primary neuronal cultures, neurons were treated with *A. ureafaciens* neuraminidase, which removes α2,3-, α2,6-, and α2,8-linked terminal SA residues, prior to infection. In contrast to vehicle-treated neurons, infectivity trends of neuraminidase-treated neurons precisely mimicked those observed from *in vivo* studies. Viruses containing T1 σ1 head sequences infected neuraminidase-treated neurons poorly (**Fig. II-6C** and **II-6D**). Of note, the diminished infectivity of neuraminidase-treated neurons by T3 Body virus suggests that infection of cultured neurons by this strain is dependent on binding to cell-surface SA. Viruses containing T3 σ1 head sequences (T3+, T3-, T1 Body, and T3 Head) infected neuraminidase-treated neurons robustly and comparably (**Fig. II-6C** and **II-6D**). T3-, T1 Body, and T3 Head viruses displayed approximately two-fold enhanced infectivity of neuraminidase-treated neurons compared with vehicle-treated neurons. Collectively, these data demonstrate that the σ1 head domain controls serotype-dependent infection of neurons and provides additional evidence that glycan engagement is not required for infection of neurons *in vivo*.

## Discussion

The reovirus S1 gene dictates serotype-dependent differences in neurotropism and disease, a finding first reported nearly 40 years ago (9). However, even as new functions are described for S1-encoded proteins, the mechanism by which S1 gene sequences dictate these differences in pathogenesis has remained elusive. In this study, I used a reverse genetics platform to engineer a panel of reoviruses that encode chimeric S1 genes to identify σ1 sequences that mediate serotype-specific differences in reovirus neurologic disease. I found that infection of neurons does not correlate with T3 sequences encoding the σ1s protein, the σ1 tail domain, or serotype-specific glycan engagement in the σ1 body domain. Instead, I discovered that sequences encoding the T3 σ1 head domain are required for infection of neurons in the murine brain (**Fig. II-5**). These same sequences also influence encephalitis induction and survival outcome (**Fig. II-4B**). Viruses expressing T3 σ1 head domain sequences replicate to high titer in the

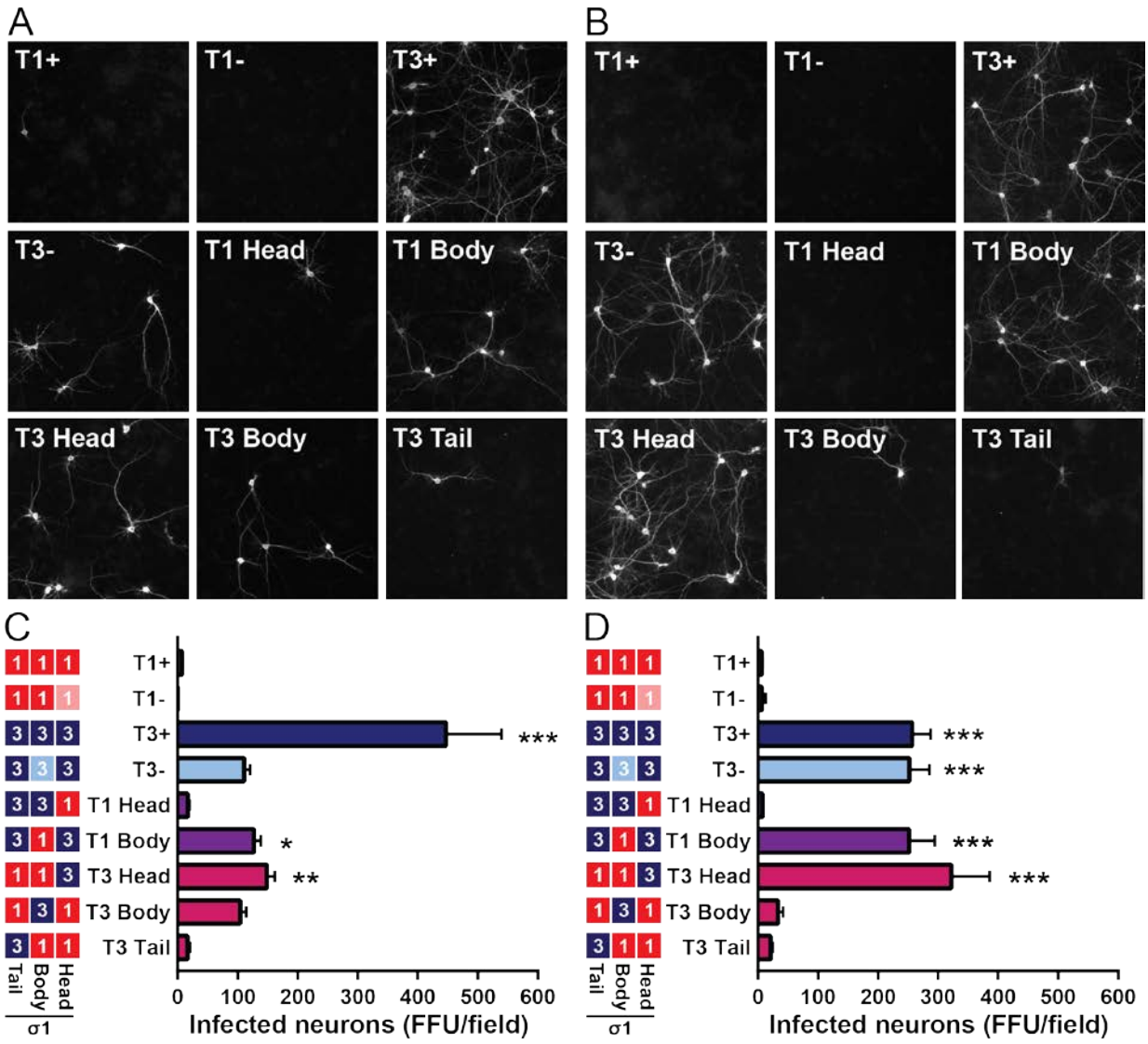


**Figure II-6: Infection of primary cortical neurons is primarily dependent on sequences in the T3 σ1 head domain.** Cultured primary rat cortical neurons were treated with a vehicle control (A,C) or 40 mU/mL of neuraminidase (B,D), inoculated with reovirus at an MOI of 500 PFU/cell, fixed at 24 hpi, and stained with reovirus-specific antiserum, an antibody to detect Tuj1, and DAPI. (A,B) Representative micrographs of reovirus-infected neurons (white staining) are shown. (C,D) Infected neurons were enumerated using indirect immunofluorescence. Results are expressed as mean number of infected neurons per field of view for six images per well in quadruplicate wells for five independent experiments. Error bars indicate SEM. Values that differ significantly from T1+ by one-way ANOVA and Dunnett's test are indicated (*, $P < 0.05$; **, $P < 0.01$; ***, $P < 0.001$).

brain, likely because of the greater number of cells targeted when compared with viruses expressing T1 σ1 head domain sequences (**Fig. II-5**). Using cultured neurons, I further demonstrate that this infection of neurons is strictly dependent on the T3 σ1 head domain when cell-surface SA is removed (**Fig. II-6B**). Furthermore, I found that reciprocal sequences in T1 σ1 mediate infection of ependyma (**Fig. II-5**), lower viral brain titers (**Fig. II-4B**), and survival (**Fig. II-4A**) following intracranial inoculation of mice. These data establish that homologous sequences in the reovirus σ1 head domain coordinate infection at discrete sites in the CNS (**Fig. II-7A** and **II-7B**).

It was not previously known whether reoviruses expressing chimeric genes derived from different serotypes could be recovered. Chimeric σ1 proteins have been expressed and purified from insect cell lysates (184), and the S1 gene of replication-competent viruses has allowed insertion of transgenes, although transgene sequences are variably stable (47, 185, 186). Our study demonstrates that replication-competent reoviruses expressing chimeric S1 genes and gene products can be recovered and are genetically preserved over multiple generations. I was not able to recover a virus expressing the T1 σ1 tail domain appended to the T3 σ1 body and head domains (T1 Tail). It is possible that the sequences chosen for T1 Tail construction would not allow proper protein folding. Alternatively, the viral RNA may contain an incompatibility between T1 and T3 sequences (45). Recently available structures of the T1 and T3 σ1 tail domains (88) should allow improved design of future σ1-chimeric proteins.

Similar to other glycan-binding viruses, reoviruses use an adhesion-strengthening mechanism of attachment to cells, in which low-affinity engagement of glycans adheres virus to the cell surface prior to ligation of a higher-affinity receptor capable of promoting internalization (99, 102, 111). Reovirus binding to SA is not thought to directly initiate viral entry, although there is some evidence that glycan engagement may influence post-binding signaling events (107). Our data are consistent with an adhesion-strengthening model of reovirus neurotropism. Viral titers in the brain and lethality are highest for T3+, a virus that engages glycans using the σ1 body domain. However, viruses with limited or absent T3 glycan-binding affinity (T3-, T1 Body, and T3 Head) retain the capacity to target neurons for infection (**Fig. II-5** and **II-6A**) and initiate lethal encephalitis (**Fig. II-4A**), albeit less efficiently than T3+.

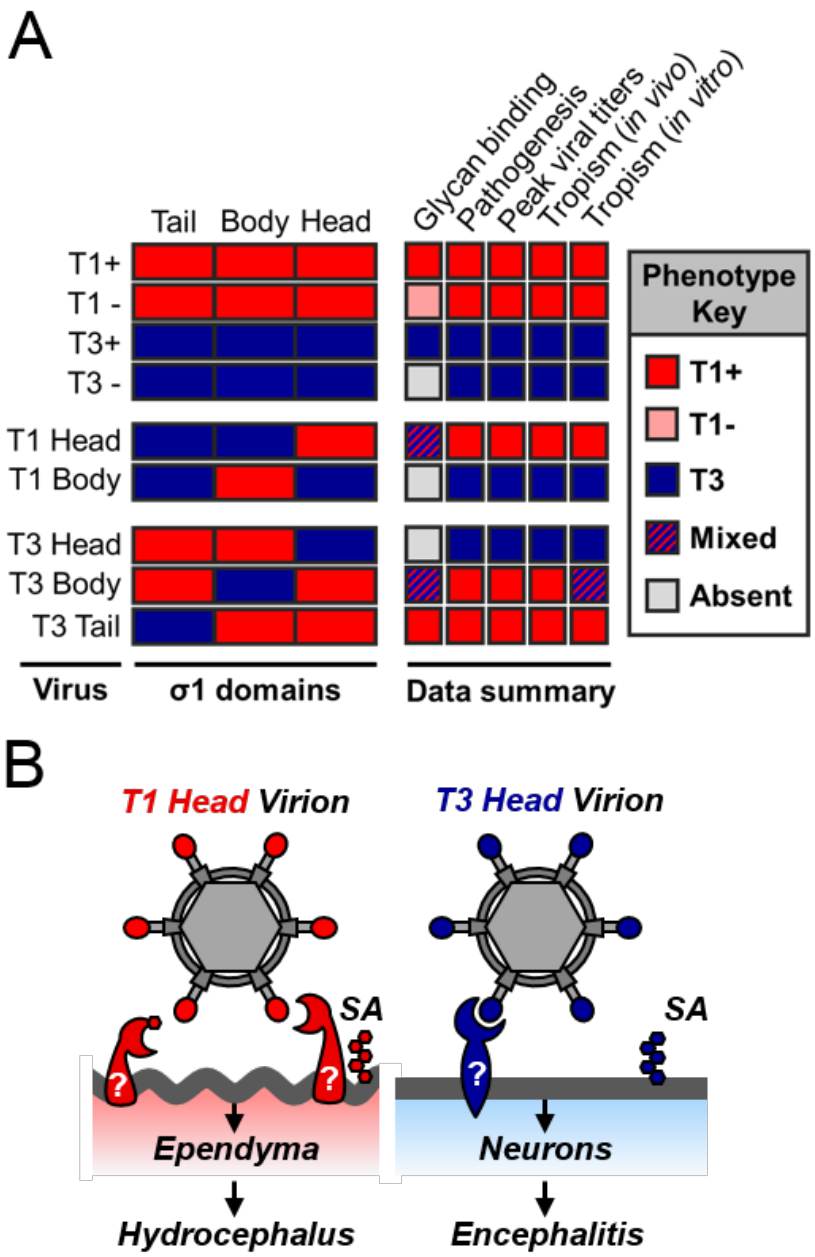


**Figure II-7: Sequences in the σ1 head domain dictate serotype-dependent patterns of viral tropism and neurologic disease in a glycan-independent manner.** (A) Summary of key findings. The σ1 protein domain for each virus strain indicated is presented as a rectangle (red, T1; blue, T3). The legend on the right displays results as more similar to T1 (red box), more similar to T3 (blue box), mix between T1 and T3 (hatched box), or absent (grey box) in the case of hemagglutination. (B) Model of serotype-dependent neurotropism. Viruses expressing T1 σ1 head domains infect ependyma, and we predict they would cause hydrocephalus with a higher inoculation MOI. Viruses expressing T3 σ1 head domains infect neurons and initiate a lethal, fulminant encephalitis.

T3 Body virus does not exhibit neurotropic capacity *in vivo* (**Fig. II-5**). However, this virus is capable of infecting cultured neurons using a SA-dependent mechanism (**Fig. II-5A** and **II-5B**). It is possible that T3 glycan engagement is sufficient to initiate infection of neurons *in vivo* at a level that was not detected or that *in vitro*-cultured neurons do not faithfully recapitulate *in vivo* receptor requirements. Interestingly, purified virion preparations of T3 Body may contain more ISVPs (indicated by the δ μ1 cleavage product) compared with other contemporaneously purified viruses (**Fig. II-2A**). Cultured neurons are significantly more susceptible to ISVPs than virions (27), and while ISVPs are presumed to use receptors comparably to virions, ISVPs hemagglutinate more efficiently than virions, and ISVP infectivity is significantly more sensitive to neuraminidase treatment than virion infectivity (96). These data indicate that receptor requirements differ for reovirus virions and *in vitro*-prepared ISVPs. Thus, I hypothesize that T3 Body ISVPs enter neurons in the absence of a receptor engaged by the T3 σ1 head domain.

Treatment of cultured neurons with *A. ureafaciens* neuraminidase diminishes T3+ virus infectivity to that of T3- virus and does not alter T3- infectivity (98, 100). Surprisingly, I observed that T3-, T1 Body, and T3 Head virus demonstrate a two-fold increase in infectivity of cultured neurons following neuraminidase treatment (**Fig. II-6A** and **II-6B**), despite the prediction that these viruses do not bind SA and should be unaffected by neuraminidase treatment. A nearly identical finding has been reported for HIV-1 in studies using both primary and cultured cells (187). It is possible that removal of SA from the cell surface in certain settings enhances the accessibility of σ1 to a T3 head-specific receptor.

How do sequences in the σ1 head domain mediate tropism? No currently known functions of σ1 account for the CNS tropism observed in our study. However, data reported here raise new questions. To efficiently infect either ependymal cells or neurons, reovirus must be able to traffic to, bind, and replicate within these cells. Because T1 and T3 tropism in the CNS is manifested following multiple different routes of inoculation, and cultured neurons recapitulate serotype-dependent differences in neurotropism (86) (**Fig. II-6A**), I do not think that trafficking to affected CNS cell types accounts for differences in tropism, as both T1 and T3 are capable of efficient

hematogenous dissemination and have been observed in and around microvasculature in the brain. While the σ1 head domain may function in post-binding/pre-entry replication steps to promote tropism differences, serotype-dependent binding to primary ependyma (85) and neurons (86) supports a receptor-dependent mechanism of target-cell selection.

In addition to JAM-A, GM2 glycan is bound by the T1 σ1 head domain (87). T1 strains deficient in glycan engagement are altered in virulence but not in tropism within the CNS (101). While the GM2 glycan bound by T1 reovirus is appended to both proteins and lipids, the full array of host components expressing this glycan is not known. I hypothesize that T1 σ1 head sequences coordinate binding to a proteinaceous receptor, which may be engaged independent of or overlapping with the GM2-glycan binding site (**Fig. II-7B**). In the case of T3 σ1, the serotype-specific, glycan-binding domain is distant from the neurotropism-determining σ1 head domain (**Fig. II-7B**). Both T1 and T3 reovirus can spread by hematogenous routes to infect multiple organs, but T3 strains also spread via neural routes (80, 82, 188). I hypothesize that T3 σ1 head sequences engage a neural-specific receptor to initiate infection of neurons, which also may mediate neural dissemination from sites of initial infection.

If the σ1 head domain binds a T1- or T3-specific proteinaceous receptor as we anticipate, then reovirus would have evolved two proximal binding sites at the virion-distal end of a long filamentous protein, one site for JAM-A and one that determines CNS tropism. I hypothesize that this location might be advantageous to either provide a larger surface area for binding and concordantly promote a more affine interaction (189) or serve as a flexible probe to interrogate molecular contacts at the cell surface. Other viruses also display receptor-binding domains at the termini of an extended trimeric protein, further highlighting a shared design for viral adhesion to cells (190, 191).

These studies contribute to an overall understanding of mechanisms of neuroinvasion and highlight the evolutionary pressure for RNA viruses to coopt viral proteins to serve multiple, critical functions in infection. By dissecting those functions, I have uncovered an important, serotype-specific determinant of reovirus neurotropism. I also consider this panel of viruses to be a useful toolbox to answer questions about the function of reovirus attachment in replication, dissemination, and tropism outside the

CNS. While reovirus does not cause disease in humans, it preferentially infects and kills cancer cells (167, 192, 193). A prototype T3 reovirus strain, licensed as Reolysin®, has been used in more than 30 clinical trials to date and shows both safety and potential efficacy in treatment of several different cancers, including those of the CNS (42). The reovirus σ1 protein shares a striking resemblance to the multifunctional attachment protein of adenovirus (194), another promising oncolytic. Adenoviruses expressing reovirus σ1 are viable and display reovirus-predicted tropism (191). By combining reovirus and adenovirus receptor-binding domains, a new class of tailored therapeutics can be envisioned. Such strategies to genetically manipulate the attachment functions of reovirus could improve cancer targeting and cell killing. Thus, understanding molecular determinants of reovirus tropism informs mechanisms of viral neuroinvasion and may contribute to tailored and improved oncolytic therapies.

# CHAPTER III

# DEFINING REOVIRUS AND NOGO RECEPTOR SEQUENCES REQUIRED FOR BINDING AND INFECTIVITY

## Introduction

Reovirus displays serotype-specific tropism in the CNS. However, the molecular basis underlying differential cell targeting is not known. It is hypothesized that T1 strains infect ependyma by engaging an ependymal receptor and T3 strains infect neurons by engaging a neural receptor. However, reovirus receptors have not been identified for these cell populations. NgR1 was first identified as a receptor that allows reovirus infection of normally non-susceptible CHO cells (98). While NgR1 is expressed at multiple sites in the body, it is most abundantly expressed in neurons of the CNS, where many of its functions have been described. In the adult CNS, NgR1 binds myelin inhibitory proteins and neuronal coreceptors to prevent neuronal outgrowth. Importantly, blockade or removal of NgR1 inhibits reovirus infection of primary cultured cortical neurons (98). It is not yet clear whether NgR1 influences viral tropism or pathogenesis.

NgR1 may serve as a neuronal receptor for T3 reovirus in a subset of CNS neurons. However, at least in overexpression systems, NgR1 is capable of mediating infection by both T1 and T3 reovirus strains. If NgR1 is a neuronal receptor, it is not clear how it functions in serotype-dependent patterns of infection, if it does at all. Furthermore, the structural and biochemical mechanisms underlying NgR1-dependent infection are almost entirely unknown. While soluble NgR1 protein is capable of immunoprecipitating reovirus virions but not ISVPs (98), the viral ligand is not known. ISVPs have lost σ3 and contain an altered conformer of σ1 (61), suggesting that one or both of these proteins binds NgR1. Understanding what sequences of NgR1 and reovirus are required for this interaction will enhance knowledge of how NgR1 mediates binding to structurally diverse proteins and may influence our understanding of reovirus neurotropism.

To identify sequences of NgR1 necessary for interaction with reovirus, I conducted on-cell binding assays with altered NgR1 constructs I engineered. I determined that NgR1 serves as a specific receptor, as a related receptor homolog

(NgR2) does not mediate reovirus binding or infection. Using NgR1 gain-of-function chimeras and loss-of-function deletion mutants, I found that N-terminal sequences of NgR1 are necessary and sufficient to interact with reovirus virions. I also demonstrated that reovirus binding to NgR1 occurs independent of known N-linked oligosaccharides. To determine the viral ligand for NgR1, I collaborated with Dr. Jennifer Konopka Anstadt and Dr. B.V. Venkataram Prasad's lab at Baylor College of Medicine to visualize NgR1 bound to reovirus particles by cryo-EM and conducted direct binding studies in collaboration with Dr. Jonathan Knowlton and Dr. Gregory Wilson. We found that reovirus outer-capsid protein σ3 interacts with NgR1. The σ3 proteins of both T1 and T3 reovirus efficiently bind NgR1, providing further support that NgR1 does not mediate serotype-specific infection. Collectively, these data demonstrate that N-terminal protein sequences of NgR1 interact with σ3 on reovirus particles to promote efficient binding and infection in a mechanism that resembles native NgR1-ligand binding interactions (133).

The second short data section in this chapter ("Elucidation of the NgR1 viral ligand, σ3") was a collaborative project with individual efforts described here. Dr. Jennifer Konopka-Anstadt and I generated viral and receptor reagents necessary for cryo-EM experiments and collaborated on experimental design and interpretation of the results (**Fig. III-6** and **III-7**). Single-particle cryo-EM was performed at Baylor College of Medicine, with special attention by Mr. Rodolfo Moreno and Dr. Liya Hu. Initial identification of direct NgR1-σ3 interactions was obtained by me with σ3 protein generously donated by Dr. Gregory Wilson. Results presented in **Figure III-8** were obtained by Dr. Jonathan Knowlton and represent collaborative experimental design and interpretation by Dr. Knowlton and me.

## Results

Identification of NgR1 sequences required for efficient reovirus binding and infectivity

NgR1 shares sequence and structural homology with two proteins, NgR2 and NgR3 (**Fig. III-1A**) (195). These homologs display differential tissue expression and, in some cases, redundant functions (196-199). To determine whether NgR2 serves as a receptor for reovirus, I expressed NgR1 or NgR2 from normally non-susceptible CHO

cells and quantified reovirus binding to and infectivity of these cells. Both NgR1 and NgR2 were detected on the cell surface (**Fig. III-1B**), indicating receptor availability to interact with adsorbed reovirus. However, only NgR1-expressing cells bind reovirus (**Fig. III-1C**) and permit infection (**Fig. III-1D**). While binding and infectivity of NgR3-expressing cells remains to be determined, these data demonstrate that NgR1, and not NgR2, serves as reovirus receptor.

NgR1 is N-glycosylated at two well-characterized sites in the central body domain, asparagine 82 and asparagine 179, and O-glycosylated at multiple less-well-characterized sites in the C-terminal GPI linker domain. Glycosylation at residue 179 is dispensable for NgR1 binding to all native ligands reported to date, whereas glycosylation at residue 82 is necessary for efficient binding to MAG, OMgp and Lingo-1 (133). Both NgR1 N-glycosylation sites display high-mannose glycans (129), which are populated by and terminate in mannose residues. Therefore, these glycans are not predicted to interact with known reovirus glycan-binding sequences. To determine whether NgR1 N-glycosylation is necessary for reovirus binding and infectivity, I altered residues N82 and N179 singly to alanine and expressed WT or mutant NgR1 in CHO cells. By immunoblot detection of whole-cell lysates, NgR1 mutants display predicted gel-shift migration patterns of ~2 kD per glycosylation site (**Fig. III-2A**). In a parallel experiment, transfected CHO cells were analyzed for cell-surface expression of NgR1 and binding by T3- reovirus particles by flow cytometry. I found that WT, N82A, or N179A NgR1 proteins are expressed by a high percentage of cells, approximately 96, 77, and 83 percent, respectively (**Fig. III-2B**). Similarly, T3- reovirus bound to an equivalent, and overlapping, population of CHO cells (**Fig. III-2C**). These data suggest that NgR1 N-glycosylation is not required for efficient reovirus binding.

It is not known whether NgR1 requires coreceptors to efficiently internalize reovirus. However, because NgR1 is GPI-anchored to the membrane, it cannot initiate intracellular signaling without cofactors. NgR1 normally functions in a complex of coreceptors and ligands (200-207). Since at least one of those coreceptors (Lingo-1) binds NgR1 in a glycosylation-dependent manner (133), I tested whether reovirus binding to to NgR1 is sufficient to mediate viral replication. CHO were transfected with WT, N82A, or N179A NgR1, adsorbed with T3- reovirus, and infected cells were

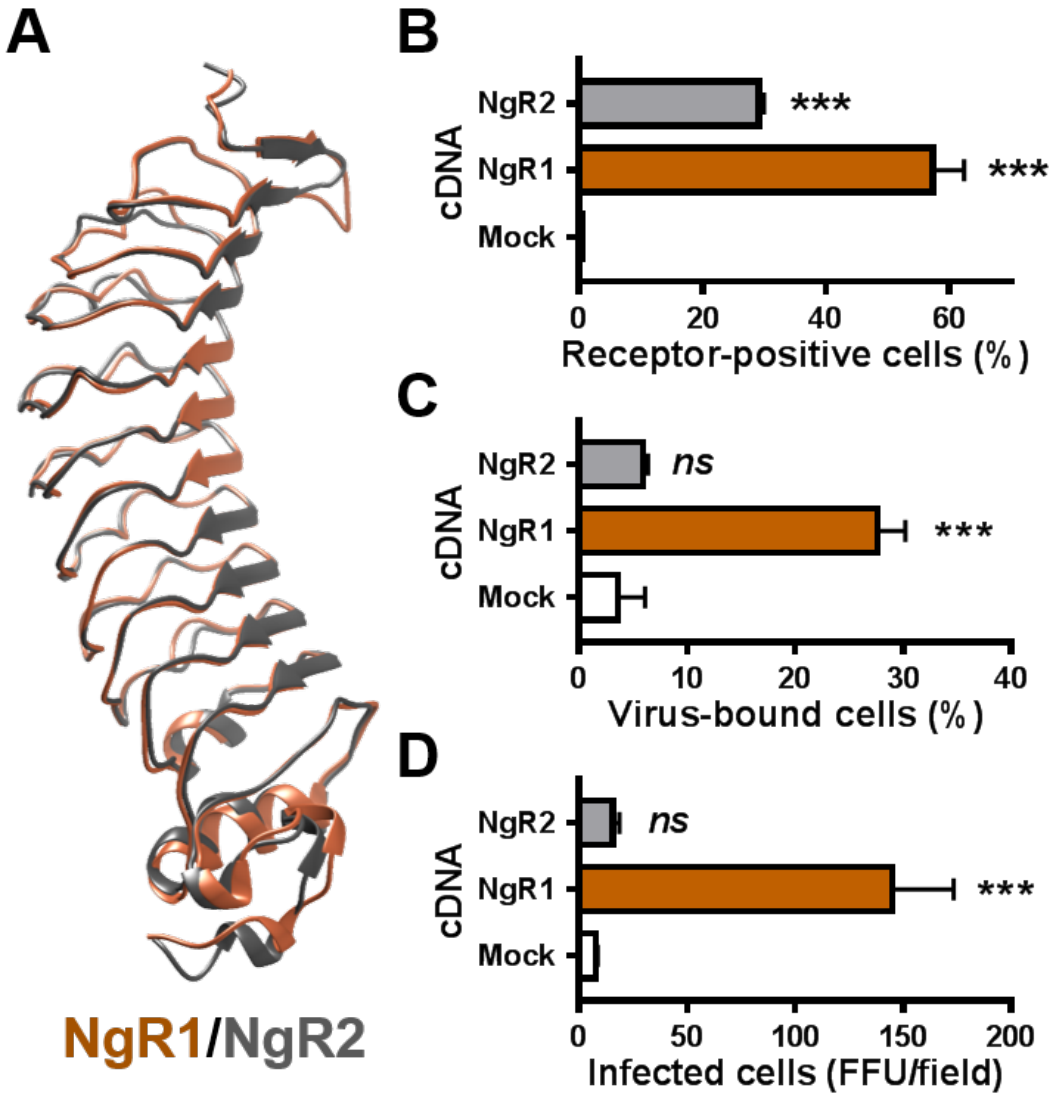


**Figure III-1: NgR1 is a specific reovirus receptor.** (**A**) NgR1 and NgR2 are structural homologs. Ribbon tracings of NgR1 (orange) (129) and NgR2 (grey) (195) (NT domain to LR-CT domain) are superimposed using UCSF Chimera software. (**B-D**) NgR2 is not a reovirus receptor. CHO cells were either mock transfected or transfected with cDNA encoding either NgR1 or NgR2 and incubated for 48 h. (**B and C**) Cells were treated with NgR1- or NgR2-specific antibodies prior to adsorption with $10^5$ particles/cell of Alexa Fluor 546-labeled reovirus T3- on ice for 1 h. The percentage of cells either (**B**) expressing receptor or (**C**) bound by virus was determined by flow cytometry. Results are expressed as the mean percentage of positive cells for three independent samples. (**D**) Transfected CHO cells were adsorbed with 10 PFU/cell of reovirus T3- and monitored for infectivity 24 hpi by indirect immunofluorescence using reovirus-specific antiserum. Results are expressed as the mean FFU/field from 4 fields of view per well in triplicate wells. Error bars indicate SD. Values that differ significantly from mock by one-way ANOVA and Dunnett's test are indicated (*, $P < 0.05$; **, $P < 0.01$; ***, $P < 0.001$). *ns* = not significantly different.

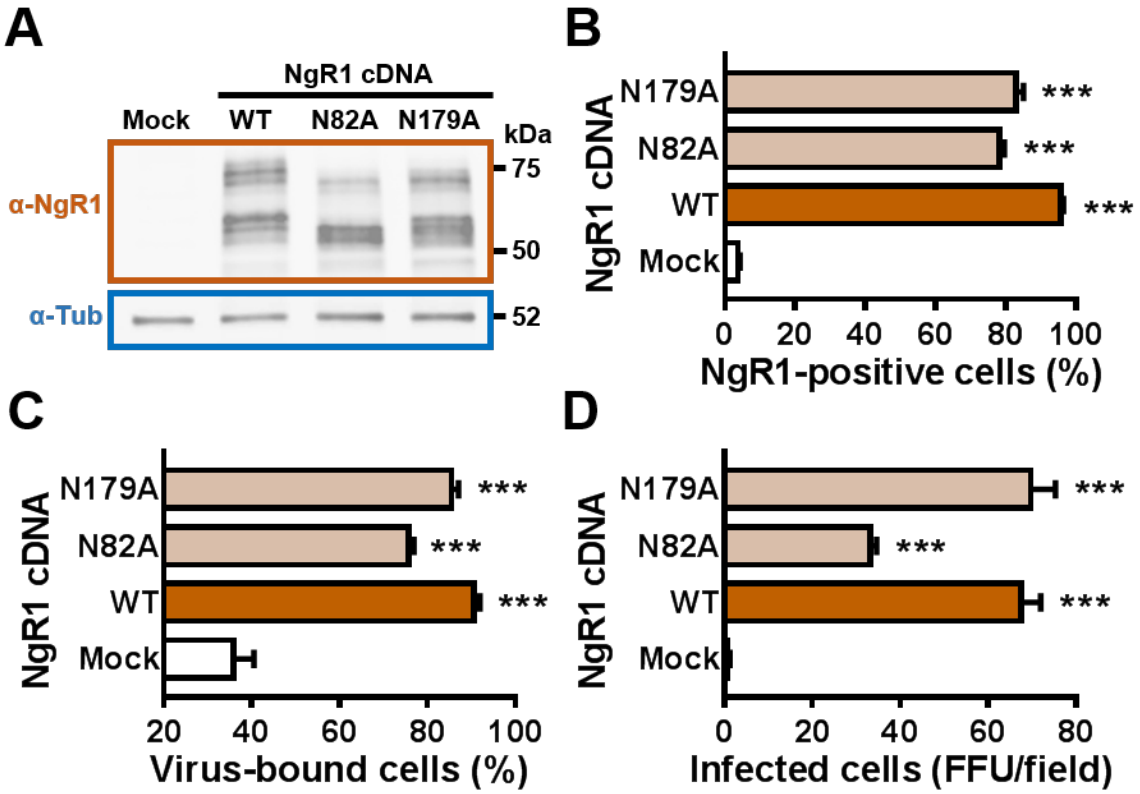


**Figure III-2: NgR1 N-glycosylation is not required for reovirus binding.** (**A-D**) CHO cells were either mock transfected or transfected with cDNA encoding WT, N82A, or N179A NgR1 and incubated for 48 h. (**A**) Glycosylation mutants demonstrate predicted gel shifts. Transfected CHO cells were lysed in protein dissociation buffer, and soluble protein was analyzed by SDS-PAGE and visualized by immunoblotting with either NgR1-specific antiserum (top panel) or α-tubulin-specific monoclonal antibody (bottom panel). (**B and C**) Transfected CHO cells were treated with antibodies specific for NgR1 prior to adsorption with $10^5$ particles/cell of Alexa Fluor 546-labeled reovirus T3- on ice for 1 h. The percentage of cells either (**B**) expressing receptor or (**C**) bound by virus was determined by flow cytometry. Results are expressed as the mean percentage of positive cells for three independent samples. (**D**) Transfected CHO cells were adsorbed with 10 PFU/cell of reovirus T3- and monitored for infectivity 24 hpi by indirect immunofluorescence using reovirus-specific antiserum. Results are expressed as the mean FFU/field from 4 fields of view per well in triplicate wells. Error bars indicate SD. Values that differ significantly from mock by one-way ANOVA and Dunnett's test are indicated (*, $P < 0.05$; **, $P < 0.01$; ***, $P < 0.001$).

quantified by indirect immunofluorescence 24 h post-adsorption. WT and N179A NgR1 mediated efficient and equivalent infection of reovirus, whereas CHO cells transfected with NgR1-N82A displayed ~ 50% of the infectivity observed with WT or N178A NgR1 (**Fig. III-2D**). These data may suggest a function for N82 glycosylation in post-binding steps.

To define domains of NgR1 required to bind reovirus, I used complementary gain-of-function and loss-of-function approaches. The solenoid structure of NgR1 resembles building blocks, in that repeated units stack via repetitive structural motifs (**Fig. I-5D-F**). This structure makes NgR1 particularly amenable to genetic manipulation (133, 198, 199). I engineered gain-of-function NgR1 constructs, in which sequences of NgR1 were replaced with sequences of NgR2. This chimera-generating strategy has been used successfully to identify chondroitin sulfate proteoglycan binding sequences in the LR-CT domains of NgR1 and NgR3 (199) and MAG binding sequences of NgR1 and NgR2 (198). The use of NgR1 deletion constructs demonstrates that the C-terminal GPI-CT is dispensable for binding to most NgR1 ligands and that the central core of LRR domains (the N-terminal two-thirds of the protein) is required for interactions with most ligands (133).

As chimeric or deletion proteins may not be effectively recognized by available NgR1 or NgR2 antibodies, modified proteins have been detected on the cell surface using an N-terminal myc tag. This small, 10-residue polypeptide is detected using commercially available antibodies and does not disrupt NgR1 binding to ligands (133). I first tested whether myc-tagged NgR1 could be expressed in CHO cells and whether the tagged protein can serve as an efficient docking and internalization receptor. While myc-tagged NgR1 is expressed well from cells (**Fig. III-3A**), this protein does not mediate efficient reovirus binding (**Fig. III-3B**) or infectivity (data not shown). Therefore, I instead used NgR1-specific antibodies to detect NgR1 deletion constructs on the surface and a combination of NgR1 and NgR2 antibodies to detect chimeric proteins on the cell surface.

The 421-amino acid length of NgR1 can be divided into approximately equivalent thirds, from NT to LRR4, from LRR5 to LR-CT, and the independent, large GPI-CT domain (**Fig. I-5**). I engineered three gain-of-function constructs called NgR-A, NgR-B,

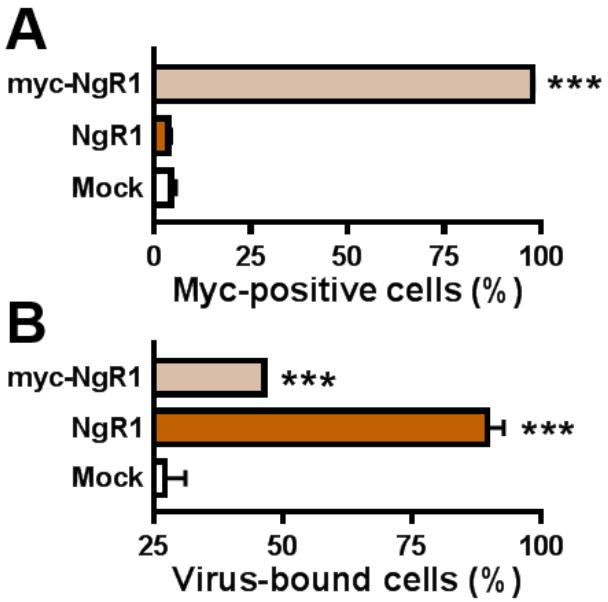


**Figure III-3: N-terminal NgR1 myc-tag disrupts reovirus binding.** (**A** and **B**) CHO cells were either mock transfected or transfected with cDNA encoding WT NgR1 or myc-tagged NgR1 and incubated for 48 h. Cells were adsorbed with $10^5$ particles/cell of Alexa Fluor 546-labeled reovirus T3- on ice for 1 h prior to treatment with a myc-specific antibody. The percentage of cells either (**A**) expressing receptor or (**B**) bound by virus was determined by flow cytometry. Results are expressed as the mean percentage of positive cells for three independent samples. Error bars indicate SD. Values that differ significantly from mock by one-way ANOVA and Dunnett's test are indicated (*, $P < 0.05$; **, $P < 0.01$; ***, $P < 0.001$).

and NgR-C with precise sequences defined in **Table III-1** and depicted schematically in **Figure III-4A**. Following transfection of NgR1, NgR2, or chimeric receptor constructs into CHO cells, I assessed cell-surface receptor expression and reovirus binding by flow cytometry. Chimeric receptors are expressed at levels similar to or greater than that of NgR2 (**Fig. III-4B**). Only NgR1 and a construct encoding the N-terminal two-thirds of NgR1 were sufficient to confer reovirus binding to (**Fig. III-4C**) and infectivity of (data not shown) CHO cells. These data indicate that NgR1 receptor specificity is conferred in the main LRR body of the protein and that the GPI-CT does not directly mediate reovirus binding, similar to many other ligands of NgR1 (133, 199).

In similar studies, I engineered loss-of-function NgR1 deletion mutants that lack the NT, GPI-CT, LR-CT, or LRR's 1-2, 3-4, 5-6, or 7-8 (**Fig. III-5A**) (**Table III-1**). Following transfection of WT or deletion mutant NgR1 into CHO cells, the cell-surface detection of all deletion constructs was less than that of WT NgR1 (**Fig. III-5B**). However, I found that deletion of the NT domain significantly diminished reovirus binding to cells, deletion of LRR 1-2 or 3-4 allowed moderate reovirus binding to cells, and deletion of more C-terminal domains had little-to-no effect on reovirus binding to cells (**Fig. III-5C**). Similar to results obtained using chimeric-NgR1 receptors, these data suggest that NgR1 C-terminal sequences are dispensable for binding to reovirus and indicate a function for N-terminal sequences in reovirus attachment. These data also suggest that NgR1 deletion constructs are not displayed in a way that can be recognized efficiently by NgR1 affinity-purified antibody. In parallel experiments, I assessed whether NgR1 deletion constructs mediate reovirus infection. Despite some receptors contributing to efficient cell binding, no deletion construct allowed infectivity (**Fig. III-5D**). These data suggest that NgR1 receptor engagement is not sufficient to permit infection and that additional functions of NgR1, contributed by receptor sequence or structural integrity, are required to promote infection.

Elucidation of the NgR1 viral ligand, σ3

To identify the viral ligand for NgR1, we visualized reovirus virions incubated alone or with NgR1 by cryo-EM. We hypothesized that NgR1 binds to a virion conformer of σ1 or σ3. Reovirus virions incubated alone were ~ 650 Å in diameter spherical

**Table III-1: Nogo receptor sequences employed in these studies**

| Receptor construct | hNgR1 a.a | hNgR2 a.a. | Notes |
|---|---|---|---|
| *Wild-type* | | | |
| NgR1 | 1-473* | | |
| NgR2 | | 1-420** | |
| NgR1-myc | 1-473 | | N-term Myc |
| *Glycosylation mutant* | | | |
| NgR1 N82A | 1-473 | | N82A |
| NgR1 N179A | 1-473 | | N179A |
| *Chimeric NgR1/NgR2* | | | |
| NgR1-A | 1-154 | 156-420 | |
| NgR1-B | 155-310 | 1-155,313-420 | |
| NgR1-C | 1-310 | 313-420 | |
| *Domain deletion* | | | |
| NgR1ΔNT | 1-25,58-473 | | |
| NgR1Δ1-2 | 1-57,106-473 | | |
| NgR1Δ3-4 | 1-105,155-473 | | |
| NgR1Δ5-6 | 1-154,203-473 | | |
| NgR1Δ7-8 | 1-202,251-473 | | |
| NgR1ΔCT | 1-259,311-473 | | |
| NgR1ΔGPI-CT | 1-310 | | |

All receptor cDNA sequences were cloned into pcDNA3.1+ (Invitrogen)

Amino acid (a.a.) sequences used from the following reference sequences:

* NgR1: NM_023004 (modified from OriGene SC126683)

** NgR2: NM_178570 (modified from OriGene RG217072)

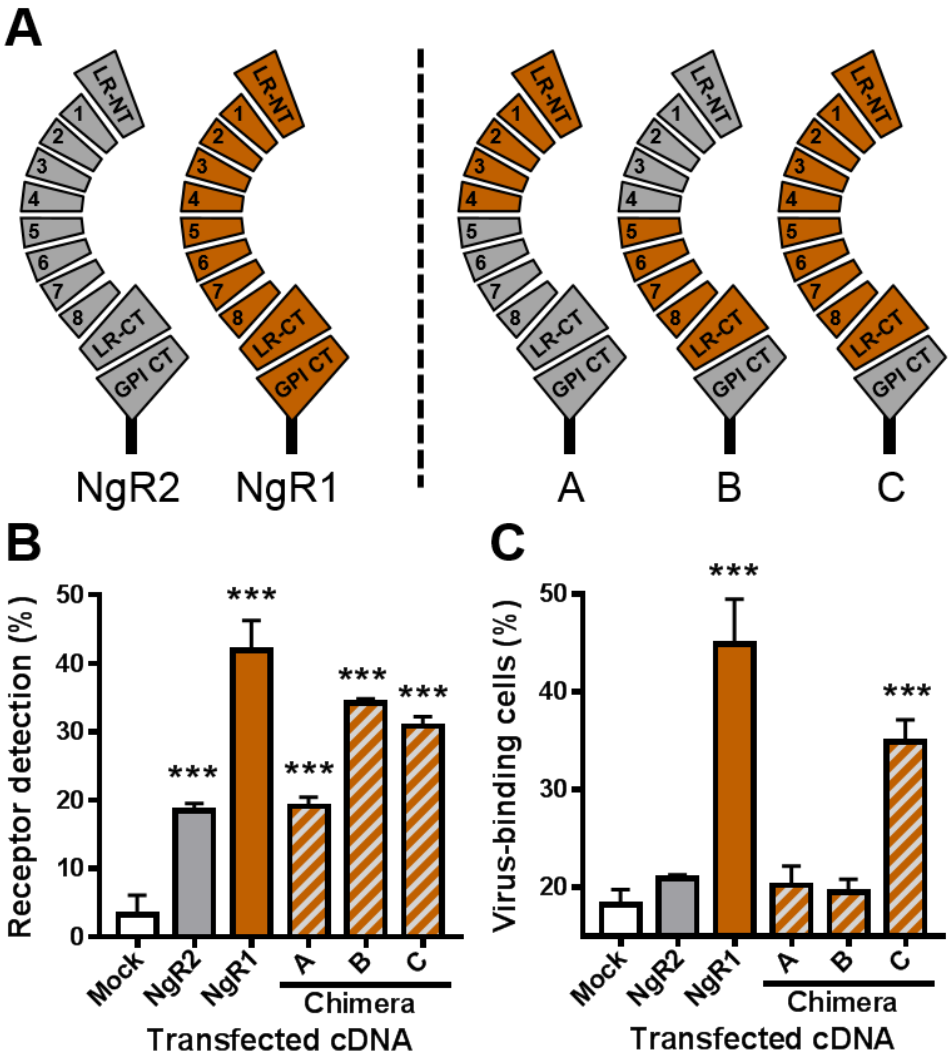


**Figure III-4: NgR1 chimeras reveal N-terminal sequences are sufficient for reovirus binding.** (**A**) Schematics of protein domains for NgR1 (orange), NgR2 (grey), or chimeric proteins (orange and grey) are shown. (**B and C**) CHO cells were either mock transfected or transfected with cDNA encoding NgR1, NgR2, or chimeric NgR1/NgR2 proteins and incubated for 48 h. Cells were treated with antibodies specific for NgR1 and NgR2 prior to adsorption with $10^5$ particles/cell of Alexa Fluor 546-labeled reovirus T3- on ice for 1 h. The percentage of cells either (**B**) expressing receptor or (**C**) bound by virus was determined by flow cytometry. Results are expressed as the mean percentage of positive cells for three independent samples. Error bars indicate SD. Values that differ significantly from mock by one-way ANOVA and Dunnett's test are indicated (*, $P < 0.05$; **, $P < 0.01$; ***, $P < 0.001$).

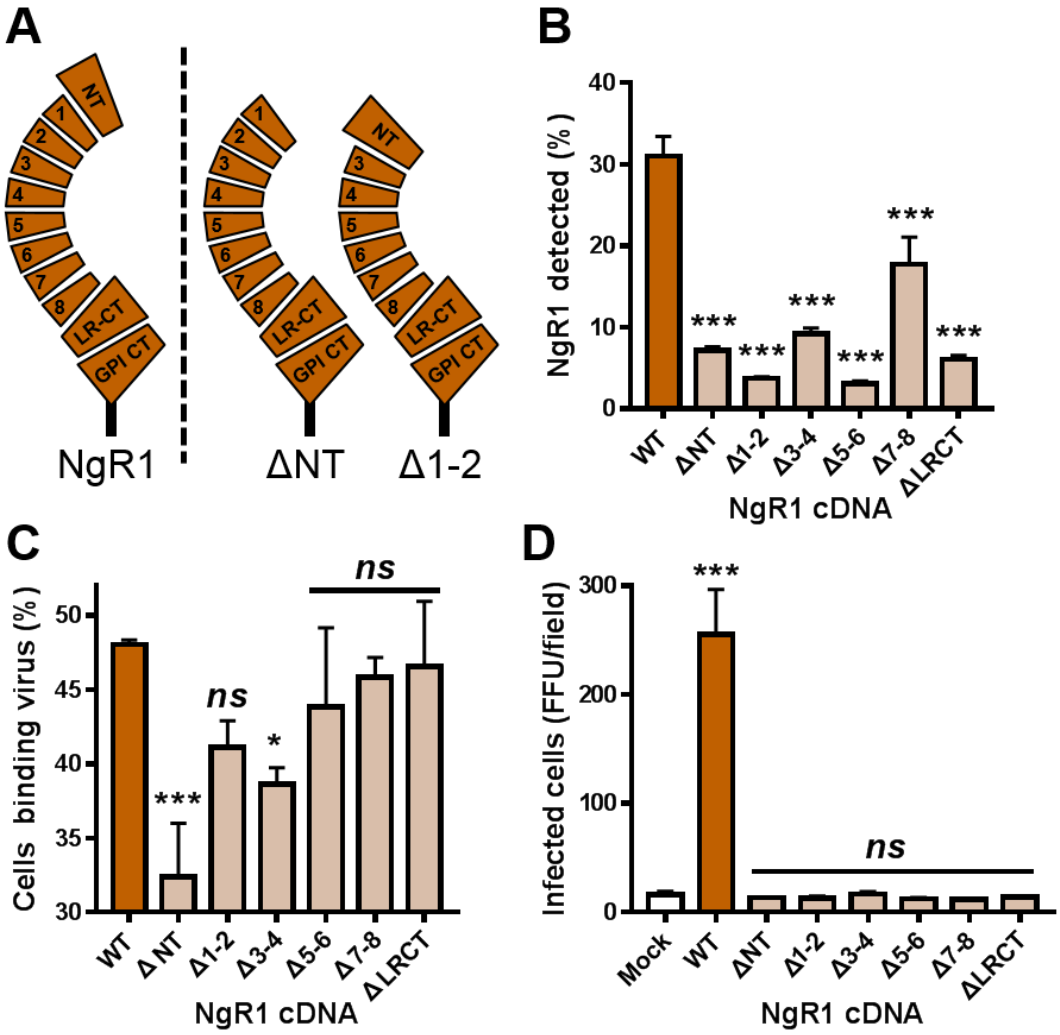


**Figure III-5: NgR1 deletion mutants demonstrate C-terminal sequences are dispensable for reovirus binding but not infectivity.** (**A**) Model of NgR1 deletions. NgR1 domains were sequentially deleted to engineer six unique mutants lacking either the NT domain, LRR 1-2, 3-4, 5-6, 7-8, or the LR-CT. NgR1ΔNT and NgR1Δ1-2 are shown for reference. (**B-D**) Deletions reveal different requirements for binding and infectivity. CHO cells were transfected with cDNA encoding WT NgR1 or the indicated deletion constructs and incubated for 48 h. (**B** and **C**) Cells were treated with NgR1-specific antibody prior to adsorption with $10^5$ particles/cell of Alexa Fluor 546-labeled reovirus T3- on ice for 1 h. The percentage of cells either (**B**) expressing receptor or (**C**) bound by virus was determined by flow cytometry. Results are expressed as the mean percentage of positive cells for three independent samples. (**D**) Transfected CHO cells were adsorbed with 10 PFU/cell of reovirus T3- and monitored for infectivity 24 hpi by indirect immunofluorescence using reovirus-specific antiserum. Results are expressed as the mean FFU/field from 4 fields of view per well in triplicate wells. Error bars indicate SD. Values that differ significantly from WT (**B** and **C**) or Mock (**D**) by one-way ANOVA and Dunnett's test are indicated (*, $P < 0.05$; **, $P < 0.01$; ***, $P < 0.001$). *ns* = not significantly different.

particles (**Fig. III-6A**). In contrast, reovirus virions incubated for 4 h with NgR1 are larger in diameter and display uneven, rough margins (**Fig. III-6A**), indicating that NgR1 binds particles with high occupancy. There are as many as 12 σ1 trimers on reovirus virions and 600 copies of σ3 (61). Collectively, these data suggest that σ3 is the viral ligand for NgR1.

In preliminary cryo-EM experiments intended to optimize the reaction incubation conditions, reovirus was incubated alone or with purified JAM-A or NgR1 for an extended interval ($>$ 48 h). Particles incubated alone or with JAM-A were unchanged, whereas particles incubated with NgR1 under these conditions displayed central lucencies and were sporadically damaged (**Fig. III-6B**). The diminished density of particles incubated with NgR1 for extended intervals resembles genome-less reovirus particles (208). This capsid disruption indicates that NgR1 may function in post-binding disassembly of reovirus particles to mediate capsid release to the cytosol. Further experiments are necessary to determine the effect of NgR1 on reovirus particle stability.

To better visualize the location and orientation of NgR1 on the surface of reovirus particles incubated for short intervals with NgR1, we conducted 3D reconstructions of more than 500 particles incubated alone or with NgR1. In both datasets, particles of approximately equivalent diameter were visualized, suggesting that the extended NgR1 density was lost during reconstructions. However, particles incubated with NgR1 display additional density in pores formed by adjacent $\mu1_3\sigma3_3$ heterohexamers (**Fig. III-7**). At these pseudo six-fold axes of symmetry, a shallow electron density is observed in P2 pores adjacent to λ2, and in P3 pores with continuous density to heterohexamers. These data indicate that NgR1 binds σ3 in shallow pockets of the capsid.

While cryo-EM experiments suggested that σ3 may be the viral ligand for NgR1, the 3D reconstructions obtained thus far are at a resolution too low to demonstrate direct molecular interactions. Furthermore, while the density observed in the P2 and P3 pores is likely NgR1, as it is not detected when particles are incubated with buffer alone, it is not sufficient to model the NgR1 structure with confidence. To confirm that NgR1 and σ3 physically interact, we conducted immunoprecipitation studies using σ3 with soluble NgR1. The σ3 protein expressed alone is prone to aggregation and can form homodimers which bury some surfaces that are normally exposed on virions (209).

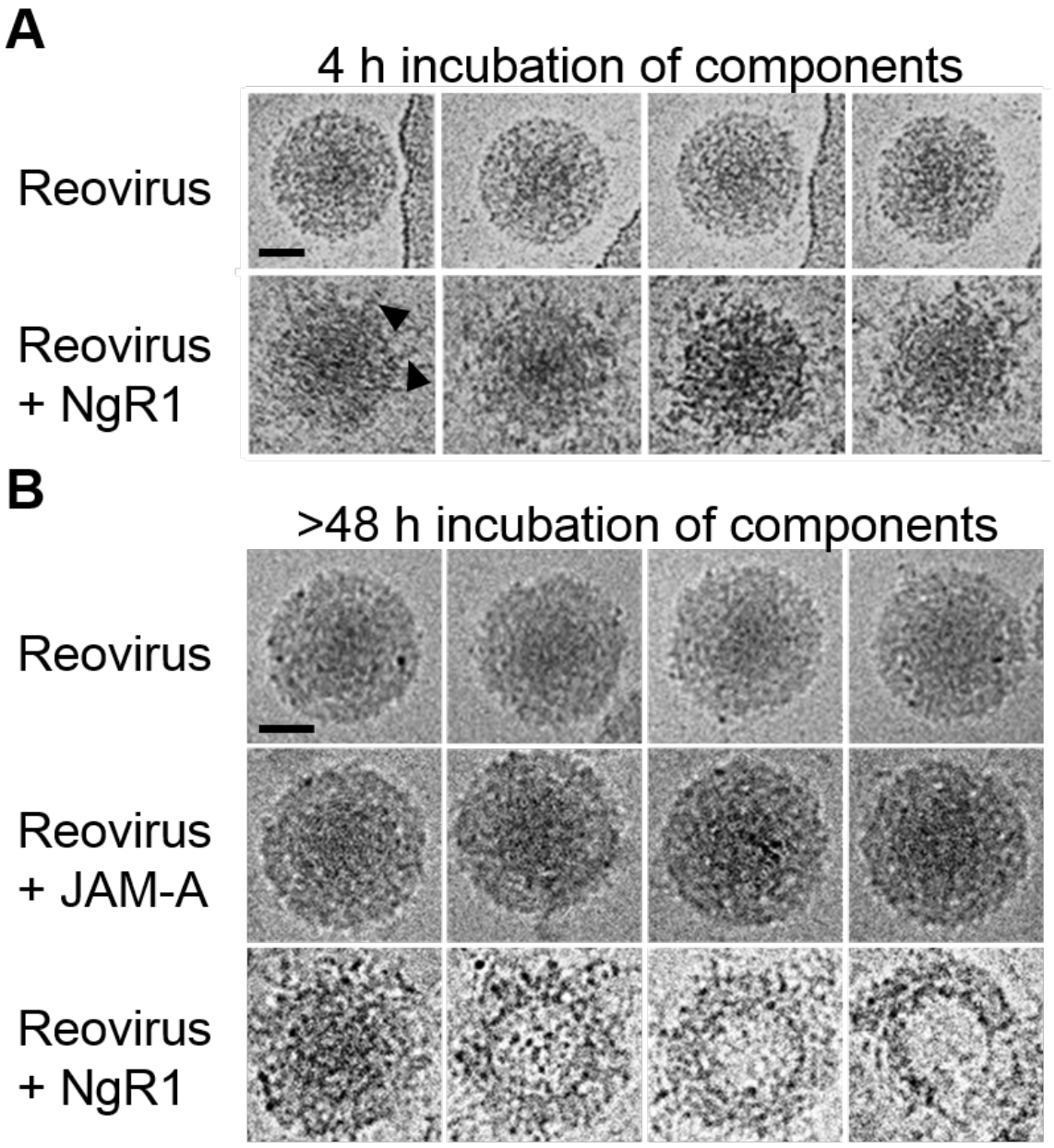


**Figure III-6: NgR1 binds reovirus particles.** Representative cryo-EM images of reovirus particles incubated alone, with JAM-A, or with NgR1 for (**A**) 4h or (**B**) more than 48 h. Receptor to predicted ligand interaction is a 1:5 ratio. Particles visualized at 50K magnification. Scale bar, ~ 200 Å. Possible bound NgR1 molecules are indicated in (**A**) by arrowheads.

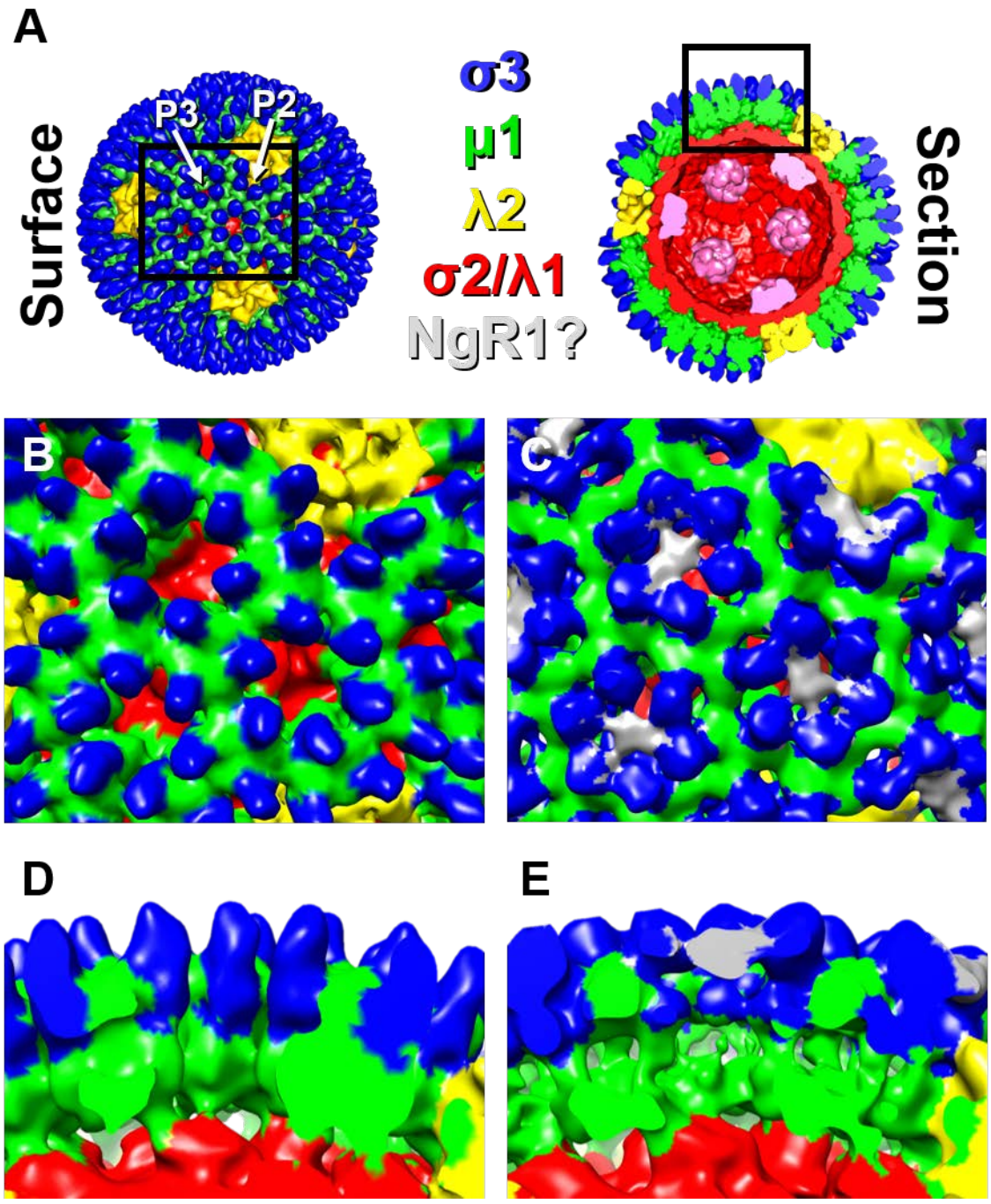


**Figure III-7: Cryo-EM image reconstruction of NgR1 bound to reovirus.** (**A**) Surface and cross-section views of the native reovirus virion (49). Reovirus proteins σ3 (blue), μ1 (green), λ2 (yellow), σ2/λ1 (red), and λ3 (pink) are shown. Representative P2 and P3 pores are marked with arrows. Insets demonstrate approximate regions for panels below. (**B**-**E**) Reovirus virions were incubated alone (**B** and **D**) or with Fc-tagged NgR1 (**C** and **E**) and viewed at the particle surface (**B** and **C**) or via cross-section (**D** and **E**). Particle density is colored to match (**A**). Additional density attributed to NgR1 (grey) is located in P2 and P3 pores (**C** and **E**). (**B**-**E**) Resolution is ~ 16 Å.

Therefore, we first tested binding to stably complexed $\mu1_3\sigma3_3$ heterohexamers. Antibodies directed against σ3 (10C1) or u1 (8H6) were used as positive controls to immunoprecipitate heterohexamers. An irrelevant receptor, coxsackievirus and adenovirus receptor (CAR), was used as a negative control for binding. 10C1, 8H6, and NgR1 efficiently immunoprecipitated heterohexamers, but CAR failed to do so (**Fig. III-8C**). These data support cryo-EM imaging results and demonstrate that NgR1 is capable of binding reovirus outer-capsid proteins.

To determine whether σ3 binds NgR1 in the absence of μ1, we performed additional immunoprecipitations, but used cellular lysates expressing radiolabeled σ3. By adding S4 reovirus cDNA and $^{35}S$ radioisotope to mRNA-depleted rabbit reticulocyte lysates (RRLs), σ3 is the only synthesized protein and can be visualized by phosphor imaging. This technique has been used to express and detect folded σ3 protein on a small scale (210). We assessed whether NgR1, 10C1, or CAR was capable of binding either T1 or T3 σ3 directly. Both NgR1 and 10C1 immunoprecipitated σ3 of either serotype, but CAR did not immunoprecipitate σ3 (**Fig. III-8D**). As NgR1 is capable of mediating both T1 and T3 infection in vitro (98), the serotype-independence of this interaction is not surprising. In addition to full-length σ3, NgR1 also immunoprecipitated lower-molecular weight fragments of σ3, which may be translation-halted σ3 products. However, in addition to the start codon, T1 and T3 σ3 proteins both contain two in-frame, conserved AUG sites, and we suspect that the lower-molecular weight species represent alternate translation initiation ORFs. These data indicate that σ3 is sufficient to interact with NgR1 and suggest that NgR1 binds more C-terminal sequences of σ3.

## Discussion

In this study, I identified NgR1 sequences that mediate binding and infection of reovirus and contributed to the discovery of σ3 as the viral ligand for NgR1. Using on-cell binding assays paired with infectivity assays, I determined that reovirus requires N-terminal protein sequences of NgR1 for efficient binding. Unexpectedly, I found that efficient binding does not strictly correlate with efficient infectivity (**Fig. III-5**). The discordance between these readouts suggests that NgR1 serves post-binding

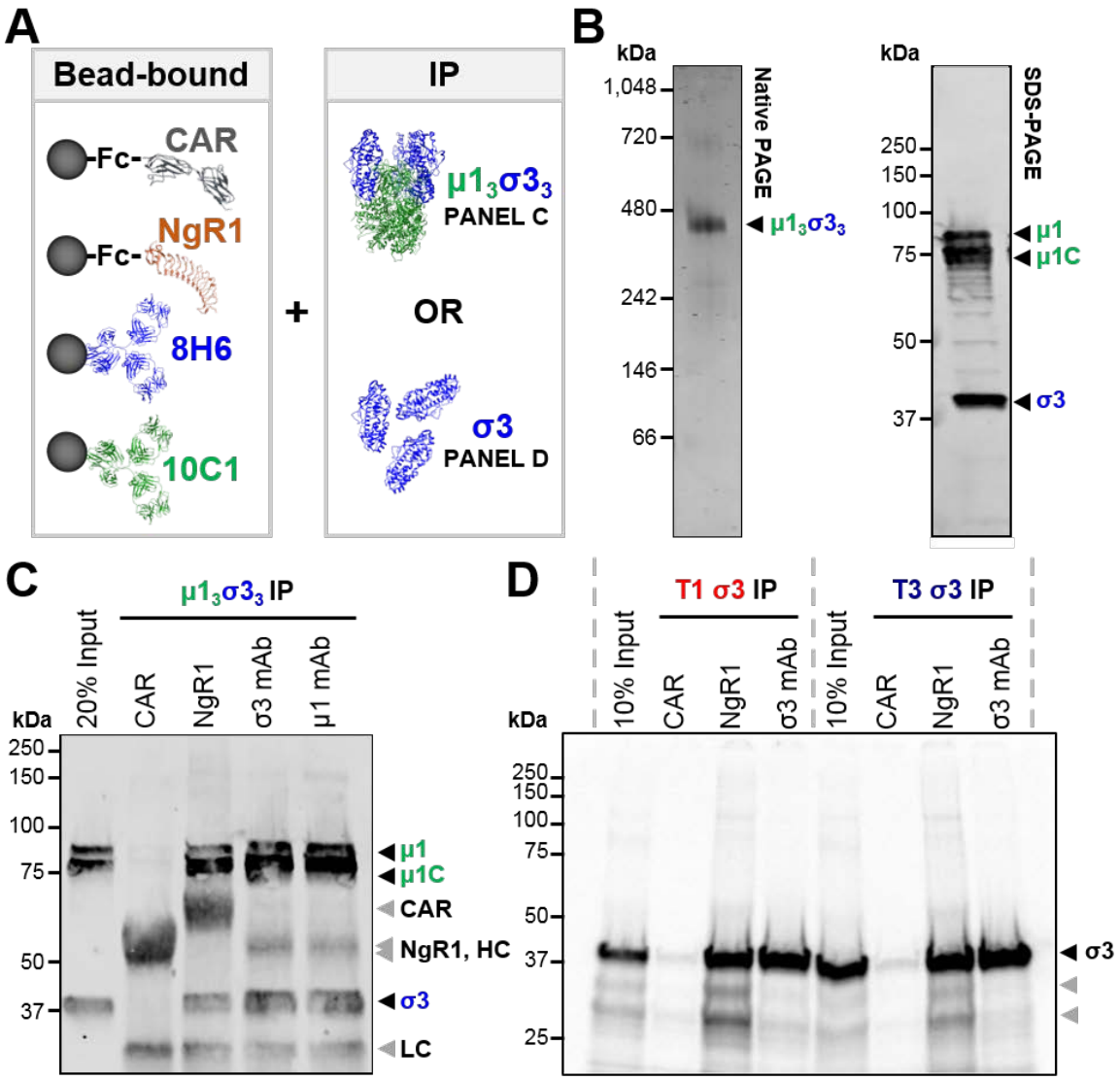


**Figure III-8: NgR1 binds reovirus outer-capsid capsid protein σ3.** (**A**) Diagram of bead-bound and immunoprecipitate (IP) protein schemes used here. Soluble Fc-tagged NgR1 or CAR, or monoclonal antibodies 8H6 (μ1-specific) or 10C1 (σ3-specific) were immobilized onto protein G beads. Protein-conjugated beads were incubated with purified $\mu1_3\sigma3_3$ heterohexamer or cell lysates expressing σ3. (**B**) Purified $\mu1_3\sigma3_3$ heterohexamer was visualized by native PAGE and colloidal blue stain (left panel) or SDS-PAGE and immunoblotting using reovirus-specific antiserum (right panel). (**C** and **D**) NgR1 immunoprecipitates capsid heterohexamer and σ3. Beads were conjugated with the proteins shown and incubated with (**C**) T1L $\mu1_3\sigma3_3$ heterohexamer or (**D**) RRLs expressing radiolabeled T1L or T3D σ3. Following extensive washing, beads were boiled in protein dissociation buffer to release bound protein. Precipitated proteins were resolved by SDS-PAGE and either visualized by (**C**) colloidal blue staining or (**D**) phosphor imaging. Major reovirus species (μ1, μ1-C, and σ3) are labelled with black arrowheads. Other proteins, including antibody heavy (HC) and light chains (LC) and σ3 translation products are indicated by grey arrowheads. Molecular weights (kDa) are shown.

functions (e.g., interacting with coreceptors or mediating conformational change in the capsid) that promote infection. Reovirus particles incubated with NgR1 display short, adhered filaments (**Fig. III-6**), and cryo-EM reconstructions demonstrate an electron density intercalated at the pseudo six-fold axes of symmetry between neighboring σ3 proteins. Further *in vitro* binding studies revealed that NgR1 immunoprecipitates $\mu1_3\sigma3_3$ heterohexamers that form the reovirus outer capsid and directly binds σ3 in a serotype-independent manner (**Fig. III-8**). While there have been suggestions that capsid components other than σ1 can contribute to cell binding (78, 79, 211), we provide the first direct evidence of an underlying interaction.

NgR1 interacts with a structurally heterogenous family of ligands and coreceptors to modulate axonal outgrowth (200-207). The central, conserved sequences of the LRR concave surface of NgR1 are required for many contacts with ligands and coreceptors (133). Similarly, we identified through three independent genetic approaches that N-terminal sequences of NgR1 in the central LRR core contribute to efficient binding of reovirus. NgR1 molecules tagged at the N-terminus are significantly less efficient at ligating reovirus. Using gain-of-function NgR1 constructs, I demonstrated that the central core of NgR1 is sufficient to allow reovirus binding and infection when adjoined to sequences of NgR2 (**Fig. III-4**). Studies using NgR1 deletion mutants also indicate that residues more C-terminal of the fourth LRR may be dispensable for ligating reovirus. However, a chimera expressing NgR1 sequences more N-terminal to this site is not sufficient to allow reovirus binding. These data highlight the power of complementary genetic approaches to identify sequences important for molecular interactions and demonstrate that membrane-distal sequences of NgR1 likely bind reovirus.

Following receptor engagement, virus structural proteins often undergo conformational changes that allow interactions with the cell membrane or promote signaling events essential for internalization. During infection of cultured cells, reovirus virions undergo acid-dependent proteolytic processing by host cathepsins. This process removes the σ3 protein and reveals the underlying membrane-penetrating μ1 protein. To my knowledge, no σ3 conformational changes have been reported for native protein in the absence of proteases. However, mutations identified in σ3 contribute to structural

changes and enhanced disassembly and infection efficiency (212-215). In preliminary experiments, we discovered that prolonged incubation of NgR1 with reovirus particles results in particle destabilization (**Fig. III-6B**) and even enhanced infectivity (216). While it has not been tested directly, these data suggest a function for NgR1 in σ3 structural rearrangements or capsid disassembly.

The mechanism of NgR1-dependent internalization is not known. As NgR1 lacks a cytoplasmic domain and is incapable of initiating signaling on its own, it is likely that NgR1 engages other cell-surface receptors to allow reovirus infection. Specialized dynamic membrane domains called lipid rafts recruit and concentrate specific lipids, proteins, and glycans and function in internalization of many viruses, including multiple *Reoviridae* family members (217, 218). NgR1 preferentially distributes to lipid-rafts, similar to many other GPI-anchored proteins, and at these sites, NgR1 may coordinate interaction with coreceptors. I found that binding to NgR1 may not be sufficient to permit reovirus infection. Using on-cell binding assays, I determined that expression of C-terminal NgR1 deletion mutants and the NgR1-N82A glycosylation mutant facilitate similar levels of virus binding relative to WT NgR1 but permit significantly less infection (**Fig. III-3** and **III-5**). While these studies should be confirmed using direct *in vitro* binding to modified NgR1 constructs, these data suggest that NgR1 serves post-binding functions. I hypothesize that reovirus binding to NgR1 leads to recruitment of coreceptors that mediate reovirus endocytosis at lipid rafts. Future studies will identify the coreceptors and other cellular factors that promote NgR1 receptor-mediated endocytosis.

We determined that NgR1 binds σ3, however, the affinity of this interaction is unknown and it is not clear whether NgR1 simultaneously interacts with other viral capsid components to mediate infectivity. EM reconstructions of reovirus incubated with NgR1 reveal density in the P2 and P3 pores formed by the reovirus outer capsid. However, at the resolution of these reconstructions (~ 16 Å), molecular contacts cannot be identified and the majority of the NgR1 fusion protein incubated with reovirus particles is lost during averaging. NgR1 density may be missing due to: 1) incomplete occupancy of pores, 2) asymmetry of binding, or 3) a flexible binding interaction. The NgR1 fusion protein used in these studies may be contributing to one or more of these

possibilities. Here, the full NgR1 protein (a.a. 27-447) was fused to a rabbit Fc by a flexible linker. Fc domains participate in homodimerization, and the NgR1 GPI-CT domain is thought to be highly flexible relative to the central LRR protein domain (129, 219). This combination of multimeric complexes and flexibility are not conducive to traditional averaging techniques. To address these problems, I engineered a truncated, His-tagged construct of NgR1, which is currently being assessed for binding to reovirus particles by cryo-EM. NgR1 sequences of the GPI-CT are not required to promote reovirus binding and internalization (**Fig. III-4**) and I confirmed that truncated NgR1 lacking the GPI-CT (a.a. 27-310) is sufficient to immunoprecipitate reovirus (data not shown).

Independent of the construct used, NgR1 binding to σ3 may be impossible to effectively image by icosahedral averaging. Assuming NgR1 binds in the P3 pore, and using molecular modeling of NgR1 with σ3, I hypothesize that the NgR1 surface could interact with one or two σ3 monomers in a P3 and, due to steric hindrance, only one NgR1 may bind per pore (**Fig. III-9**). NgR1 could then select from three or six identical binding sites per P3 pore, making it impractical to use single-particle cryo-EM to determine the structure of the complex. Therefore, in tandem to modifying conditions of the cryo-EM experiments using whole virus particles, it is reasonable to pursue other strategies to identify residues required for ligand-receptor binding. NgR1 bound to purified heterohexamers could be visualized by either cryo-EM or crystallography. Recent advances in single-particle cryo-EM allow crystallographic resolution without many of the limitations of traditional crystallography (220). The molecular weight and uniformity of the $\mu1_3\sigma3_3$ complex are amenable to cryo-EM, and if NgR1 does not bind $\mu1_3\sigma3_3$ with full occupancy, class averaging could distinguish complexes bound to one, two, or three copies of NgR1.

Data presented in this chapter identify both viral and receptor sequences required for critical steps in reovirus infection. By genetically manipulating NgR1, I determined that N-terminal sequences are necessary for interaction with reovirus. Complemented with cryo-EM image reconstructions and an understanding of NgR1 presentation on the cell surface, these data are compatible with a new model of NgR1-dependent reovirus infection (**Fig. III-9**). Membrane-distal NgR1 sequences would be

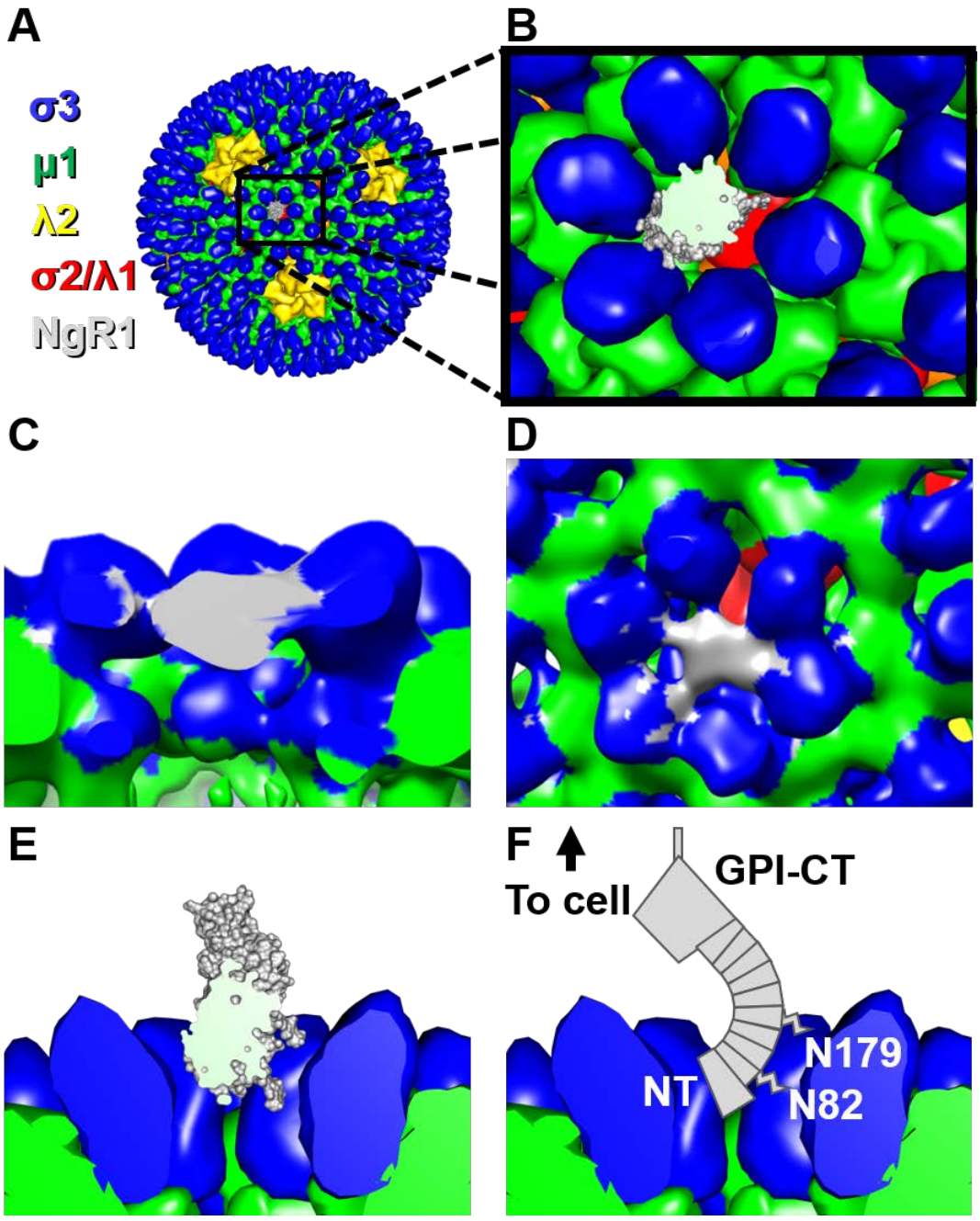


**Figure III-9: Proposed model of NgR1 binding to reovirus.** (**A**) Surface view of the native reovirus virion (49). Reovirus proteins σ3 (blue), μ1 (green), λ2 (yellow), and σ2/λ1 (red) are shown. NgR1 (grey) (219) is modeled into a representative P3 pore. Box shows location of inset for panel (**B**). (**B** and **D**) Surface view or (**C** and **E**) cross-section of either single-particle cryo-EM data (**C** and **D**) or NgR1 modelled with native reovirus particle (2CSE) (**B**, **E**). (**F**) Schematic of NgR1 orientation shown in (**E**) with the NgR1 GPI-CT, NT, and glycosylation sites N82 and N179 annotated. Cell membrane is not shown.

the first to encounter virus and embed within pores of the outer-capsid. This interaction could even promote early steps in particle disassembly, thereby promoting μ1 interaction with cellular membranes and advancing the infectious cycle.

# CHAPTER IV

# SUMMARY AND FUTURE DIRECTIONS

## Thesis Summary

All viruses must overcome an initial, critical barrier to succeed in infection: the cell membrane. For nonenveloped viruses in particular, understanding the cascade of molecular interactions between virus and host that allows infection is an area of important research with many translational applications. Often, several receptors are engaged by the same virus on different cells to coordinate dissemination to sites distant from inoculation or on the same cell to enhance entry efficiency and modulate signaling events. As the first step in the viral life cycle, receptors serve multiple critical functions in the viral replication cycle, dictating species and cell tropism and governing disease type and severity. Therefore, viral receptor interactions are attractive targets for prophylactic and therapeutic intervention. Indeed, several clinically implemented antivirals inhibit receptor binding for significant human pathogens like human immunodeficiency virus (HIV), respiratory syncytial virus (RSV), influenza virus, and HSV.

However, therapies for viral disease in the CNS remain limited, and treatment plans often consist entirely of supportive care. This therapeutic paucity is in part due to the intrinsic complexity of the CNS, which, in healthy individuals, selectively regulates molecule uptake and is resistant to entry of many drugs. Understanding interactions that permit initial viral entry into the CNS and promote replication in the brain is essential to prevent and treat these serious and often life-threatening infections. The primary goal of the research presented in this thesis was to identify viral and host sequences that mediate neuroinvasion by studying the reovirus-receptor interface during infection of discrete cell populations within the CNS.

Reoviruses display serotype-dependent tropism and disease in the CNS of many young mammals, a property that has been attributed to the σ1 viral attachment protein. The σ1 protein is structurally organized into head, body, and tail domains that display distinct functions. However, the specific protein sequences and coordinating functions that mediate serotype-dependent neurotropism were unclear. Using reverse genetics, I

engineered a panel of chimeric σ1-expressing reoviruses to identify sequences that contribute to infection in the CNS. I discovered that sequences forming the globular σ1 head domain dictate viral tropism, replication capacity, and virulence in the CNS of mice. These studies further revealed that homologous protein domains coordinate serotype-dependent phenotypes. Thus, my work contributes new knowledge about mechanisms of neuroinvasion and will enhance the rational design of reovirus oncolytic therapeutics.

In Chapter III of my thesis, I elucidated viral and host sequences required for reovirus engagement of the neuronally expressed receptor, NgR1. I found that N-terminal protein, and not glycan, residues of NgR1 are required for reovirus binding and infection. In collaborative studies, I determined that NgR1 directly binds viral outer-capsid protein σ3. Unexpectedly, I discovered that enhanced binding to NgR1-construct-transfected cells does not strictly dictate infection, suggesting that post-binding steps are mediated by NgR1 to facilitate productive infection. Collectively, studies presented in Chapter III enhance our understanding of how reovirus and NgR1 interact to promote infection and raise new and interesting questions about this binding event and steps facilitated thereafter.

## Future Directions

Determine function of the σ1 head domain in neuron binding and tropism

The σ1 head domains of both T1 and T3 σ1 dictate infection of their respective target cell types in the CNS. However, the mechanism of this interaction, and direct evidence of it, has remained elusive. Early studies report differential binding of T1 (85) and T3 (86) strains to neurons and ependyma and used S1 single-gene reassortant viruses to conclude that the viral attachment protein dictates differential binding to target cells. Furthermore, the authors predict that these binding differences dictate infection of these cells. It is important to test this hypothesis with σ1-chimeric reoviruses.

To determine whether the neural tropism of T3-σ1-head-containing viruses correlates with enhanced binding to neurons, several methods could be used. Systems to culture primary embryonic mouse and rat neurons for reovirus infection are well-established and these cells display predicted serotype-specific patterns of infection (**Fig.**

**II-6**) (27, 98). Binding to in-plate cultured neurons could be assessed. Alternatively, brain slice cultures (221) or synaptosomes could be bound with reovirus and analyzed by microscopy or flow cytometry, respectively. In contrast to neurons, which are not amenable to flow cytometry, sub-cellular synaptosome fractions can be analyzed by flow cytometry, which would enable identification of receptors present on fractions binding more virus. Furthermore, reovirus (124) and many other viruses (222) are thought to enter neurons at the synapse and these subcellular fractions may concentrate T3-specific receptors.

Unlike for T3 reovirus, serotype-specific model systems of T1 ependymal cell infection are not established. Cultured primary ependymal cells undergo autotomy, shed cilia, differentiate, and die. However, they remain viable *in vitro* for short intervals that might allow reovirus binding and infectivity studies (223). Alternatively, a number of ependymoma cell lines are available (224, 225), and the BXD-1425EPN ependymoma cell line is susceptible to T1+ infection (101). The capacity to infect these cells should be assessed using T1 and T3 glycan-blind viruses to identify a model system of T1-specific infection. Furthermore, once a model system is established, the contribution of T1-specific glycans and other receptors can be more directly assessed. It is possible that the T1 σ1 head domain mediates infection of ependymal cells by binding GM2 attached to proteins or lipids and that T1- virus retains some residual binding to this receptor. Evidence that may support this hypothesis is the diminished, but significant, infection that T1- establishes in BXD-1425EPN cells (101). Alternatively, it is possible that sequences in the T1 σ1 head domain mediate binding to an ependymal receptor at a site distinct from GM2 glycan-binding sequences.

Identify ependymal and neuronal receptors

It is possible that currently known receptors may be coordinating unknown functions in neural and ependymal tropism. Alternatively, there may be additional key receptors that dictate infection of discrete CNS cell types. A variety of strategies have been used in attempts to identify ependymal and neuronal receptors used by reovirus. These techniques include bioinformatic expression analyses, glycan microarrays, screens of cDNA libraries from NT2 cells and JAM-A$^{-/-}$ mouse brain, and genome-wide

siRNA and CRISPR screens using cultured cells. Despite extensive efforts, T1 receptors used on ependyma and T3 receptors used on neurons are not known. A few potential reasons why these techniques have not been successful thus far are that the cell-surface receptor is displayed in low abundance or not expressed in the model system, tissue-specific post-translational modifications in the receptor are required for infection, or ligation of multiple receptors is required for entry. Furthermore, cell lines may not recapitulate the complexities of primary neural and ependymal tissue, both of which are challenging to culture and scale for *in vitro* screens. Recent advances in model systems, including microfluidic systems, iPS cells, co-culture systems, and organoid models, should allow enhanced exploration of reovirus receptor use and entry mechanisms in systems that better recapitulate *in vivo* conditions. Furthermore, chimeric σ1 proteins can be used in affinity purification methods to identify glycan-independent receptors. T3 Head and T1 Body viruses do not engage any known glycans and can be used as affinity ligands.

Identify non-receptor-mediated determinants of tropism

It is possible that σ1-head domain determinants of tropism occur independent of receptor use. Following inoculation in the footpad with $10^7$ PFU of T1, T2, or T3 reovirus, viral antigen is detected in peripheral motor and sensory neurons in newborn mice (124). T1 and T2 infection of motor neurons and interneurons is limited, but infection of sensory neurons, is comparable to T3 reovirus (124). Furthermore, reovirus entry is dependent on functional microtubules (226), and trafficking to the CNS from peripheral infection also requires functional microtubules in a fast-axonal transport mechanism (80). Molecular details of reovirus fast-axonal trafficking are not known, but it is possible that the σ1 head domain mediates a post-binding function in tropism by engaging transport molecules that direct virus to productive (T3) or non-productive (T1) endocytic pathways in neurons. The σ1 protein is shed in late endosomes during reovirus uncoating, and therefore, I do not think that sequences in the σ1 head domain could contribute to post-entry-dependent mechanisms of serotype-specific infection observed in the CNS. It would be informative to quantify reovirus binding, internalization, and trafficking in cultured motor and sensory neurons to define the step

at which T1 and T3 reoviruses differ. It should be noted that reovirus on-cell binding is not sufficient for infection (**Fig. III-5**). Early studies demonstrating differences in reovirus binding to neurons did not exclude SA-dependent binding (86) and SA binding is not required for infection of neurons (**Fig. II-6**). Therefore, binding to neurons may not be indicative of the capacity to efficiently infect neurons. Similar studies should be conducted to precisely identify the block to T3 infection of ependymal cells, once these T1-specific systems have been established.

Design and test improved reovirus oncolytics

Only one strain of reovirus, T3D, is currently being assessed for the treatment of human cancers. Heterogeneity from natural or engineered reovirus isolates could improve oncolytic efficiency. Several aspects of reovirus biology are governable, including virion stability (96, 227), interaction with immune cells (228), cell targeting, immune stimulation or evasion (229-231), replication efficiency (173, 175), cell-death induction (172, 232), and more. In particular, reovirus receptor use should be manipulated to improve viral targeting to specific tumor biomarkers.

Here, for the first time, we have engineered a reovirus capable of binding both T1 and T3 glycans (T3 Body) (**Fig. II-3**). The exchange of T1 for T3 σ1 body sequences allows synergistic binding efficiency of T3 Body to erythrocytes (**Fig. II-3**) and even confers replication in MEL cells (data not shown), which are normally not susceptible to T1 reovirus infection (50). This gain-of-function is a proof of concept that σ1 chimeric viruses, and other new strains presented here, should be implemented in pre-clinical studies to assess relative targeting and oncolytic capacity for a battery of transformed cell lines. Promising oncolytic candidates should then be accelerated to clinical trials to assess safety and efficacy in combination therapies.

Elucidate the function of NgR1 in tropism and disease

Blockade or ablation of murine NgR1 inhibits reovirus infection of cultured cortical neurons (98). However, preliminary data from experiments with mice deficient for NgR1 ($NgR1^{-/-}$) suggests that NgR1 is not a major contributor to T3 replication in the brain, and $NgR1^{-/-}$ mice still succumb to lethal T3 infection (233). These data indicate that

neuronal infection and inflammation still occur in NgR1$^{-/-}$ mice, although more detailed studies should be performed to determine the extent of reovirus tropism and disease. It is possible that NgR1 functions as a receptor in discrete neuronal populations. Moreover, NgR1 is expressed in several non-neural tissues (196). To elucidate whether NgR1 functions in tropism and pathogenesis, cohorts of WT and NgR1$^{-/-}$ mice should be inoculated by peroral, footpad, and intracranial routes with T1 and T3 strains. Viral titer, lethality, and tropism should be assessed in several tissues to determine if and where NgR1 contributes to pathogenesis. It is possible that a function for NgR1 will not be found in these studies. If that is the case, a pilot experiment using mice ablated for NgR1, NgR2, and NgR3 (NgR1$^{-/-}$/NgR2$^{-/-}$/NgR3$^{-/-}$) (199) should be performed to rule out complementary receptor use. While NgR2 does not function as a reovirus receptor following transfection into CHO cells (**Fig. III-1**), NgR2 and NgR3 display some functional redundancy with NgR1 (198, 199) and may contribute to reovirus replication or pathogenesis in mice.

<u>Characterize the importance of NgR1:reovirus interactions in oncolytics and neuronal plasticity regulation</u>

Independent of NgR1 function in reovirus tropism and pathogenesis in mice, studies presented in Chapter III inform two important fields of study: viral oncolytics and neuronal plasticity. NgR1 was first identified as a reovirus receptor in an immortalized cell line originating from a cervical cancer and is expressed by several transformed cell lines (234). All studies presented in this dissertation used a human isotype of NgR1 (hNgR1). Transfection of cDNA encoding murine NgR1 (mNgR1) into CHO cells or MEL cells does not result in productive infection (data not shown) for unknown reasons. It may be that hNgR1 serves as a reovirus receptor and mNgR1 does not, due to sequence polymorphisms between the two molecules. However, studies using cortical neurons cultured from NgR1$^{-/-}$ mice and blockade of mNgR1 on WT neurons (98) suggest a function for mNgR1.

NgR1 expression should be profiled for human tumors and cancer cell lines to identify whether titration of NgR1 expression influences reovirus oncolysis. Furthermore, reovirus or reovirus capsid subunits should be assessed in competition assays with

known NgR1 ligands. These studies could provide clues about structural interactions of reovirus and NgR1. Moreover, interruption of NgR1-mediating signaling can improve disease progression or outcome for several neuropathies. Studies presented here may illuminate therapeutic options for scientists studying various NgR1-influencing maladies, such as spinal crush injury, Alzheimer's disease, or multiple sclerosis.

Identify mechanisms of NgR1-depedent reovirus internalization

Much remains to be learned about how NgR1 permits reovirus infection. In studies described in Chapter III of my thesis, I found that binding to NgR1-expressing cells was not sufficient to permit reovirus infection (**Fig. III-5**), suggesting that NgR1 serves post-binding functions. NgR1 lacks a cytoplasmic domain and therefore is not predicted to initiate intracellular signaling events alone. To modulate axonal plasticity, NgR1 recruits a complex of coreceptors that either directly mediate (201, 203, 235) or enhance (202, 205) intracellular signaling. I hypothesize that NgR1 structural changes induced by deletions may allow NgR1 binding to reovirus but prevent interaction with co-receptors important for reovirus internalization. It would be informative to assess whether known coreceptors of NgR1 are expressed in CHO cells and whether these receptors influence reovirus entry.

Previous proteomic analyses have identified that at least one NgR1 coreceptor, p75, is expressed in CHO cells (236). Using siRNA knockdown, dominant-negative constructs, or chemical inhibitors, where appropriate, the contribution of p75, TROY, Lingo-1, and Amigo3 to reovirus infectivity of CHO cells and neurons should be defined. In parallel experiments, over-expression of NgR1 co-receptors in CHO cells may demonstrate enhanced infectivity and provide an alternative method to identify functional coreceptors. Membrane distribution of NgR1 and co-receptors should be visualized before and after reovirus binding to identify whether recruitment to specific membrane microdomains occurs. If reovirus infection is not altered by disruption or overexpression of the most well-characterized coreceptors of NgR1, others could be assessed, or an unbiased cross-linking approach or immunoprecipitations could be used to identify components of a receptor complex.

Receptors often effect structural changes in capsid or envelope proteins to promote viral entry. NgR1 may modulate the stability of reovirus particles (**Fig. III-6**) by binding and destabilizing σ3. The effect of NgR1 on reovirus virion stability should be assessed *in vitro* and *in situ*, by quantifying production of reovirus disassembly intermediates incubated with soluble NgR1 or NgR1-expressing cells, respectively. NgR1 deletion mutants that contribute to reovirus binding but not infectivity (**Fig. III-5**) also could be assessed, as these differences may be dictated by a failure of NgR1 to mediate structural rearrangements of σ3.

Reovirus can use several methods of entry (57, 58). However, mechanisms of neuronal and NgR1-dependent entry are not known. To my knowledge, NgR1 is not thought to be internalized following receptor-ligand interactions in the CNS. A functional truncation peptide of Nogo-A is internalized into neuronal cells via a macropinocytosis-dependent uptake into signalosomes that mediate RhoA activation (237). However, this mechanism occurs independently of NgR1 expression (237). Therefore, it is important to define reovirus uptake mechanisms and determine whether these internalized components mediate signaling events.

Assess whether NgR1 is used by other neurotropic reoviruses

Baboon orthoreovirus (BRV) is a fusogenic orthoreovirus that initiates lethal meningoencephalitis in baboons (33, 238). While BRV virions are structurally similar to reovirus (239), they lack a σ1-equivalent fiber protein. Receptors for BRV have not been reported. However, the σ3 homolog of BRV (σB) has been implicated as a potential ligand for receptors (239), due to its high-copy number and surface exposure. NgR1 should be assessed for the capacity to mediate infection of BRV and the related human pathogen, Colorado tick fever virus.

## Conclusions

The work presented in my thesis has generated new knowledge about determinants of reovirus tropism, neuroinvasion, and disease. Studies presented here establish important strategies and tools to identify the precise mechanism of reovirus-mediated neuropathogenesis. Collectively, results presented here enhance our

understanding of viral pathogenesis and inform diverse fields of study ranging from oncolytic therapeutics to interventions for several neuropathies.

# CHAPTER V

# MATERIALS AND METHODS

## Cells and antibodies

Spinner-adapted L929 fibroblasts were maintained in Joklik's minimal essential medium (JMEM) supplemented to contain 5% fetal bovine serum, 2 mM L-glutamine, 100 U/ml penicillin, 100 µg/ml streptomycin, and 0.25 µg/ml amphotericin B. BHK-T7 cells were maintained as previously described (46). CHO K12 (ATCC CCL-61) cells were maintained in F12 medium (DMEM; Gibco) supplemented to contain 10% FBS, 100 U/ml penicillin, 100 µg/ml streptomycin, and 0.25 µg/ml amphotericin B. High Five insect cells (ThermoFisher, B85502) were maintained in Express Five (ThermoFisher, 10486025) serum-free medium and cultured at 27°C.

Reovirus-neutralizing antibodies 5C6 (240) and 9BG5 (241) were purified from hybridoma cell supernatants using protein G chromatography (GE Healthcare) (94). Hybridoma cell lines are deposited at the Developmental Studies Hybridoma Bank (Iowa City, IA, USA). Reovirus polyclonal serum was collected from rabbits immunized and boosted with reovirus strain T1L or T3D. Sera from T1L- and T3D-inoculated rabbits were mixed 1:1 (vol:vol) and cross-adsorbed on L929 cells to deplete non-specific antibodies. NgR1- and NgR2-specific antibodies were affinity-purified from goat polyclonal antiserum (AF1208 and AF2776, respectively; R&D Systems) and used at 0.1 µg/mL for immunoblot and flow cytometry experiments. Tubulin β 3 (TUBB3)-specific antibody was used to detect neurons (801201; BioLegend). Mouse monoclonal antibody DM1A was used at a 1:2000 dilution to immunoblot for α-tubulin. Mouse monoclonal antibodies 8H6 (σ3-specific) (242) and 10C1 (µ1/µ1δ-specific) (240) were used in NgR1 immunoprecipitation studies. Purified mouse monoclonal recognizing the human c-Myc epitope (EQKLISEEDL) was used at a 1:8000 dilution (clone 9B11; Cell Signaling Technology). All primary and secondary antibodies (Licor) were diluted in TBS-T for immunoblot studies.

## Viruses

All viruses were recovered using plasmid-based reverse genetics (3, 46) to contain nine gene segments from reovirus strain T1L (46) and a unique S1 gene.

Unique S1 gene sequences are published with NCBI. The S1 gene of T1+ is of strain T1L. T1- differs from T1+ at two point-mutations (S370P and Q371E) (101). The S1 gene of T3+ was designed to express the same primary protein sequence of strain T3C44-MA and was engineered by site-directed mutagenesis of cDNA encoding strain T3D S1 (accession no. EF494441) to encode five σ1 polymorphisms (V22I, I88T, I246T, T249I, and T408A) (182) and one σ1s polymorphism (P70S). T3- differs from strain T3+ at a single polymorphism (P204L).

T1 Head, T1 Tail, and T3 Body S1 genes were synthesized (GenScript) with a 5' T7 promotor site and 3' sequences encoding an HDZ ribozyme and initially packaged in the pUC57 vector by Xba1 flanking sequences. Genes and flanking sequences were excised by restriction-enzyme digest (Xba-I-HF; NEB) and subcloned into existing Xba1 sites of pBacPak8 (Clontech).

T3 Head and T3 Tail S1 genes were engineered by sticky-ended cloning of T3 S1 sequences into modified T1L-S1-pBacPak plasmids (modified from (46)). A 5' NcoI and a 3' NheI site were engineered by site-directed mutagenesis into T1L-S1-pBacPak. Primers encoding terminal NcoI or NheI sequences were used to amplify heterologous cDNA fragments of the T3+ S1 sequence. T1L sequences of the σ1 head or tail regions of S1 were excised by restriction enzyme digestion and replaced with PCR-amplified and NcoI/NheI-digested linear cDNA fragments encoding the T3+ σ1 head or tail. NcoI and NheI restriction sites in the newly-created chimeric gene were reverted to intended protein-coding sequence by site-directed mutagenesis.

The T1 Body S1 gene was engineered similar to T3-Head and T3-Tail S1 genes, in that NcoI and NheI sites were introduced in the T3+-pBacPak plasmid and T3+ sequences corresponding to a body domain were excised by restriction enzyme digest and replaced using sticky-ended addition of T1-body sequences. However, T1-Body sequences were synthesized (GenScript). NcoI and NheI sites of the chimeric gene were removed by site-directed mutagenesis.

Virus was purified from infected L929 cells by cesium chloride gradient centrifugation (48), and viral titers were determined by plaque assay (242) or fluorescent focus unit assay using L929 cells (described below). Particle number was estimated by spectral absorbance at 260 nm (1 $OD_{260}$ = $2.1 \times 10^{12}$ particles/mL).

Reovirus virions were labeled with succinimydl ester Alexa Flour 546 (Invitrogen) to generate directly fluoresceinated particles.

### Quantification of σ1 abundance in virions by colloidal-blue stained acrylamide gels

Purified reovirus particles ($5 \times 10^{10}$) were incubated 1:1 (vol:vol) with 2X laemmli sample buffer containing 5% β-mercaptoethanol at 95° for 5 min and electrophoresed in 16-cm long 10% polyacrylamide gels under laemmli buffer using the Protean II Xi system (Bio-Rad) at room temperature for 6 h at 37 mA. Gels were stained with colloidal blue (Invitrogen) and scanned using an Odyssey CLx imager (LI-COR) at 700 nm λ. Optical density (OD) of bands corresponding to σ1 and μ (includes μ1, μ1C, and μ2) proteins were quantified using ImageStudio software (LI-COR). Relative OD of σ1 was calculated per gel using the equation: Relative $OD_{\sigma1} = [(\sigma1_x - \sigma1_{blank}) \div (\sigma1_{max} - \sigma1_{blank})] \times 100$, where raw OD values are reported for experimental lanes ($\sigma1_x$), lanes containing the maximum σ1 intensity measured per gel ($\sigma1_{max}$), and for lanes measured at the same relative electrophoretic mobility in the gel where virus was not loaded ($\sigma1_{blank}$). Relative OD for μ ($OD_\mu$) was calculated similarly. Normalized σ1 per virus = relative $OD_{\sigma1} \div$ relative $OD_\mu$.

### Assessment of reovirus replication by plaque assay

L929 cells ($2 \times 10^5$) were adsorbed with reovirus in Dulbecco's phosphate-buffered saline (PBS) at an MOI of 0.5 PFU/cell at 37°C for 1 h, washed with PBS, and incubated in 1 mL of fresh medium. At various intervals, cells were frozen and thawed twice before determination of viral titer by plaque assay using L929 cells. Viral yields were calculated using the equation: $\log_{10}(\text{PFU/mL})t_x - \log_{10}(\text{PFU/mL})t_{x=0}$, where $t_x$ is the time post-infection.

### FFU neutralization with conformation-specific antibodies

L929 cells were adsorbed with serial two-fold dilutions of virus in complete JMEM at 37°C for 1 h, washed with PBS, incubated in fresh medium at 37° for 24 h, washed with PBS, and fixed with cold methanol. Fixed cells were incubated with reovirus

polyclonal serum diluted 1:1000 in 0.5% Triton X-100, followed by incubation with Alexa Fluor 488-labeled secondary IgG. Cells were counterstained with DAPI and imaged using a Lionheart FX imaging system (BioTek). The percentage of infected cells was quantified using Gen5 software (BioTek), and the concentration of virus required to infect approximately 60% of cells ($TCID_{60}$) was determined.

Antibody neutralization efficiency was determined by incubating virus at a concentration of 1 $TCID_{60}$ of virus with an equal volume of complete JMEM or four-fold serial dilutions of 9BG5 or 5C6 antibody at room temperature for 1 h, followed by virus adsorption to cells at 37°C for 1 h. Cells were washed, fixed, imaged, and enumerated as described above. The percent neutralization was determined using the equation: $\text{percent infection}_{[mAb]} \div \text{mean percent infection}_{JMEM}$.

## Hemagglutination assay

Purified reovirus virions were serially diluted two-fold in 0.05 mL of PBS. Viral concentrations used ranged from $5.0 \times 10^{10}$ particles in 0.05 mL to $2.4 \times 10^{7}$ particles in 0.05 mL. Bovine erythrocytes (Innovative Research) or human type $O^-$ erythrocytes (University of Pittsburgh Medical Center Blood Bank) were washed with PBS and diluted to 1% in PBS (vol:vol). Equal volumes (0.05 mL) of virus and erythrocyte mixtures were gently mixed in U-bottom assay plates and incubated at 4°C for 4 h. Hemagglutination (HA) was defined as a partial or complete shield of erythrocytes within the well. The lowest number of reovirus particles required to produce HA, termed $HA_{Low}$, is used to calculate the HA titer using the equation: HA titer = $(5.0 \times 10^{10}$ reovirus particles$) \div (HA_{Low})$.

## Mice and rats

C57BL/6J mice (Jackson) were used to establish breeding colonies in specific-pathogen free facilities at Vanderbilt University and the University of Pittsburgh and experiments were performed using ABSL2 facilities and guidelines. Timed pregnant Sprague-Dawley rats (Charles River) were housed in specific-pathogen free facilities at the University of Pittsburgh before euthanasia and embryo resection. Experiments using mice and rats included approximately equivalent numbers of males and females.

All animal husbandry and experimental procedures were performed in accordance with U.S. Public Health Service policy and approved by the Institutional Animal Care and Use Committees at Vanderbilt University and the University of Pittsburgh.

### Infection of mice and histology

Two to three litters of two-to-three-day-old C57BL/6J mice weighing between 1.4-2.2 g were inoculated intracranially in the right cerebral hemisphere with 100 PFU of virus (± 3–fold) diluted in PBS using a 30-gauge needle and syringe (Hamilton). Viral titers of inocula were confirmed by plaque assay. For analyses of virulence, inoculated mice were monitored daily for symptoms of disease. Death was not used as an endpoint in these studies; moribund mice were euthanized. Qualifications for moribundity included severe lethargy or seizures, paralysis, or 25% body weight loss.

For analyses of viral replication and immunohistopathology, mice were euthanized 8 days post-inoculation, and brains were excised and hemisected along the longitudinal fissure. The right-brain hemisphere was collected into 1 mL of PBS and frozen and thawed twice prior to homogenization using a TissueLyser (Qiagen). Viral titers were determined by plaque assay using L929 cells. The left-brain hemisphere was fixed in 10% neutral buffered formalin for at least 24 h, imbedded in paraffin wax, and cut into 5 μM thick sections. Using the BOND-MAX automated system (Leica), tissue was deparaffinized, incubated with Epitope Retrieval Solution 2 (BOND) at 100°C for 20 min (followed by gradual, stepwise temperature reduction), blocked with Serum Free Protein Block (DAKO) at room temperature for 10 min, and incubated with reovirus polyclonal serum diluted 1:45,000 in Primary Antibody Diluent (BOND). Polymer Refine Detection reagents (BOND) were used to visualize reovirus antigen and nuclei using 3,3'-diaminobenzidin-conjugated rabbit secondary IgG and a hematoxylin counterstain, respectively. Stained slides were scanned using a Lionheart FX imager.

### Cortical neuron culture

Surfaces of 48-well tissue-culture grade plates were treated with Neurobasal medium (Gibco) containing 10 μg/mL poly-D-lysine (BD Biosciences) and 1 μg/mL

laminin (BD Biosciences) at 4°C overnight and washed three times with PBS. Plating medium (Neurobasal medium supplemented to contain 10% fetal bovine serum, 50 U/mL penicillin, 50 µg/mL streptomycin, and 0.6 mM GlutaMAX [GIBCO]) was added to treated wells, and plates were incubated at 37°C until use.

Cortices of embryonic day 17.5 Sprague-Dawley rats were isolated, separated from meninges, and collected in Hanks' balanced salt solution$^{-/-}$ (HBSS) on ice. Cortices were incubated with 130 U/mL trypsin (Worthington) in HBSS at room temperature for 30 min, washed twice with HBSS, and dissociated in 5 mL of plating medium by trituration with fire-polished borosilicate glass Pasteur pipettes. Debris was allowed to settle for 2 min, and the supernatant was transferred to 5 mL of plating medium for additional trituration. Cell viability was assessed by trypan blue exclusion, and $10^5$ viable cells were suspended in plating medium per well and incubated overnight. Plating medium was removed and cells were maintained in Neurobasal medium supplemented to contain 1X B27 supplement (Gibco), 50 U/mL penicillin, 50 µg/mL streptomycin, and 0.6 mM GlutaMAX. Half of the medium was replaced every 4 days, and neurons were cultivated *in vitro* for 10-12 days prior to infection.

### Defining sialic-acid (SA) dependent and independent infectivity of cultured neurons

Cultured cortical neurons were incubated with either vehicle control or 40 mU/mL of *Arthrobacter ureafaciens* neuraminidase (MP Biomedicals, LLC) diluted in complete Neurobasal medium at 37°C for 1 h. Neurons were washed with PBS and adsorbed with reovirus diluted in PBS with added calcium and magnesium at an MOI of 500 PFU/cell at 37°C for 1 h. The inoculum was removed, warm complete medium was added to cells, and cells were incubated for 24 h prior to fixation with 4% paraformaldehyde and 0.2% glutaraldehyde in PBS at 37°C for 15 min. Fixation was quenched with 100 mM glycine in PBS, and cells were blocked with 5% bovine serum albumin in PBS.

Fixed cells were incubated with reovirus polyclonal serum diluted 1:1000 in 0.5% Triton X-100, followed by incubation with Alexa Fluor 488-labeled secondary IgG. Cells were counterstained with DAPI, and neurons were identified by indirect immunofluorescence using a mouse anti-tubulin beta 3 (Tuj1) antibody (BioLegend)

diluted 1:1,000, followed by incubation with Alexa Fluor 546-labeled secondary IgG. Neurons were imaged at 4X magnification with 6 images/well in quadruplicate wells per virus per experiment using a LionHeart FX imager. DAPI-positive nuclei were enumerated using Gen5 software, and reovirus-positive neurons were manually counted.

### Receptor cDNA transfection and infection of CHO cells

One day before transfection, CHO cells were seeded in 1 mL of completed F12 medium at a density of $1 \times 10^5$ cells/well in 24-well tissue culture plates. Apporximately 0.5 µg of pcDNA3.1$^+$ expression vector was combined with FuGene 6 (Promega, E2691) in Opti-MEM (Gibco) and incubated at RT for 20 min. Opti-MEM mixture was added dropwise to cell supernatants and cells were incubated for 48 h post-transfection at 37°C before infection or flow cytometry experiments.

For infections, transfected CHO cells were inoculated with T3- diluted in PBS$^{-/-}$ at an MOI of 500 PFU/cell at 37°C for 1 h. Virus was removed and cells were washed with PBS and incubated in completed F12 medium. At 24 hpi, cells were fixed with cold methanol at -20°C for 30+ min. Fixed cells were stained with reovirus antiserum, anti-rabbit Alexa Fluor 488, and DAPI and imaged manually. Infected cells (FFU) were counted per 20X field of view on a Zeiss Axiovert 200 fluorescent microscope. At least four fields of view were counted per well in triplicate wells.

### Flow cytometry assessment of reovirus binding or receptor expression

Monolayers of mock- or cDNA-transfected CHO cells were washed with PBS, detached using CellStripper Dissociation Reagent (Corning), and quenched with an equal volume of PBS$^{-/-}$ supplemented to contain 2% FBS (FACS buffer). All further washes and dilutions were performed in FACS buffer in 1.5 mL tubes. Cells were pelleted at 1000 revolutions per minute (rpm) at 4°C for 5 min. Cells were washed, pelleted, and incubated with $10^5$ particles of T3- reovirus/cell on ice for 1 h. Cells were pelleted to remove unbound virus, washed 3X, and incubated with NgR1 and/or NgR2-specific antibodies or myc-specific antibodies on ice for 1 h. Cells were washed 3X and fixed in PBS$^{-/-}$ supplemented to contain 1% paraformaldehyde. Cells were analyzed

using a Fortessa flow cytometer (BD Bioscience) and results were quantified with FlowJo software.

### Expression and purification of the $\mu1_3\sigma3_3$ heterohexamer

Hi5 insect cells (1 L) were infected with 20 mL of third passage rBV expressing the T1L reovirus μ1 and σ3 heterohexamer proteins. Cells were incubated at 27°C for 72 h, pelleted by centrifugation at 500*g* for 10 min, and resuspended in heterohexamer lysis buffer (150 mM KCl, 20 mM Tris pH 8.5, 2 mM $MgCl_2$, 2 mM β-mercaptoethanol [BME], 3 mM PMSF, and completed with benzonase [1,000 units] and complete protease inhibitors [Roche] prior to use). Cells were lysed by emulsiflex and debris was cleared by ultracentrifugation at 31,200 rpm for 40 min at 4°C. The supernatant was loaded onto a MonoQ ion-exchange column and washed with buffer A (20 mM Tris pH 8.5, 20 mM $MgCl_2$, 2 mM BME) containing 150 mM NaCl. The heterohexamer was eluted with a linear buffer A gradient from 150 to 450 mM NaCl. Fractions containing μ1 and σ3 were pooled and concentrated to 1 mL with a 30 kDa molecular weight cut-off (MWCO) centricon. Protein was diluted to 4 mL with buffer A lacking NaCl and mixed dropwise with ammonium sulfate buffer (4 M ammonium sulfate, 20 mM Tris pH 8.5) to a final concentration of 0.7 M ammonium sulfate. Protein was loaded onto a phenyl sepharose column and eluted with a linear buffer A gradient from 0.7 M to 0 M ammonium sulfate. Fractions containing heterohexamer were pooled and concentrated with a 30 kDA MWCO centricon. Protein was passed through a Superdex 200 size-exclusion column equilibrated with buffer B (20 mM Bicine pH 9, 100 mM NaCl, 2 mM $MgCl_2$, 2 mM BME). Heterohexamer fractions were pooled and concentrated to 1 mg/mL.

### Production of $^{35}$S-labeled σ3

Coupled *in vitro* transcription and translation reactions were conducted using the TNT coupled rabbit reticulocyte lysate system (Promega, L4610) according to the manufacturer's instructions. Reactions were supplemented with [$^{35}$S]-methionine (Perkin Elmer, NEG709A500UC) for radiolabeling and RNasin Plus RNase Inhibitor (N2611). Using pcDNA3.1+ encoding T1L or T3D S4 for *in vitro* transcription and translation,

reactions were incubated at 30°C for 30 min. Translation reactions were terminated by four-fold dilution in stop buffer (20 mM HEPES-KOH pH 7.4, 100 mM potassium acetate, 5 mM magnesium acetate, 5 mM EDTA, 2 mM methionine) supplemented with a final concentration of 1 mM dithiothreitol (DTT) and 2 mM puromycin.

## Immunoprecipitations; Native and SDS-PAGE, immunoblotting and phosphor imaging

**Immunoprecipitation:** To immunoprecipitate proteins translated *in vitro* in RRLs, 5 µg of mouse 10C1 or 8H6 monoclonal antibody or NgR1-Fc or CAR-Fc were incubated with σ3-expressing reactions at 4°C for 1 h with rotation. Samples were added to Protein G Dynabeads and incubated at 4°C for 1 h with rotation. The flow-through containing unbound protein was resolved by native PAGE. Dynabeads were washed four times with Tris-buffered saline (20 mM Tris-HCl pH 7.5, 150 mM NaCl) containing 0.1% Tween-20, eluted with SDS sample buffer, and resolved by SDS-PAGE.

**Native PAGE:** Samples for native PAGE were diluted in 4X Native PAGE Sample Buffer (ThermoFisher, BN2003) and loaded into wells of 4-16% Native PAGE Bis-Tris acrylamide gels (ThermoFisher). Samples were electrophoresed using the blue native PAGE Novex Bis-Tris gel system (ThermoFisher) at 150V at 4°C for 60 min, followed by 250V at 4°C for 40 min. Light blue anode buffer was supplemented with 0.1% L-cysteine and 1 mM ATP.

Following electrophoresis, proteins were transferred to a polyvinylidene difluoride (PVDF) membrane (BioRad, 162-0177) at 25 V at 4°C for 2 h. Following transfer, the membrane was soaked in 8% acetic acid for 15 min, rinsed with $ddH_2O$, and dried. The membrane was incubated with 100% methanol for 1 min, rinsed with $ddH_2O$, blocked with 5% bovine serum albumin (BSA) diluted in PBS-/- and incubated with antibodies for immunoblotting. All native gels were electrophoresed with the NativeMark Protein Standard (ThermoFisher, LC0725) for molecular weight estimation.

**SDS-PAGE:** Samples for SDS-PAGE were diluted in 5X SDS-PAGE sample buffer and incubated at 95°C for 10 min. Samples were loaded into wells of 10% acrylamide gels (BioRad, 4561036) and electrophoresed at 100V for 90 min. Following

electrophoresis, proteins were either stained with colloidal blue (ThermoFisher, LC6025) or transferred to nitrocellulose for immunoblotting. Immunoblot analysis was performed as described (243) and gels were scanned using an Odyssey CLx imaging system (Li-Cor).

**Phosphor Imaging:** Following electrophoresis, gels were incubated in 40% methanol, 10% acetic acid at RT for 1 h, washed three times with dd$H_2O$, and dried on filter paper at 80°C for 2 h using a BioRad model 583 gel dyer. Dried gels were applied to a phosphor imaging screen for 12-36 h, followed by imaging using a Perkin Elmer Cyclone Phosphor System Scanner (B431200). Protein bands labeled with $^{35}$S-methionine were analyzed using ImageJ software (244).

### Cryo-EM Reconstructions of NgR1 and reovirus

Purified T3- reovirus virions were incubated with buffer alone, soluble NgR1-Fc, or JAM-Fc at RT for 4 h or >48 h and embedded in a thin layer of vitreous ice on holey carbon films (245). Frozen hydrated specimens were imaged using low electron dose conditions with JEOL 2010F or JEOL 3200 FSC cryo-electron microscopes equipped with direction detection cameras in the NIH-funded National Center for Macromolecular Imaging at Baylor College of Medicine. Image processing (~ 600 particles) and three-dimensional reconstruction (~ 16 Å resolution) were conducted using EMAN2 software to visualize how NgR1 interacts with the reovirus capsid.

### Statistical analysis

All statistical tests were conducted using Prism 7 (GraphPad Software). *P* values of less than 0.05 were considered to be statistically significant. Descriptions of the specific tests used are found in the figure legends, and differences are calculated relative to T1+ virus unless otherwise noted.

## REFERENCES


1. **Dahm T, Rudolph H, Schwerk C, Schroten H, Tenenbaum T.** 2016. Neuroinvasion and inflammation in viral central nervous system infections. Mediators Inflamm **2016:**8562805.
2. **Kanai Y, Komoto S, Kawagishi T, Nouda R, Nagasawa N, Onishi M, Matsuura Y, Taniguchi K, Kobayashi T.** 2017. Entirely plasmid-based reverse genetics system for rotaviruses. Proc Natl Acad Sci U S A **114:**2349-2354.
3. **Kobayashi T, Ooms LS, Ikizler M, Chappell JD, Dermody TS.** 2010. An improved reverse genetics system for mammalian orthoreoviruses. Virology **398:**194-200.
4. **Margolis G, Kilham L.** 1969. Hydrocephalus in hamsters, ferrets, rats, and mice following inoculations with reovirus type I. II. Pathologic studies. Lab Invest **21:**189-198.
5. **Raine CS, Fields BN.** 1973. Reovirus type 3 encephalitis--a virologic and ultrastructural study. J Neuropathol Exp Neurol **32:**19-33.
6. **Wu AG, Pruijssers AJ, Brown JJ, Stencel-Baerenwald JE, Sutherland DM, Iskarpatyoti JA, Dermody TS.** 2018. Age-dependent susceptibility to reovirus encephalitis in mice is influenced by maturation of the type-I interferon response. Pediatr Res **83:**1057-1066.
7. **Masters C, Alpers M, Kakulas B.** 1977. Pathogenesis of reovirus type 1 hydrocephalus in mice. Significance of aqueductal changes. Arch Neurol **34:**18-28.
8. **Weiner HL, Drayna D, Averill DR, Jr., Fields BN.** 1977. Molecular basis of reovirus virulence: role of the S1 gene. Proc Natl Acad Sci U S A **74:**5744-5748.
9. **Weiner HL, Powers ML, Fields BN.** 1980. Absolute linkage of virulence and central nervous system cell tropism of reoviruses to viral hemagglutinin. J Infect Dis **141:**609-616.
10. **Jayaraman B, Smith AM, Fernandes JD, Frankel AD.** 2016. Oligomeric viral proteins: small in size, large in presence. Crit Rev Biochem Mol Biol **51:**379-394.
11. **Freire JM, Santos NC, Veiga AS, Da Poian AT, Castanho MA.** 2015. Rethinking the capsid proteins of enveloped viruses: multifunctionality from genome packaging to genome transfection. FEBS J **282:**2267-2278.
12. **Rotbart HA.** 2000. Viral meningitis. Semin Neurol **20:**277-292.
13. **Romero JR, Newland JG.** 2003. Viral meningitis and encephalitis: traditional and emerging viral agents. Semin Pediatr Infect Dis **14:**72-82.
14. **Wong AD, Ye M, Levy AF, Rothstein JD, Bergles DE, Searson PC.** 2013. The blood-brain barrier: an engineering perspective. Front Neuroeng **6:**7.
15. **Wolburg H, Paulus W.** 2010. Choroid plexus: biology and pathology. Acta Neuropathol **119:**75-88.
16. **Ransohoff RM, Engelhardt B.** 2012. The anatomical and cellular basis of immune surveillance in the central nervous system. Nat Rev Immunol **12:**623-635.
17. **Schwerk C, Tenenbaum T, Kim KS, Schroten H.** 2015. The choroid plexus-a multi-role player during infectious diseases of the CNS. Front Cell Neurosci **9:**80.

18. **Fiala M, Looney DJ, Stins M, Way DD, Zhang L, Gan X, Chiappelli F, Schweitzer ES, Shapshak P, Weinand M, Graves MC, Witte M, Kim KS.** 1997. TNF-alpha opens a paracellular route for HIV-1 invasion across the blood-brain barrier. Mol Med **3:**553-564.
19. **Hazleton JE, Berman JW, Eugenin EA.** 2010. Novel mechanisms of central nervous system damage in HIV infection. HIV AIDS (Auckl) **2:**39-49.
20. **Stamatovic SM, Keep RF, Andjelkovic AV.** 2008. Brain endothelial cell-cell junctions: how to "open" the blood brain barrier. Curr Neuropharmacol **6:**179-192.
21. **Spindler KR, Hsu TH.** 2012. Viral disruption of the blood-brain barrier. Trends Microbiol **20:**282-290.
22. **Pohl D, Alper G, Van Haren K, Kornberg AJ, Lucchinetti CF, Tenembaum S, Belman AL.** 2016. Acute disseminated encephalomyelitis: Updates on an inflammatory CNS syndrome. Neurology **87:**S38-45.
23. **Modlin JF, Dagan R, Berlin LE, Virshup DM, Yolken RH, Menegus M.** 1991. Focal encephalitis with enterovirus infections. Pediatrics **88:**841-845.
24. **Emmons RW.** 1988. Ecology of Colorado tick fever. Annu Rev Microbiol **42:**49-64.
25. **Lambert AJ, Blair CD, D'Anton M, Ewing W, Harborth M, Seiferth R, Xiang J, Lanciotti RS.** 2010. La Crosse virus in Aedes albopictus mosquitoes, Texas, USA, 2009. Emerg Infect Dis **16:**856-858.
26. **Gandelman-Marton R, Kimiagar I, Itzhaki A, Klein C, Theitler J, Rabey JM.** 2003. Electroencephalography findings in adult patients with West Nile virus-associated meningitis and meningoencephalitis. Clin Infect Dis **37:**1573-1578.
27. **Pruijssers AJ, Hengel H, Abel TW, Dermody TS.** 2013. Apoptosis induction influences reovirus replication and virulence in newborn mice. J Virol **87:**12980-12989.
28. **Schoneboom BA, Catlin KM, Marty AM, Grieder FB.** 2000. Inflammation is a component of neurodegeneration in response to Venezuelan equine encephalitis virus infection in mice. J Neuroimmunol **109:**132-146.
29. **Jan JT, Griffin DE.** 1999. Induction of apoptosis by sindbis virus occurs at cell entry and does not require virus replication. Journal of Virology **73:**10296-10302.
30. **Kuo RL, Kung SH, Hsu YY, Liu WT.** 2002. Infection with enterovirus 71 or expression of its 2A protease induces apoptotic cell death. J Gen Virol **83:**1367-1376.
31. **Samuel MA, Morrey JD, Diamond MS.** 2007. Caspase 3-dependent cell death of neurons contributes to the pathogenesis of West Nile virus encephalitis. J Virol **81:**2614-2623.
32. **Tate JE, Burton AH, Boschi-Pinto C, Parashar UD, World Health Organization-Coordinated Global Rotavirus Surveillance N.** 2016. Global, regional, and national estimates of rotavirus mortality in children <5 years of age, 2000-2013. Clin Infect Dis **62 Suppl 2:**S96-S105.
33. **Leland MM, Hubbard GB, Sentmore HT, 3rd, Soike KF, Hilliard JK.** 2000. Outbreak of Orthoreovirus-induced meningoencephalomyelitis in baboons. Comp Med **50:**199-205.

34. **Hermann L, Embree J, Hazelton P, Wells B, Coombs RT.** 2004. Reovirus type 2 isolated from cerebrospinal fluid. Pediatr Infect Dis J **23:**373-375.
35. **Johansson PJ, Sveger T, Ahlfors K, Ekstrand J, Svensson L.** 1996. Reovirus type 1 associated with meningitis. Scand J Infect Dis **28:**117-120.
36. **Stanley NF, Dorman DC, Ponsford J.** 1953. Studies on the pathogenesis of a hitherto undescribed virus (hepato-encephalomyelitis) producing unusual symptoms in suckling mice. Aust J Exp Biol Med Sci **31:**147-159.
37. **Tyler KL, Barton ES, Ibach ML, Robinson C, Campbell JA, O'Donnell SM, Valyi-Nagy T, Clarke P, Wetzel JD, Dermody TS.** 2004. Isolation and molecular characterization of a novel type 3 reovirus from a child with meningitis. J Infect Dis **189:**1664-1675.
38. **Van Tongeren HAE.** 1957. A familial infection with hepatoencephalomyelitis virus in the Netherlands: study on some properties of the infective agent. Arch Gesamte Virusforsch **7:**429-448.
39. **Sabin AB.** 1959. Reoviruses: a new group of respiratory and enteric viruses formerly classified as ECHO type 10 is described. Science **130:**1387-1389.
40. **Dermody TS, Parker JS, Sherry B.** 2013. Orthoreoviruses, p 1304-1346. *In* Knipe DM, Howley PM (ed), Fields Virology, Sixth ed, vol 2. Lippincott Williams & Wilkins, Philadelphia.
41. **Bouziat R, Hinterleitner R, Brown JJ, Stencel-Baerenwald JE, Ikizler M, Mayassi T, Meisel M, Kim SM, Discepolo V, Pruijssers AJ, Ernest JD, Iskarpatyoti JA, Costes LM, Lawrence I, Palanski BA, Varma M, Zurenski MA, Khomandiak S, McAllister N, Aravamudhan P, Boehme KW, Hu F, Samsom JN, Reinecker HC, Kupfer SS, Guandalini S, Semrad CE, Abadie V, Khosla C, Barreiro LB, Xavier RJ, Ng A, Dermody TS, Jabri B.** 2017. Reovirus infection triggers inflammatory responses to dietary antigens and development of celiac disease. Science **356:**44-50.
42. **Clements D, Helson E, Gujar SA, Lee PW.** 2014. Reovirus in cancer therapy: An evidence-based review. Oncolytic Virother **3:**69-82.
43. **Skup D, Millward S.** 1980. mRNA capping enzymes are masked in reovirus progeny subviral particles. J Virol **34:**490-496.
44. **Zou S, Brown EG.** 1992. Identification of sequence elements containing signals for replication and encapsidation of the reovirus M1 genome segment. Virology **186:**377-388.
45. **Chappell JD, Goral MI, Rodgers SE, Depamphilis CW, Dermody TS.** 1994. Sequence diversity within the reovirus S2 gene - Reovirus genes reassort in nature, and their termini are predicted to form a panhandle motif. J Virol **68:**750-756.
46. **Kobayashi T, Antar AA, Boehme KW, Danthi P, Eby EA, Guglielmi KM, Holm GH, Johnson EM, Maginnis MS, Naik S, Skelton WB, Wetzel JD, Wilson GJ, Chappell JD, Dermody TS.** 2007. A plasmid-based reverse genetics system for animal double-stranded RNA viruses. Cell Host Microbe **1:**147-157.
47. **Eaton HE, Kobayashi T, Dermody TS, Johnston RN, Jais PH, Shmulevitz M.** 2017. African Swine Fever Virus NP868R Capping Enzyme Promotes Reovirus Rescue during Reverse Genetics by Promoting Reovirus Protein Expression, Virion Assembly, and RNA Incorporation into Infectious Virions. J Virol **91**.

48. **Furlong DB, Nibert ML, Fields BN.** 1988. Sigma 1 protein of mammalian reoviruses extends from the surfaces of viral particles. J Virol **62:**246-256.
49. **Zhang X, Ji Y, Zhang L, Harrison SC, Marinescu DC, Nibert ML, Baker TS.** 2005. Features of reovirus outer capsid protein mu1 revealed by electron cryomicroscopy and image reconstruction of the virion at 7.0 Angstrom resolution. Structure **13:**1545-1557.
50. **Reiter DM, Frierson JM, Halvorson EE, Kobayashi T, Dermody TS, Stehle T.** 2011. Crystal structure of reovirus attachment protein sigma1 in complex with sialylated oligosaccharides. PLoS Pathog **7:**e1002166.
51. **Rosen L.** 1960. Serologic grouping of reovirus by hemagglutination-inhibition. American Journal of Hygiene **71:**242-249.
52. **Lerner AM, Cherry JD, Klein JO, Finland M.** 1962. Infections with reoviruses. N Engl J Med **267:**947-952.
53. **Tai JH, Williams JV, Edwards KM, Wright PF, Crowe JE, Jr., Dermody TS.** 2005. Prevalence of reovirus-specific antibodies in young children in Nashville, Tennessee. J Infect Dis **191:**1221-1224.
54. **Weiner HL, Fields BN.** 1977. Neutralization of reovirus: the gene responsible for the neutralization antigen. J Exp Med **146:**1305-1310.
55. **Breun LA, Broering TJ, McCutcheon AM, Harrison SJ, Luongo CL, Nibert ML.** 2001. Mammalian reovirus L2 gene and lambda2 core spike protein sequences and whole-genome comparisons of reoviruses type 1 Lang, type 2 Jones, and type 3 Dearing. Virology **287:**333-348.
56. **Steyer A, Gutierrez-Aguire I, Kolenc M, Koren S, Kutnjak D, Pokorn M, Poljsak-Prijatelj M, Racki N, Ravnikar M, Sagadin M, Fratnik Steyer A, Toplak N.** 2013. High similarity of novel orthoreovirus detected in a child hospitalized with acute gastroenteritis to mammalian orthoreoviruses found in bats in Europe. J Clin Microbiol **51:**3818-3825.
57. **Maginnis MS, Mainou BA, Derdowski AM, Johnson EM, Zent R, Dermody TS.** 2008. NPXY motifs in the β1 integrin cytoplasmic tail are required for functional reovirus entry. J Virol **82:**3181-3191.
58. **Schulz WL, Haj AK, Schiff LA.** 2012. Reovirus uses multiple endocytic pathways for cell entry. J Virol **86:**12665-12675.
59. **Sturzenbecker LJ, Nibert ML, Furlong DB, Fields BN.** 1987. Intracellular digestion of reovirus particles requires a low pH and is an essential step in the viral infectious cycle. J Virol **61:**2351-2361.
60. **Ebert DH, Deussing J, Peters C, Dermody TS.** 2002. Cathepsin L and cathepsin B mediate reovirus disassembly in murine fibroblast cells. J Biol Chem **277:**24609-24617.
61. **Dryden KA, Wang G, Yeager M, Nibert ML, Coombs KM, Furlong DB, Fields BN, Baker TS.** 1993. Early steps in reovirus infection are associated with dramatic changes in supramolecular structure and protein conformation: analysis of virions and subviral particles by cryoelectron microscopy and image reconstruction. J Cell Biol **122:**1023-1041.
62. **Chandran K, Nibert ML.** 2003. Animal cell invasion by a large nonenveloped virus: reovirus delivers the goods. Trends Microbiol **11:**374-382.

63. **Coombs KM.** 1998. Stoichiometry of reovirus structural proteins in virus, ISVP, and core particles. Virology **243:**218-228.
64. **Silverstein SC, Astell C, Levin DH, Schonberg M, Acs G.** 1972. The mechanism of reovirus uncoating and gene activation in vivo. Virology **47:**797-806.
65. **Danthi P, Coffey CM, Parker JS, Abel TW, Dermody TS.** 2008. Independent regulation of reovirus membrane penetration and apoptosis by the mu1 phi domain. PLoS Pathog **4:**e1000248.
66. **Banerjee AK, Shatkin AJ.** 1970. Transcription in vitro by reovirus-associated ribonucleic acid-dependent polymerase. J Virol **6:**1-11.
67. **Chang CT, Zweerink HJ.** 1971. Fate of parental reovirus in infected cell. Virology **46:**544-555.
68. **Schonberg M, Silverstein SC, Levin DH, Acs G.** 1971. Asynchronous synthesis of the complementary strands of the reovirus genome. Proc Natl Acad Sci U S A **68:**505-508.
69. **Li JK-K, Scheible PP, Keene JD, Joklik WK.** 1980. The plus strand of reovirus gene S2 is identical with its in vitro transcript. Virology **105:**282-286.
70. **Shatkin AJ, Kozak M.** 1983. Biochemical aspects of reovirus transcription and translation, p 79-106. *In* Joklik WJ (ed), The Reoviridae. Plenum Press, New York.
71. **Antczak JB, Joklik WK.** 1992. Reovirus genome segment assortment into progeny genomes studied by the use of monoclonal-antibodies directed against reovirus proteins. Virology **187:**760-776.
72. **Excoffon KJDA, Guglielmi KM, Wetzel JD, Gansemer ND, Campbell JA, Dermody TS, Zabner J.** 2008. Reovirus preferentially infects the basolateral surface and is released from the apical surface of polarized human respiratory epithelial cells. J Infect Dis **197:**1189-1197.
73. **Lai CM, Mainou BA, Kim KS, Dermody TS.** 2013. Directional release of reovirus from the apical surface of polarized endothelial cells. MBio **4:**e00049-00013.
74. **Oberhaus SM, Smith RL, Clayton GH, Dermody TS, Tyler KL.** 1997. Reovirus infection and tissue injury in the mouse central nervous system are associated with apoptosis. J Virol **71:**2100-2106.
75. **Wolf JL, Rubin DH, Finberg R, Kaufman RS, Sharpe AH, Trier JS, Fields BN.** 1981. Intestinal M cells: a pathway of entry for reovirus into the host. Science **212:**471-472.
76. **Bass DM, Trier JS, Dambrauskas R, Wolf JL.** 1988. Reovirus type I infection of small intestinal epithelium in suckling mice and its effect on M cells. Lab Invest **58:**226-235.
77. **Antar AAR, Konopka JL, Campbell JA, Henry RA, Perdigoto AL, Carter BD, Pozzi A, Abel TW, Dermody TS.** 2009. Junctional adhesion molecule-A is required for hematogenous dissemination of reovirus. Cell Host Microbe **5:**59-71.
78. **Maginnis MS, Forrest JC, Kopecky-Bromberg SA, Dickeson SK, Santoro SA, Zutter MM, Nemerow GR, Bergelson JM, Dermody TS.** 2006. β1 integrin mediates internalization of mammalian reovirus. Journal of Virology **80:**2760-2770.

79. **Thete D, Snyder AJ, Mainou BA, Danthi P.** 2016. Reovirus mu1 protein affects infectivity by altering virus-receptor interactions. J Virol **90:**10951-10962.
80. **Tyler KL, McPhee DA, Fields BN.** 1986. Distinct pathways of viral spread in the host determined by reovirus S1 gene segment. Science **233:**770-774.
81. **Boehme KW, Guglielmi KM, Dermody TS.** 2009. Reovirus nonstructural protein sigma1s is required for establishment of viremia and systemic dissemination. Proc Natl Acad Sci U S A **106:**19986-19991.
82. **Boehme KW, Frierson JM, Konopka JL, Kobayashi T, Dermody TS.** 2011. The reovirus sigma1s protein is a determinant of hematogenous but not neural virus dissemination in mice. J Virol **85:**11781-11790.
83. **Pacitti AF, Gentsch JR.** 1987. Inhibition of Reovirus Type-3 Binding to Host-Cells by Sialylated Glycoproteins Is Mediated through the Viral Attachment Protein. Journal of Virology **61:**1407-1415.
84. **Iskarpatyoti JA, Morse EA, McClung RP, Ikizler M, Wetzel JD, Contractor N, Dermody TS.** 2012. Serotype-specific differences in inhibition of reovirus infectivity by human-milk glycans are determined by viral attachment protein sigma1. Virology **433:**489-497.
85. **Tardieu M, Weiner HL.** 1982. Viral receptors on isolated murine and human ependymal cells. Science **215:**419-421.
86. **Dichter MA, Weiner HL.** 1984. Infection of neuronal cell cultures with reovirus mimics in vitro patterns of neurotropism. Ann Neurol **16:**603-610.
87. **Reiss K, Stencel JE, Liu Y, Blaum BS, Reiter DM, Feizi T, Dermody TS, Stehle T.** 2012. The GM2 glycan serves as a functional co-receptor for serotype 1 reovirus. PLoS Pathogens **8:**e1003078.
88. **Dietrich MH, Ogden KM, Long JM, Ebenhoch R, Thor A, Dermody TS, Stehle T.** 2018. Structural and functional features of the reovirus sigma1 tail. J Virol doi:10.1128/JVI.00336-18.
89. **Nibert ML, Dermody TS, Fields BN.** 1990. Structure of the reovirus cell-attachment protein: a model for the domain organization of σ1. Journal of Virology **64:**2976-2989.
90. **Kirchner E, Guglielmi KM, Strauss HM, Dermody TS, Stehle T.** 2008. Structure of reovirus sigma1 in complex with its receptor junctional adhesion molecule-A. PLoS Pathog **4:**e1000235.
91. **Mohamed A, Teicher C, Haefliger S, Shmulevitz M.** 2015. Reduction of virion-associated sigma1 fibers on oncolytic reovirus variants promotes adaptation toward tumorigenic cells. J Virol **89:**4319-4334.
92. **Nagata L, Masri SA, Pon RT, Lee PWK.** 1987. Analysis of functional domains on reovirus cell attachment protein sigma 1 using cloned S1 gene deletion mutants. Virology **160:**162-168.
93. **Katen SP, Dermody, T.S.** 2018. Unpublished observations.
94. **Dietrich MH, Ogden KM, Katen SP, Reiss K, Sutherland DM, Carnahan RH, Goff M, Cooper T, Dermody TS, Stehle T.** 2017. Structural insights into reovirus sigma1 interactions with two neutralizing antibodies. J Virol **91:**e01621-01616.

95. **Borsa J, Morash BD, Sargent MD, Copps TP, Lievaart PA, Szekely JG.** 1979. Two modes of entry of reovirus particles into L cells. Journal of General Virology **45:**161-170.
96. **Nibert ML, Chappell JD, Dermody TS.** 1995. Infectious subvirion particles of reovirus type 3 Dearing exhibit a loss in infectivity and contain a cleaved σ1 protein. Journal of Virology **69:**5057-5067.
97. **Stettner E, Dietrich MH, Reiss K, Dermody TS, Stehle T.** 2015. Structure of serotype 1 reovirus attachment protein sigma1 in complex with junctional adhesion molecule A reveals a conserved serotype-independent binding epitope. J Virol **89:**6136-6140.
98. **Konopka-Anstadt JL, Mainou BA, Sutherland DM, Sekine Y, Strittmatter SM, Dermody TS.** 2014. The Nogo receptor NgR1 mediates infection by mammalian reovirus. Cell Host Microbe **15:**681-691.
99. **Barton ES, Connolly JL, Forrest JC, Chappell JD, Dermody TS.** 2001. Utilization of sialic acid as a coreceptor enhances reovirus attachment by multistep adhesion strengthening. Journal of Biological Chemistry **276:**2200-2211.
100. **Frierson JM, Pruijssers AJ, Konopka JL, Reiter DM, Abel TW, Stehle T, Dermod TS.** 2012. Utilization of sialylated glycans as coreceptors enhances the neurovirulence of serotype 3 reovirus. J Virol **86:**13164-13173.
101. **Stencel-Baerenwald J, Reiss K, Blaum BS, Colvin D, Li XN, Abel T, Boyd K, Stehle T, Dermody TS.** 2015. Glycan engagement dictates hydrocephalus induction by serotype 1 reovirus. MBio **6:**e02356.
102. **Haywood AM.** 1994. Virus receptors: binding, adhesion strengthening, and changes in viral structure. J Virol **68:**1-5.
103. **Matrosovich M, Herrler G, Klenk HD.** 2015. Sialic acid receptors of viruses, p 1-28. *In* Gerardy-Schahn R, Delannoy P, von Itzstein M (ed), SialoGlyco Chemistry and Biology II, 2013/07/23 ed, vol 367. Springer International Publishing, New York, NY.
104. **Stroh LJ, Stehle T.** 2014. Glycan Engagement by Viruses: Receptor Switches and Specificity. Annu Rev Virol **1:**285-306.
105. **Varki A, Schauer R.** 2009. Sialic Acids. *In* Varki A, Cummings RD, Esko JD, Freeze HH, Stanley P, Bertozzi CR, Hart GW, Etzler ME (ed), Essentials of Glycobiology, 2nd ed. Cold Spring Harbor Laboratory Press, Cold Spring Harbor (NY).
106. **Barton ES, Youree BE, Ebert DH, Forrest JC, Connolly JL, Valyi-Nagy T, Washington K, Wetzel JD, Dermody TS.** 2003. Utilization of sialic acid as a coreceptor is required for reovirus-induced biliary disease. J Clin Invest **111:**1823-1833.
107. **Connolly JL, Barton ES, Dermody TS.** 2001. Reovirus binding to cell surface sialic acid potentiates virus-induced apoptosis. J Virol **75:**4029-4039.
108. **Prota AE, Campbell JA, Schelling P, Forrest JC, Watson MJ, Peters TR, Aurrand-Lions M, Imhof BA, Dermody TS, Stehle T.** 2003. Crystal structure of human junctional adhesion molecule 1: implications for reovirus binding. Proc Natl Acad Sci U S A **100:**5366-5371.

109. **Eierhoff T, Hrincius ER, Rescher U, Ludwig S, Ehrhardt C.** 2010. The epidermal growth factor receptor (EGFR) promotes uptake of influenza A viruses (IAV) into host cells. PLoS Pathog **6:**e1001099.
110. **Hofman EG, Bader AN, Voortman J, van den Heuvel DJ, Sigismund S, Verkleij AJ, Gerritsen HC, van Bergen en Henegouwen PM.** 2010. Ligand-induced EGF receptor oligomerization is kinase-dependent and enhances internalization. J Biol Chem **285:**39481-39489.
111. **Barton ES, Forrest JC, Connolly JL, Chappell JD, Liu Y, Schnell FJ, Nusrat A, Parkos CA, Dermody TS.** 2001. Junction adhesion molecule is a receptor for reovirus. Cell **104:**441-451.
112. **Martin-Padura I, Lostaglio S, Schneemann M, Williams L, Romano M, Fruscella P, Panzeri C, Stoppacciaro A, Ruco L, Villa A, Simmons D, Dejana E.** 1998. Junctional adhesion molecule, a novel member of the immunoglobulin superfamily that distributes at intercellular junctions and modulates monocyte transmigration. Journal of Cell Biology **142:**117-127.
113. **Williams LA, Martin-Padura I, Dejana E, Hogg N, Simmons DL.** 1999. Identification and characterisation of human Junctional Adhesion Molecule (JAM). Mol Immunol **36:**1175-1188.
114. **Stelzer S, Ebnet K, Schwamborn JC.** 2010. JAM-A is a novel surface marker for NG2-Glia in the adult mouse brain. BMC Neurosci **11:**27.
115. **Hwang I, An BS, Yang H, Kang HS, Jung EM, Jeung EB.** 2013. Tissue-specific expression of occludin, zona occludens-1, and junction adhesion molecule A in the duodenum, ileum, colon, kidney, liver, lung, brain, and skeletal muscle of C57BL mice. J Physiol Pharmacol **64:**11-18.
116. **Del Maschio A, De Luigi A, Martin-Padura I, Brockhaus M, Bartfai T, Fruscella P, Adorini L, Martino G, Furlan R, DeSimoni MG, Dejana E.** 1999. Leukocyte recruitment in the cerebrospinal fluid of mice with experimental meningitis is inhabited by an antibody to junctional adhesion molecule (JAM). J Exp Med **190:**1351-1356.
117. **Liu Y, Nusrat A, Schnell FJ, Reaves TA, Walsh S, Pochet M, Parkos CA.** 2000. Human junction adhesion molecule regulates tight junction resealing in epithelia. J Cell Sci **113 ( Pt 13):**2363-2374.
118. **Bhella D.** 2015. The role of cellular adhesion molecules in virus attachment and entry. Philos Trans R Soc Lond B Biol Sci **370:**20140035.
119. **Dermody TS, Kirchner E, Guglielmi KM, Stehle T.** 2009. Immunoglobulin superfamily virus receptors and the evolution of adaptive immunity. PLoS Pathog **5:**e1000481.
120. **Kostrewa D, Brockhaus M, D'Arcy A, Dale GE, Nelboeck P, Schmid G, Mueller F, Bazzoni G, Dejana E, Bartfai T, Winkler FK, Hennig M.** 2001. X-ray structure of junctional adhesion molecule: structural basis for homophilic adhesion via a novel dimerization motif. EMBO J **20:**4391-4398.
121. **Campbell JA, Schelling P, Wetzel JD, Johnson EM, Forrest JC, Wilson GAR, Aurrand-Lions M, Imhof BA, Stehle T, Dermody TS.** 2005. Junctional adhesion molecule a serves as a receptor for prototype and field-isolate strains of mammalian reovirus. Journal of Virology **79:**7967-7978.

122. **Salinas S, Zussy C, Loustalot F, Henaff D, Menendez G, Morton PE, Parsons M, Schiavo G, Kremer EJ.** 2014. Disruption of the coxsackievirus and adenovirus receptor-homodimeric interaction triggers lipid microdomain- and dynamin-dependent endocytosis and lysosomal targeting. J Biol Chem **289:**680-695.
123. **Lai CM, Boehme KW, Pruijssers AJ, Parekh VV, Van Kaer L, Parkos CA, Dermody TS.** 2015. Endothelial JAM-A promotes reovirus viremia and bloodstream dissemination. J Infect Dis **211:**383-393.
124. **Flamand A, Gagner JP, Morrison LA, Fields BN.** 1991. Penetration of the nervous systems of suckling mice by mammalian reoviruses. J Virol **65:**123-131.
125. **Barrette B, Vallieres N, Dube M, Lacroix S.** 2007. Expression profile of receptors for myelin-associated inhibitors of axonal regeneration in the intact and injured mouse central nervous system. Mol Cell Neurosci **34:**519-538.
126. **Hunt D, Coffin RS, Anderson PN.** 2002. The Nogo receptor, its ligands and axonal regeneration in the spinal cord; a review. J Neurocytol **31:**93-120.
127. **Llorens F, Gil V, del Rio JA.** 2011. Emerging functions of myelin-associated proteins during development, neuronal plasticity, and neurodegeneration. FASEB J **25:**463-475.
128. **Tardieu M, Powers ML, Weiner HL.** 1983. Age dependent susceptibility to Reovirus type 3 encephalitis: role of viral and host factors. Ann Neurol **13:**602-607.
129. **He XL, Bazan JF, McDermott G, Park JB, Wang K, Tessier-Lavigne M, He Z, Garcia KC.** 2003. Structure of the Nogo receptor ectodomain: a recognition module implicated in myelin inhibition. Neuron **38:**177-185.
130. **Botos I, Segal DM, Davies DR.** 2011. The structural biology of Toll-like receptors. Structure **19:**447-459.
131. **Motta V, Soares F, Sun T, Philpott DJ.** 2015. NOD-like receptors: Versatile cytosolic sentinels. Physiol Rev **95:**149-178.
132. **Deng L, Luo M, Velikovsky A, Mariuzza RA.** 2013. Structural insights into the evolution of the adaptive immune system. Annu Rev Biophys **42:**191-215.
133. **Lauren J, Hu F, Chin J, Liao J, Airaksinen MS, Strittmatter SM.** 2007. Characterization of myelin ligand complexes with neuronal Nogo-66 receptor family members. J Biol Chem **282:**5715-5725.
134. **Nikolic M.** 2002. The role of Rho GTPases and associated kinases in regulating neurite outgrowth. Int J Biochem Cell Biol **34:**731-745.
135. **Taylor MP, Koyuncu OO, Enquist LW.** 2011. Subversion of the actin cytoskeleton during viral infection. Nat Rev Microbiol **9:**427-439.
136. **Wang X, Chun SJ, Treloar H, Vartanian T, Greer CA, Strittmatter SM.** 2002. Localization of Nogo-A and Nogo-66 receptor proteins at sites of axon-myelin and synaptic contact. J Neurosci **22:**5505-5515.
137. **Organization WH.** 2018. Cancer, *on* World Health Organization. http://www.who.int/en/news-room/fact-sheets/detail/cancer. Accessed
138. **Kelly E, Russell SJ.** 2007. History of oncolytic viruses: genesis to genetic engineering. Mol Ther **15:**651-659.

139. **Gujar S, Pol JG, Kim Y, Lee PW, Kroemer G.** 2018. Antitumor benefits of antiviral immunity: An underappreciated aspect of oncolytic virotherapies. Trends Immunol **39:**209-221.
140. **Andtbacka RH, Agarwala SS, Ollila DW, Hallmeyer S, Milhem M, Amatruda T, Nemunaitis JJ, Harrington KJ, Chen L, Shilkrut M, Ross M, Kaufman HL.** 2016. Cutaneous head and neck melanoma in OPTiM, a randomized phase 3 trial of talimogene laherparepvec versus granulocyte-macrophage colony-stimulating factor for the treatment of unresected stage IIIB/IIIC/IV melanoma. Head Neck **38:**1752-1758.
141. **Andtbacka RH, Kaufman HL, Collichio F, Amatruda T, Senzer N, Chesney J, Delman KA, Spitler LE, Puzanov I, Agarwala SS, Milhem M, Cranmer L, Curti B, Lewis K, Ross M, Guthrie T, Linette GP, Daniels GA, Harrington K, Middleton MR, Miller WH, Jr., Zager JS, Ye Y, Yao B, Li A, Doleman S, VanderWalde A, Gansert J, Coffin RS.** 2015. Talimogene laherparepvec improves durable response rate in patients with advanced melanoma. J Clin Oncol **33:**2780-2788.
142. **Liu BL, Robinson M, Han ZQ, Branston RH, English C, Reay P, McGrath Y, Thomas SK, Thornton M, Bullock P, Love CA, Coffin RS.** 2003. ICP34.5 deleted herpes simplex virus with enhanced oncolytic, immune stimulating, and anti-tumour properties. Gene Ther **10:**292-303.
143. **Hu JC, Coffin RS, Davis CJ, Graham NJ, Groves N, Guest PJ, Harrington KJ, James ND, Love CA, McNeish I, Medley LC, Michael A, Nutting CM, Pandha HS, Shorrock CA, Simpson J, Steiner J, Steven NM, Wright D, Coombes RC.** 2006. A phase I study of OncoVEXGM-CSF, a second-generation oncolytic herpes simplex virus expressing granulocyte macrophage colony-stimulating factor. Clin Cancer Res **12:**6737-6747.
144. **Senzer NN, Kaufman HL, Amatruda T, Nemunaitis M, Reid T, Daniels G, Gonzalez R, Glaspy J, Whitman E, Harrington K, Goldsweig H, Marshall T, Love C, Coffin R, Nemunaitis JJ.** 2009. Phase II clinical trial of a granulocyte-macrophage colony-stimulating factor-encoding, second-generation oncolytic herpesvirus in patients with unresectable metastatic melanoma. J Clin Oncol **27:**5763-5771.
145. **Hashiro G, Loh PC, Yau JT.** 1977. The preferential cytotoxicity of reovirus for certain transformed cell lines. Arch Virol **54:**307-315.
146. **Coffey MC, Strong JE, Forsyth PA, Lee PW.** 1998. Reovirus therapy of tumors with activated Ras pathway. Science **282:**1332-1334.
147. **Thirukkumaran CM, Nodwell MJ, Hirasawa K, Shi ZQ, Diaz R, Luider J, Johnston RN, Forsyth PA, Magliocco AM, Lee P, Nishikawa S, Donnelly B, Coffey M, Trpkov K, Fonseca K, Spurrell J, Morris DG.** 2010. Oncolytic viral therapy for prostate cancer: efficacy of reovirus as a biological therapeutic. Cancer Res **70:**2435-2444.
148. **Gollamudi R, Ghalib MH, Desai KK, Chaudhary I, Wong B, Einstein M, Coffey M, Gill GM, Mettinger K, Mariadason JM, Mani S, Goel S.** 2010. Intravenous administration of Reolysin, a live replication competent RNA virus is safe in patients with advanced solid tumors. Invest New Drugs **28:**641-649.

149. **Vidal L, Pandha HS, Yap TA, White CL, Twigger K, Vile RG, Melcher A, Coffey M, Harrington KJ, DeBono JS.** 2008. A phase I study of intravenous oncolytic reovirus type 3 Dearing in patients with advanced cancer. Clin Cancer Res **14:**7127-7137.
150. **Harrington KJ, Karapanagiotou EM, Roulstone V, Twigger KR, White CL, Vidal L, Beirne D, Prestwich R, Newbold K, Ahmed M, Thway K, Nutting CM, Coffey M, Harris D, Vile RG, Pandha HS, Debono JS, Melcher AA.** 2010. Two-stage phase I dose-escalation study of intratumoral reovirus type 3 dearing and palliative radiotherapy in patients with advanced cancers. Clin Cancer Res **16:**3067-3077.
151. **Galanis E, Markovic SN, Suman VJ, Nuovo GJ, Vile RG, Kottke TJ, Nevala WK, Thompson MA, Lewis JE, Rumilla KM, Roulstone V, Harrington K, Linette GP, Maples WJ, Coffey M, Zwiebel J, Kendra K.** 2012. Phase II trial of intravenous administration of Reolysin((R)) (Reovirus Serotype-3-dearing Strain) in patients with metastatic melanoma. Mol Ther **20:**1998-2003.
152. **Karapanagiotou EM, Roulstone V, Twigger K, Ball M, Tanay M, Nutting C, Newbold K, Gore ME, Larkin J, Syrigos KN, Coffey M, Thompson B, Mettinger K, Vile RG, Pandha HS, Hall GD, Melcher AA, Chester J, Harrington KJ.** 2012. Phase I/II trial of carboplatin and paclitaxel chemotherapy in combination with intravenous oncolytic reovirus in patients with advanced malignancies. Clin Cancer Res **18:**2080-2089.
153. **Errington F, Steele L, Prestwich R, Harrington KJ, Pandha HS, Vidal L, de Bono J, Selby P, Coffey M, Vile R, Melcher A.** 2008. Reovirus activates human dendritic cells to promote innate antitumor immunity. J Immunol **180:**6018-6026.
154. **Prestwich RJ, Errington F, Ilett EJ, Morgan RS, Scott KJ, Kottke T, Thompson J, Morrison EE, Harrington KJ, Pandha HS, Selby PJ, Vile RG, Melcher AA.** 2008. Tumor infection by oncolytic reovirus primes adaptive antitumor immunity. Clin Cancer Res **14:**7358-7366.
155. **Prestwich RJ, Ilett EJ, Errington F, Diaz RM, Steele LP, Kottke T, Thompson J, Galivo F, Harrington KJ, Pandha HS, Selby PJ, Vile RG, Melcher AA.** 2009. Immune-mediated antitumor activity of reovirus is required for therapy and is independent of direct viral oncolysis and replication. Clin Cancer Res **15:**4374-4381.
156. **Samson A, Scott KJ, Taggart D, West EJ, Wilson E, Nuovo GJ, Thomson S, Corns R, Mathew RK, Fuller MJ, Kottke TJ, Thompson JM, Ilett EJ, Cockle JV, van Hille P, Sivakumar G, Polson ES, Turnbull SJ, Appleton ES, Migneco G, Rose AS, Coffey MC, Beirne DA, Collinson FJ, Ralph C, Alan Anthoney D, Twelves CJ, Furness AJ, Quezada SA, Wurdak H, Errington-Mais F, Pandha H, Harrington KJ, Selby PJ, Vile RG, Griffin SD, Stead LF, Short SC, Melcher AA.** 2018. Intravenous delivery of oncolytic reovirus to brain tumor patients immunologically primes for subsequent checkpoint blockade. Sci Transl Med **10:**eaam7577.
157. **Gujar SA, Marcato P, Pan D, Lee PW.** 2010. Reovirus virotherapy overrides tumor antigen presentation evasion and promotes protective antitumor immunity. Mol Cancer Ther **9:**2924-2933.
158. **Society AC.** 2017. Breast Cancer Facts & Figures

*on* American Cancer Society, Inc. https://www.cancer.org/content/dam/cancer-org/research/cancer-facts-and-statistics/breast-cancer-facts-and-figures/breast-cancer-facts-and-figures-2017-2018.pdf. Accessed
159. **Boehme KW, Lai CM, Dermody TS.** 2013. Mechanisms of reovirus bloodstream dissemination. Adv Virus Res **87:**1-35.
160. **Solimando AG, Brandl A, Mattenheimer K, Graf C, Ritz M, Ruckdeschel A, Stuhmer T, Mokhtari Z, Rudelius M, Dotterweich J, Bittrich M, Desantis V, Ebert R, Trerotoli P, Frassanito MA, Rosenwald A, Vacca A, Einsele H, Jakob F, Beilhack A.** 2018. JAM-A as a prognostic factor and new therapeutic target in multiple myeloma. Leukemia **32:**736-743.
161. **Tian Y, Tian Y, Zhang W, Wei F, Yang J, Luo X, Zhou T, Hou B, Qian S, Deng X, Qiu Y, Yao K.** 2015. Junctional adhesion molecule-A, an epithelial-mesenchymal transition inducer, correlates with metastasis and poor prognosis in human nasopharyngeal cancer. Carcinogenesis **36:**41-48.
162. **Ikeo K, Oshima T, Shan J, Matsui H, Tomita T, Fukui H, Watari J, Miwa H.** 2015. Junctional adhesion molecule-A promotes proliferation and inhibits apoptosis of gastric cancer. Hepatogastroenterology **62:**540-545.
163. **Zhao C, Lu F, Chen H, Zhao X, Sun J, Chen H.** 2014. Dysregulation of JAM-A plays an important role in human tumor progression. Int J Clin Exp Pathol **7:**7242-7248.
164. **Zhang M, Luo W, Huang B, Liu Z, Sun L, Zhang Q, Qiu X, Xu K, Wang E.** 2013. Overexpression of JAM-A in non-small cell lung cancer correlates with tumor progression. PLoS One **8:**e79173.
165. **Murakami M, Giampietro C, Giannotta M, Corada M, Torselli I, Orsenigo F, Cocito A, d'Ario G, Mazzarol G, Confalonieri S, Di Fiore PP, Dejana E.** 2011. Abrogation of junctional adhesion molecule-A expression induces cell apoptosis and reduces breast cancer progression. PLoS One **6:**e21242.
166. **Twigger K, Roulstone V, Kyula J, Karapanagiotou EM, Syrigos KN, Morgan R, White C, Bhide S, Nuovo G, Coffey M, Thompson B, Jebar A, Errington F, Melcher AA, Vile RG, Pandha HS, Harrington KJ.** 2012. Reovirus exerts potent oncolytic effects in head and neck cancer cell lines that are independent of signalling in the EGFR pathway. BMC Cancer **12:**368.
167. **Strong JE, Coffey MC, Tang D, Sabinin P, Lee PW.** 1998. The molecular basis of viral oncolysis: usurpation of the Ras signaling pathway by reovirus. EMBO J **17:**3351-3362.
168. **Marcato P, Shmulevitz M, Pan D, Stoltz D, Lee PW.** 2007. Ras transformation mediates reovirus oncolysis by enhancing virus uncoating, particle infectivity, and apoptosis-dependent release. Mol Ther **15:**1522-1530.
169. **Hezel AF, Kimmelman AC, Stanger BZ, Bardeesy N, Depinho RA.** 2006. Genetics and biology of pancreatic ductal adenocarcinoma. Genes Dev **20:**1218-1249.
170. **Fernandez-Medarde A, Santos E.** 2011. Ras in cancer and developmental diseases. Genes Cancer **2:**344-358.
171. **Carew JS, Espitia CM, Zhao W, Mita MM, Mita AC, Nawrocki ST.** 2017. Oncolytic reovirus inhibits angiogenesis through induction of CXCL10/IP-10 and abrogation of HIF activity in soft tissue sarcomas. Oncotarget **8:**86769-86783.

172. **Simon EJ, Howells MA, Stuart JD, Boehme KW.** 2017. Serotype-specific killing of large cell carcinoma cells by reovirus. Viruses **9**.
173. **Ooms LS, Kobayashi T, Dermody TS, Chappell JD.** 2010. A post-entry step in the mammalian orthoreovirus replication cycle is a determinant of cell tropism. J Biol Chem **285:**41604-41613.
174. **Ooms LS, Jerome WG, Dermody TS, Chappell JD.** 2012. Reovirus replication protein mu2 influences cell tropism by promoting particle assembly within viral inclusions. J Virol **86:**10979-10987.
175. **Shah PNM, Stanifer ML, Hohn K, Engel U, Haselmann U, Bartenschlager R, Krausslich HG, Krijnse-Locker J, Boulant S.** 2017. Genome packaging of reovirus is mediated by the scaffolding property of the microtubule network. Cell Microbiol **19**.
176. **Roner MR, Roehr J.** 2006. The 3' sequences required for incorporation of an engineered ssRNA into the Reovirus genome. Virol J **3:**1.
177. **Leone G, Mah DCW, Lee PWK.** 1991. The incorporation of reovirus cell attachment protein σ1 into virions requires the amino-terminal hydrophobic tail and the adjacent heptad repeat region. Virology **182:**346-350.
178. **Brubaker MM, West B, Eillis RJ.** 1964. Human blood group influence on reovirus hemagglutination titers. Proc Soc Exp Biol Med **115:**1118-1120.
179. **Eggers HJ, Gomatos PJ, Tamm I.** 1962. Agglutination of bovine erythrocytes: a general characteristic of reovirus type 3. Proc Soc Exp Biol Med **110:**879-881.
180. **Gentsch JR, Pacitti AF.** 1987. Differential interaction of reovirus type 3 with sialylated receptor components on animal cells. Virology **161:**245-248.
181. **Paul RW, Lee PWK.** 1987. Glycophorin Is the Reovirus Receptor on Human-Erythrocytes. Virology **159:**94-101.
182. **Chappell JD, Gunn VL, Wetzel JD, Baer GS, Dermody TS.** 1997. Mutations in type 3 reovirus that determine binding to sialic acid are contained in the fibrous tail domain of viral attachment protein σ1. Journal of Virology **71:**1834-1841.
183. **Tyler KL.** 1998. Pathogenesis of reovirus infections of the central nervous system. Curr Top Microbiol Immunol **233:**93-124.
184. **Chappell JD, Duong JL, Wright BW, Dermody TS.** 2000. Identification of carbohydrate-binding domains in the attachment proteins of type 1 and type 3 reoviruses. J Virol **74:**8472-8479.
185. **Demidenko AA, Blattman JN, Blattman NN, Greenberg PD, Nibert ML.** 2013. Engineering recombinant reoviruses with tandem repeats and a tetravirus 2A-like element for exogenous polypeptide expression. Proc Natl Acad Sci U S A **110:**E1867-1876.
186. **van den Wollenberg DJ, Dautzenberg IJ, Ros W, Lipinska AD, van den Hengel SK, Hoeben RC.** 2015. Replicating reoviruses with a transgene replacing the codons for the head domain of the viral spike. Gene Ther **22:**267-279.
187. **Sun J, Barbeau B, Sato S, Tremblay MJ.** 2001. Neuraminidase from a bacterial source enhances both HIV-1-mediated syncytium formation and the virus binding/entry process. Virology **284:**26-36.

188. **Morrison LA, Sidman RL, Fields BN.** 1991. Direct spread of reovirus from the intestinal lumen to the central nervous system through vagal autonomic nerve fibers. Proceedings of the National Academy of Sciences USA **88:**3852-3856.
189. **Chen J, Sawyer N, Regan L.** 2013. Protein-protein interactions: General trends in the relationship between binding affinity and interfacial buried surface area. Protein Sci **22:**510-515.
190. **Bewley MC, Springer K, Zhang YB, Freimuth P, Flanagan JM.** 1999. Structural analysis of the mechanism of adenovirus binding to its human cellular receptor, CAR. Science **286:**1579-1583.
191. **Mercier GT, Campbell JA, Chappell JD, Stehle T, Dermody TS, Barry MA.** 2004. A chimeric adenovirus vector encoding reovirus attachment protein σ1 targets cells expressing junctional adhesion molecule 1. Proc Natl Acad Sci U S A **101:**6188-6193.
192. **Duncan MR, Stanish SM, Cox DC.** 1978. Differential sensitivity of normal and transformed human cells to reovirus infection. J Virol **28:**444-449.
193. **Strong JE, Lee PW.** 1996. The v-erbB oncogene confers enhanced cellular susceptibility to reovirus infection. J Virol **70:**612-616.
194. **Chappell JD, Prota A, Dermody TS, Stehle T.** 2002. Crystal structure of reovirus attachment protein σ1 reveals evolutionary relationship to adenovirus fiber. EMBO Journal **21:**1-11.
195. **Semavina M, Saha N, Kolev MV, Goldgur Y, Giger RJ, Himanen JP, Nikolov DB.** 2011. Crystal structure of the Nogo-receptor-2. Protein Sci **20:**684-689.
196. **Lauren J, Airaksinen MS, Saarma M, Timmusk T.** 2003. Two novel mammalian Nogo receptor homologs differentially expressed in the central and peripheral nervous systems. Mol Cell Neurosci **24:**581-594.
197. **Robak LA, Venkatesh K, Lee H, Raiker SJ, Duan Y, Lee-Osbourne J, Hofer T, Mage RG, Rader C, Giger RJ.** 2009. Molecular basis of the interactions of the Nogo-66 receptor and its homolog NgR2 with myelin-associated glycoprotein: development of NgROMNI-Fc, a novel antagonist of CNS myelin inhibition. J Neurosci **29:**5768-5783.
198. **Venkatesh K, Chivatakarn O, Lee H, Joshi PS, Kantor DB, Newman BA, Mage R, Rader C, Giger RJ.** 2005. The Nogo-66 receptor homolog NgR2 is a sialic acid-dependent receptor selective for myelin-associated glycoprotein. J Neurosci **25:**808-822.
199. **Dickendesher TL, Baldwin KT, Mironova YA, Koriyama Y, Raiker SJ, Askew KL, Wood A, Geoffroy CG, Zheng B, Liepmann CD, Katagiri Y, Benowitz LI, Geller HM, Giger RJ.** 2012. NgR1 and NgR3 are receptors for chondroitin sulfate proteoglycans. Nat Neurosci **15:**703-712.
200. **Fournier AE, GrandPre T, Strittmatter SM.** 2001. Identification of a receptor mediating Nogo-66 inhibition of axonal regeneration. Nature **409:**341-346.
201. **Wang KC, Kim JA, Sivasankaran R, Segal R, He Z.** 2002. P75 interacts with the Nogo receptor as a co-receptor for Nogo, MAG and OMgp. Nature **420:**74-78.
202. **Mi S, Lee X, Shao Z, Thill G, Ji B, Relton J, Levesque M, Allaire N, Perrin S, Sands B, Crowell T, Cate RL, McCoy JM, Pepinsky RB.** 2004. LINGO-1 is a

component of the Nogo-66 receptor/p75 signaling complex. Nat Neurosci **7:**221-228.
203. **Park JB, Yiu G, Kaneko S, Wang J, Chang J, He XL, Garcia KC, He Z.** 2005. A TNF receptor family member, TROY, is a coreceptor with Nogo receptor in mediating the inhibitory activity of myelin inhibitors. Neuron **45:**345-351.
204. **Harel NY, Song KH, Tang X, Strittmatter SM.** 2010. Nogo receptor deletion and multimodal exercise improve distinct aspects of recovery in cervical spinal cord injury. J Neurotrauma **27:**2055-2066.
205. **Ahmed Z, Douglas MR, John G, Berry M, Logan A.** 2013. AMIGO3 is an NgR1/p75 co-receptor signalling axon growth inhibition in the acute phase of adult central nervous system injury. PLoS One **8:**e61878.
206. **Schwab ME, Strittmatter SM.** 2014. Nogo limits neural plasticity and recovery from injury. Curr Opin Neurobiol **27:**53-60.
207. **Saha N, Kolev M, Nikolov DB.** 2014. Structural features of the Nogo receptor signaling complexes at the neuron/myelin interface. Neurosci Res **87:**1-7.
208. **Smith RE, Zweerink HJ, Joklik WK.** 1969. Polypeptide components of virions, top component and cores of reovirus type 3. Virology **39:**791-810.
209. **Olland AM, Jané-Valbuena J, Schiff LA, Nibert ML, Harrison SC.** 2001. Structure of the reovirus outer capsid and dsRNA-binding protein σ3 at 1.8 Å resolution. EMBO J **20:**979-989.
210. **Knowlton JJ, Fernandez de Castro I, Ashbrook AW, Gestaut DR, Zamora PF, Bauer JA, Forrest JC, Frydman J, Risco C, Dermody TS.** 2018. The TRiC chaperonin controls reovirus replication through outer-capsid folding. Nat Microbiol **3:**481-493.
211. **Snyder AJ, Danthi P.** 2015. Lipid membranes facilitate conformational changes required for reovirus cell entry. J Virol **90:**2628-2638.
212. **Baer GS, Dermody TS.** 1997. Mutations in reovirus outer-capsid protein σ3 selected during persistent infections of L cells confer resistance to protease inhibitor E64. Journal of Virology **71:**4921-4928.
213. **Wilson GJ, Nason EL, Hardy CS, Ebert DH, Wetzel JD, Venkataram Prasad BV, Dermody TS.** 2002. A single mutation in the carboxy terminus of reovirus outer-capsid protein sigma 3 confers enhanced kinetics of sigma 3 proteolysis, resistance to inhibitors of viral disassembly, and alterations in sigma 3 structure. J Virol **76:**9832-9843.
214. **Clark KM, Wetzel JD, Gu Y, Ebert DH, McAbee SA, Stoneman EK, Baer GS, Zhu Y, Wilson GJ, Prasad BVV, Dermody TS.** 2006. Reovirus variants selected for resistance to ammonium chloride have mutations in viral outer-capsid protein σ3. Journal of Virology **80:**671-681.
215. **Doyle JD, Stencel-Baerenwald JE, Copeland CA, Rhoads JP, Brown JJ, Boyd KL, Atkinson JB, Dermody TS.** 2015. Diminished reovirus capsid stability alters disease pathogenesis and littermate transmission. PLoS Pathog **11:**e1004693.
216. **Konopka-Anstadt JL, Dermody TS.** 2017. Unpublished observations.
217. **Bhattacharya B, Roy P.** 2008. Bluetongue virus outer capsid protein VP5 interacts with membrane lipid rafts via a SNARE domain. J Virol **82:**10600-10612.

218. **Guerrero CA, Moreno LP.** 2012. Rotavirus receptor proteins Hsc70 and integrin αvβ3 are located in the lipid microdomains of animal intestinal cells. Acta Virol **56:**63-70.
219. **Barton WA, Liu BP, Tzvetkova D, Jeffrey PD, Fournier AE, Sah D, Cate R, Strittmatter SM, Nikolov DB.** 2003. Structure and axon outgrowth inhibitor binding of the Nogo-66 receptor and related proteins. EMBO J **22:**3291-3302.
220. **Cheng Y.** 2015. Single-particle cryo-EM at crystallographic resolution. Cell **161:**450-457.
221. **Dionne KR, Leser JS, Lorenzen KA, Beckham JD, Tyler KL.** 2011. A brain slice culture model of viral encephalitis reveals an innate CNS cytokine response profile and the therapeutic potential of caspase inhibition. Exp Neurol **228:**222-231.
222. **Sattentau Q.** 2008. Avoiding the void: Cell-to-cell spread of human viruses. Nat Rev Microbiol **6:**815-826.
223. **Grondona JM, Granados-Duran P, Fernandez-Llebrez P, Lopez-Avalos MD.** 2013. A simple method to obtain pure cultures of multiciliated ependymal cells from adult rodents. Histochem Cell Biol **139:**205-220.
224. **Yu L, Baxter PA, Voicu H, Gurusiddappa S, Zhao Y, Adesina A, Man TK, Shu Q, Zhang YJ, Zhao XM, Su JM, Perlaky L, Dauser R, Chintagumpala M, Lau CC, Blaney SM, Rao PH, Leung HC, Li XN.** 2010. A clinically relevant orthotopic xenograft model of ependymoma that maintains the genomic signature of the primary tumor and preserves cancer stem cells in vivo. Neuro Oncol **12:**580-594.
225. **Amani V, Donson AM, Lummus SC, Prince EW, Griesinger AM, Witt DA, Hankinson TC, Handler MH, Dorris K, Vibhakar R, Foreman NK, Hoffman LM.** 2017. Characterization of 2 novel ependymoma cell lines with chromosome 1q gain derived from posterior fossa tumors of childhood. J Neuropathol Exp Neurol **76:**595-604.
226. **Mainou BA, Zamora PF, Ashbrook AW, Dorset DC, Kim KS, Dermody TS.** 2013. Reovirus cell entry requires functional microtubules. MBio **4:**e00405-00413.
227. **Chappell JD, Barton ES, Smith TH, Baer GS, Duong DT, Nibert ML, Dermody TS.** 1998. Cleavage susceptibility of reovirus attachment protein σ1 during proteolytic disassembly of virions is determined by a sequence polymorphism in the σ1 neck. Journal of Virology **72:**8205-8213.
228. **Adair RA, Roulstone V, Scott KJ, Morgan R, Nuovo GJ, Fuller M, Beirne D, West EJ, Jennings VA, Rose A, Kyula J, Fraser S, Dave R, Anthoney DA, Merrick A, Prestwich R, Aldouri A, Donnelly O, Pandha H, Coffey M, Selby P, Vile R, Toogood G, Harrington K, Melcher AA.** 2012. Cell carriage, delivery, and selective replication of an oncolytic virus in tumor in patients. Sci Transl Med **4:**138ra177.
229. **Stuart JD, Holm GH, Boehme KW.** 2018. Differential delivery of genomic double-stranded RNA causes reovirus strain-specific differences in interferon regulatory factor 3 activation. J Virol **92**.

230. **Zurney J, Kobayashi T, Holm GH, Dermody TS, Sherry B.** 2009. Reovirus mu2 protein inhibits interferon signaling through a novel mechanism involving nuclear accumulation of interferon regulatory factor 9. J Virol **83:**2178-2187.
231. **Irvin SC, Zurney J, Ooms LS, Chappell JD, Dermody TS, Sherry B.** 2012. A single-amino-acid polymorphism in reovirus protein mu2 determines repression of interferon signaling and modulates myocarditis. J Virol **86:**2302-2311.
232. **Tyler KL, Squier MK, Rodgers SE, Schneider SE, Oberhaus SM, Grdina TA, Cohen JJ, Dermody TS.** 1995. Differences in the capacity of reovirus strains to induce apoptosis are determined by the viral attachment protein σ1. J Virol **69:**6972-6979.
233. **Aravamudhan P, Guzman, C.C., Konopka-Anstadt, J.L., Dermody, T.S.** 2018. Unpublished observations.
234. **Consortium HPA.** 2017. The Human Protein Atlas. https://www.proteinatlas.org/. Accessed
235. **Shao Z, Browning JL, Lee X, Scott ML, Shulga-Morskaya S, Allaire N, Thill G, Levesque M, Sah D, McCoy JM, Murray B, Jung V, Pepinsky RB, Mi S.** 2005. TAJ/TROY, an orphan TNF receptor family member, binds Nogo-66 receptor 1 and regulates axonal regeneration. Neuron **45:**353-359.
236. **Baycin-Hizal D, Tabb DL, Chaerkady R, Chen L, Lewis NE, Nagarajan H, Sarkaria V, Kumar A, Wolozny D, Colao J, Jacobson E, Tian Y, O'Meally RN, Krag SS, Cole RN, Palsson BO, Zhang H, Betenbaugh M.** 2012. Proteomic analysis of Chinese hamster ovary cells. J Proteome Res **11:**5265-5276.
237. **Joset A, Dodd DA, Halegoua S, Schwab ME.** 2010. Pincher-generated Nogo-A endosomes mediate growth cone collapse and retrograde signaling. J Cell Biol **188:**271-285.
238. **Kumar S, Dick EJ, Jr., Bommineni YR, Yang A, Mubiru J, Hubbard GB, Owston MA.** 2014. Reovirus-associated meningoencephalomyelitis in baboons. Vet Pathol **51:**641-650.
239. **Yan X, Parent KN, Goodman RP, Tang J, Shou J, Nibert ML, Duncan R, Baker TS.** 2011. Virion structure of baboon reovirus, a fusogenic orthoreovirus that lacks an adhesion fiber. J Virol **85:**7483-7495.
240. **Virgin HW, IV, Mann MA, Fields BN, Tyler KL.** 1991. Monoclonal antibodies to reovirus reveal structure/function relationships between capsid proteins and genetics of susceptibility to antibody action. Journal of Virology **65:**6772-6781.
241. **Burstin SJ, Spriggs DR, Fields BN.** 1982. Evidence for functional domains on the reovirus type 3 hemagglutinin. Virology **117:**146-155.
242. **Virgin HWt, Bassel-Duby R, Fields BN, Tyler KL.** 1988. Antibody protects against lethal infection with the neurally spreading reovirus type 3 (Dearing). J Virol **62:**4594-4604.
243. **Mainou BA, Dermody TS.** 2011. Src kinase mediates productive endocytic sorting of reovirus during cell entry. J Virol **85:**3203-3213.
244. **Schindelin J, Arganda-Carreras I, Frise E, Kaynig V, Longair M, Pietzsch T, Preibisch S, Rueden C, Saalfeld S, Schmid B, Tinevez JY, White DJ, Hartenstein V, Eliceiri K, Tomancak P, Cardona A.** 2012. Fiji: An open-source platform for biological-image analysis. Nat Methods **9:**676-682.

245. **Dubochet J, Adrian M, Chang JJ, Homo JC, Lepault J, McDowall AW, Schultz P.** 1988. Cryo-electron microscopy of vitrified specimens. Q Rev Biophys **21:**129-228.